

General Disclaimer

One or more of the Following Statements may affect this Document

- This document has been reproduced from the best copy furnished by the organizational source. It is being released in the interest of making available as much information as possible.
- This document may contain data, which exceeds the sheet parameters. It was furnished in this condition by the organizational source and is the best copy available.
- This document may contain tone-on-tone or color graphs, charts and/or pictures, which have been reproduced in black and white.
- This document is paginated as submitted by the original source.
- Portions of this document are not fully legible due to the historical nature of some of the material. However, it is the best reproduction available from the original submission.

1983

(NASA-CR-175558) JPL HIGHLIGHTS, 1983 (Jet
Propulsion Lab.) 101 p HC AGO/MF AC1
CSCL 05B

N85-22256

Unclas

G3/82 19502

JPL

JET PROPULSION LABORATORY
CALIFORNIA INSTITUTE OF TECHNOLOGY
PASADENA, CALIFORNIA



JPL HIGHLIGHTS

1983

ORIGINAL CONTENT
COLOR ILLUSTRATIONS



JET PROPULSION LABORATORY
CALIFORNIA INSTITUTE OF TECHNOLOGY
PASADENA, CALIFORNIA

CONTENTS

INTRODUCTION	1
I. DEEP SPACE EXPLORATION	
A. Planets and Their Satellites	
CCD Imaging of the Outer Planets	4
Plasma Physics at Saturn	6
B. Astrophysics	
Infrared Astronomical Satellite	8
Testing Relativity With Solar System Dynamics	11
X-Ray CCD Spectrometer	12
Far-Ultraviolet CCD Imager	14
Gamma-Ray Line Emission From SS 433	16
Radio Astronomy at the Milliarcsecond Level	18
Electron Impact Excitation of Ions From Energy-Loss Spectra Measurements	20
C. Deep Space Navigation and Communication	
Technology Upgrade of DSN Antennas from 64 to 70 m	22
VLSI Multicode Convolutional Encoder Chip	24
2.5 Bits/Detected Photon Demonstration	26
Data Acquisition and Command of Pioneer 8 From an Unattended Station	29
Microwave Holographic Surface Measurement of the Tidbinbilla 64-m Antenna	30
Diffraction-Coupled Semiconductor Laser Arrays	32

REPRODUCING PAGE BLANK NOT FILLED

D. Small Bodies--Asteroids and Comets

Properties of Residues From Sublimed Dirty Ice:

Comet and Mars Applications	34
Palomar Asteroid Search Program	36
Radar Detection of Comets	38

II. INFORMATION SYSTEMS AND SPACE TECHNOLOGY DEVELOPMENT

Hydride-Absorption Cryogenic Refrigerator	42
Particulate Contamination Environment Observed on STS-3	44
Flow-Field Diagnostics Using Digital Imaging Techniques	46
Computer-Vision and Robotics Research	48
Improved-Performance Shuttle-Nozzle Test	50
Gaseous Oxygen/Hydrogen Thruster Technology	52
Hybrid Topology Developments	54
The VLSI Design Center	56
Pulsed Plasma Thruster Ignition System Lifetime	57
Development of Safe, High-Energy Lithium Cells for NASA Applications	58

III. TECHNOLOGY APPLICATIONS

Measuring Trace Amounts of Contaminants Present in a Gaseous Environment	62
Metal Shell Technology and Its Applications	64
Hydrocephalus Shunt	66
Pressure Distribution and Flow Separation in Arterial Branch Cast and Models	68
Analysis of Individual Biological Particles by Mass Spectrometry	70

IV. ENERGY AND ENERGY CONVERSION TECHNOLOGY	
Low-Cost Polycrystalline Silicon-Process Development	74
Characterization of Silicon Materials Pertinent to Terrestrial Solar-Cell Applications	76
V. EARTH OBSERVATIONAL SYSTEMS	
The New Airborne Thermal Infrared Multispectral Scanner	80
Airborne Imaging Spectrometer: First Use of Imaging Spectrometry in Earth Remote Sensing	83
Development of Reliable Excimer Laser Sources for Spaceborne Active Remote Sensing	84
A Dual-Mode Horn for Submillimeter Wavelengths	86
Hybrid SAR Data Processor	88
Pilot Ocean Data System	90
Radio Interferometric Measurement of the JPL/Owens Valley/ Goldstone Baselines Using the Mobile VLBI Systems	92
SERIES GPS Receiver	94
INDEX OF NATIONAL AERONAUTICS AND SPACE ADMINISTRATION SPONSORING PROGRAM OFFICES	97

INTRODUCTION

The 43 papers contained in this report discuss the most significant accomplishments during FY'83 in a wide range of ongoing research and development tasks at the Jet Propulsion Laboratory.

JPL Highlights is not a status report, but describes annual research and technology achievements in six major categories: Deep Space Exploration, Information Systems and Space Technology Development, Technology Applications, Energy and Energy Conversion Technology, and Earth Observational Systems.

The selections emphasize programmatic goals of JPL: 1) implementation of deep-space missions for NASA; (2) participation in Earth-orbital projects and experiments; and (3) the application of advanced technology to selected fields, such as energy, that involve major national interests.

The NASA Headquarters office sponsoring the work described in each paper is included in the index. In addition, each paper includes the name, telephone number, and address of the individual(s) to be contacted should the reader wish to make inquiries regarding a particular report.

RECEIVING PAGE BLANK NOT FILLED

I. Deep Space Exploration

CCD IMAGING OF THE OUTER PLANETS

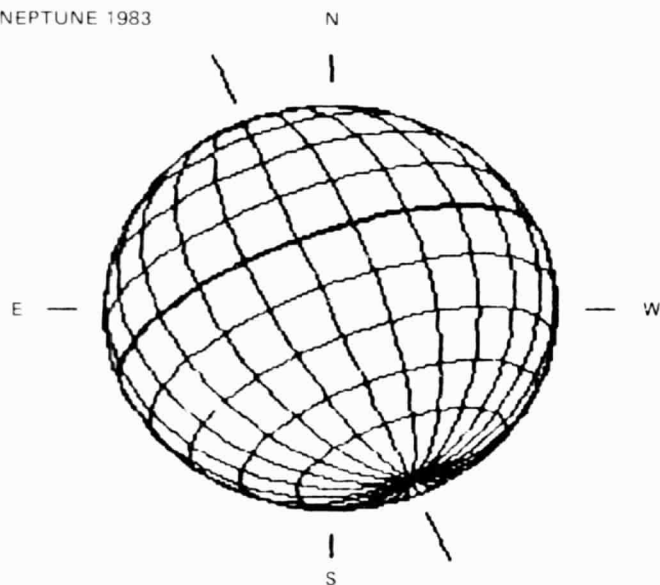
JPL and University of Arizona astronomers used the Las Campanas du Pont 2.5-m telescope on 8 nights to obtain some of the highest-resolution images ever recorded of Uranus and Neptune. Additionally they collected data which will allow a search for new satellites around Uranus and Neptune at least 2 orders of magnitude deeper than previous searches. This program involves using the Wide-Field/Planetary Camera instrument-definition 500-by-500-element Texas Instruments CCD in combination with a planetary coronagraph. The coronagraph forms an image of the entrance pupil of the telescope, which contains a mask that covers the edges of the primary and secondary mirrors and the secondary spider. This baffling virtually eliminates all diffraction from mirror edges and support structures. Furthermore, also within the coronagraph is an image of the focal plane where occulting masks can be placed in order to block out light from bright objects within the field of view. It is this combination of properties that allows the imaging of very faint satellites and rings very close to bright planets. Additionally, because of the high probability of subarcsecond seeing at Las Campanas

and the fact that Jupiter, Saturn, Uranus, and Neptune are all southern-hemisphere objects, the coronagraph has also been designed with a high-resolution direct-imaging mode.

Direct imaging of Saturn, Uranus, and Neptune was done with the planetary coronagraph in a high-resolution mode. In this mode, the plate scale becomes 0.17 arcsecond/pixel. This oversampling takes advantage of the periods of very good seeing to provide subarcsecond-resolution images. On two nights this year this system was used to acquire the best direct images of Uranus and Neptune ever recorded. Of particular interest are the images of Uranus and Neptune that were taken in the strong methane-absorption band at 8900 Å. These images show distinct cloud features, which can be seen rotating across the 2.4-arcsecond-diameter disk. This is of great interest because only very crude spectroscopic-measurement numbers exist for the rotation rate of Neptune. These new data will allow a rotation-rate determination from direct measurement of cloud motions.

Richard J. Terrile
183-301
(213) 354-6158

NEPTUNE 1983



This diagram shows the angle of Neptune when the three CCD images in the accompanying figure were taken.



Neptune's prograde rotation is evident in these three CCD images taken 40 min apart: large cloud features can be seen transiting the face of the planet. This is the first time clear cloud features have been seen on Neptune.

PLASMA PHYSICS AT SATURN

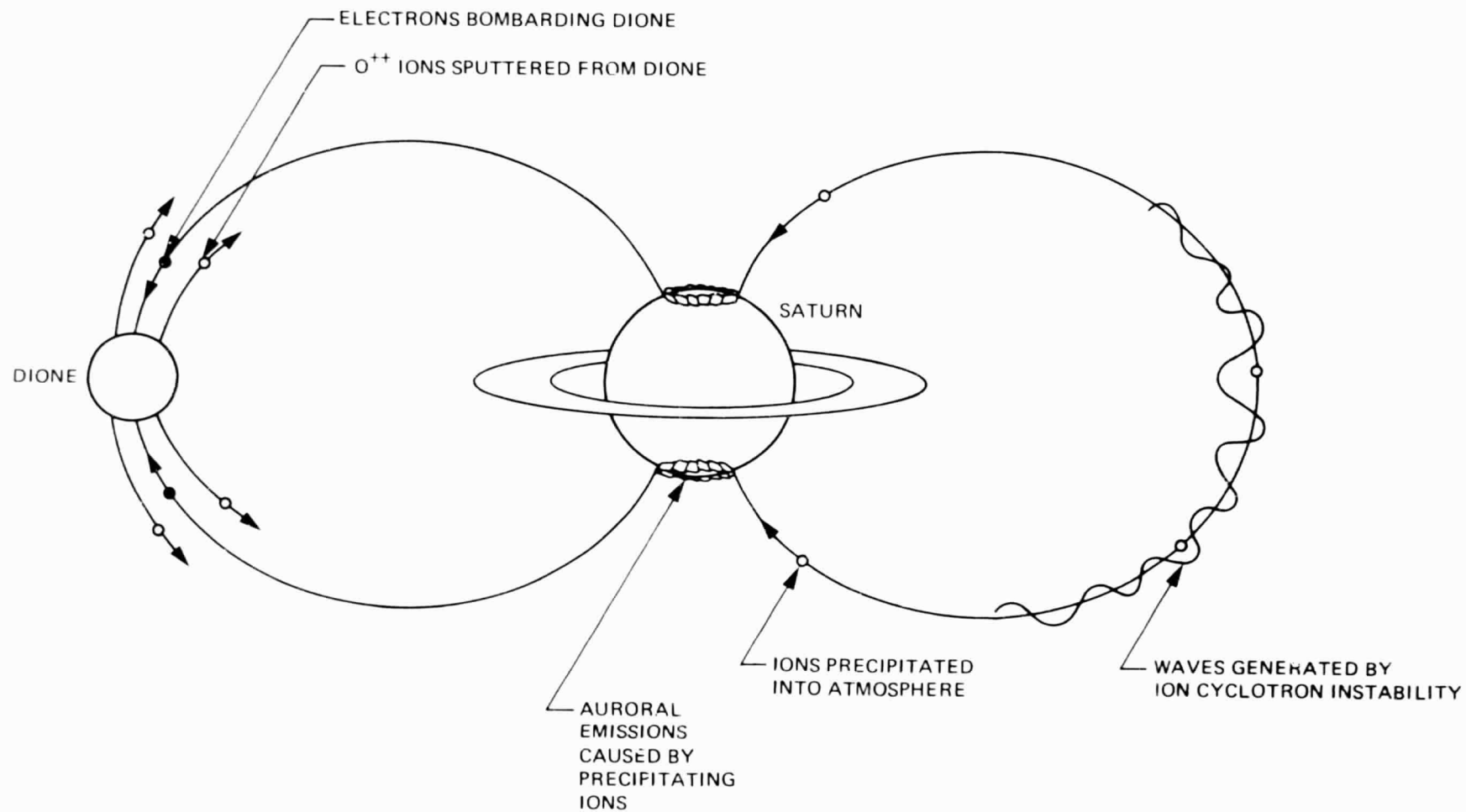
It has recently been discovered that unstable plasmas occur naturally at Saturn. The JPL magnetometer on board the Pioneer 11 spacecraft, which encountered Saturn, measured the global magnetic field of the planet and detected plasma waves near the orbit of Dione. Results of analyses of the waves indicate that they are left-hand circularly polarized emissions, identifying them as electromagnetic ion-cyclotron waves. The latter phrase refers to the spiraling of the ions around the magnetic field, a motion which is basic to the large particle accelerators (cyclotrons) used in Earth-based laboratories. The 18-s period of the waves has lead JPL researchers to believe that they are generated by doubly ionized oxygen atoms.

The scenario that has been developed by JPL researchers is as follows: as Dione orbits Saturn, it

is continuously bombarded by trapped radiation-belt electrons. As a consequence, ions are sputtered from its surface, escape Dione, and are themselves caught in the magnetic field. As these ions move about in the field they generate waves, which travel along the lines of force. As a consequence of generating the waves, some of the ions escape from the magnetic field and enter the atmosphere, where they are believed to cause an aurora, the equivalent of the northern lights seen in Earth's arctic regions.

The above explanation is similar to one developed several years ago to explain similar observations in the space surrounding Earth. During some solar magnetic storms, ions ejected into Earth's magnetic field give rise to ion cyclotron waves and to the production of the red auroral arcs seen in the skies over the northern continental United States.

Edward J. Smith
169-506
(213) 354-2248



INFRARED ASTRONOMICAL SATELLITE

After seven years of planning and preparation, the Infrared Astronomical Satellite (IRAS) is carrying out the first all-sky survey in the infrared (IR).

The telescope on the American-Dutch-British satellite observes IR radiation of wavelengths between 8 and 120 μm , with a sensitivity more than 100 times and a duration more than 1000 times greater than any earlier surveys. It is providing the basic data for the next several decades of infrared astronomy.

A prime objective of modern astronomy is to understand the birth of stars, a process that takes place initially at low temperatures in regions that have a high density of dust. Infrared radiation emitted from cold objects penetrates the dust and is ideal for studying the process. The dust-shrouded central region of our galaxy (the Milky Way) is clearly visible to the IRAS telescope. Asteroids, comets, and planets radiate mainly in the infrared.

One remarkable IRAS discovery came serendipitously out of the routine observations made for calibrating the telescope. One of the primary preselected calibration sources was the bright star Vega (Alpha Lyrae). The first observation revealed that the star is many times brighter, at the two longest wavelengths, than expected from previous visible and near-infrared observations. Repeated observations combined with theoretical considerations led to the conclusion that

Vega is surrounded by an immense halo of cold solid material at a distance of about 85 AU. Since there is no evidence for mass outflow from Vega, it is concluded that the material must be left over from the formation of Vega ~ 1 billion years ago. If this is true, then the particles must be larger than $\sim 1/20$ in., since smaller debris would have been swept away by the pressure of Vega's starlight. This is the first discovery of such macroscopic chunks of matter around a star. The possibility that it could be an emerging planetary system is under discussion.

Another IRAS achievement has been the record-setting discovery of four new comets within a six-week period. Shortly thereafter, IRAS also found that the well-known Comet Tempel 2 has a long, thin tail of dust, which, although very bright in the far infrared, is too faint at visible wavelengths to have ever been detected. With this discovery, it now seems probable that many aged comets, which had been thought to have no tails, are actually still shedding sufficient dust to be seen in the infrared.

Before the end of its mission (expected in early January 1984), IRAS will have recorded the positions and intensities of $\sim 1/4$ million infrared sources. It is probable that many more exciting discoveries are still hidden in the great bulk of data, which is being recorded faster than it can be examined.

Conway Snyder
264-338
(213) 354-5974

Figure (opposite page). IRAS view of the Milky Way. The bright band is caused by dust in the central plane of the galaxy; the bright ellipsoidal bulge is the galactic center. The colors were produced by printing the 12- μm IRAS band in blue, the 60- μm band in green, and the 100- μm band in red.



ORIGINAL PAGE
COLOR PHOTOGRAPH

TESTING RELATIVITY WITH SOLAR SYSTEM DYNAMICS

In over six years of operation since landing on Mars in July, 1976, the Viking landers have provided a set of ranging data that are sufficiently accurate to enable the distance between Earth and Mars to be modeled to within ± 18 m. This unprecedented accuracy in a Solar System data set has been responsible for a major breakthrough in the accuracy of Solar System dynamical tests of relativistic gravity.

We searched for two kinds of effects. The first derives from an idea, due originally to Dirac, that the coincidence of certain dimensionless large numbers relating fundamental cosmic to atomic quantities is not such a coincidence after all, but that the constants of local physics, such as the Newtonian gravitational constant, may be changing on a cosmic time scale. If such an effect were to exist, then it would have observable effects on the orbits of Earth and Mars. Our analysis of the Viking data gives a limit $\dot{G}/G = (0.2 \pm 0.4) \times 10^{-11} \text{ yr}^{-1}$. The conclusion is that we see no evidence for the existence of these effects at the level of accuracy of the experiment.

The second test is a test to determine which theory of gravity, Einstein's Theory of General Relativity or some other theory, correctly describes the motion of the planets. This question was raised about a year ago when Henry Hill at the University of Arizona published a value for the solar quadrupole moment, derived from his measurements of normal mode oscillations of the Sun. He pointed out that, given

his value of $J_2 = 6 \times 10^{-6}$, General Relativity would predict motion for the planet Mercury that was inconsistent with observations. Hill's value, however, is determined only indirectly and depends for its calculation on having an adequate model of the solar interior. It would clearly be desirable in testing a fundamental theory like gravitation to have an independent, direct, dynamical determination of J_2 .

This is what the acquisition of the Mars data has given. With Viking data from Mars and radar data from Mercury, it is possible to solve for J_2 at the same time one is testing gravitational theory (by estimating the value of a theory-dependent parameter β , whose value in General Relativity is 1.0). The preferred values of J_2 and β , estimated in least squares fits to the Solar System data, are:

$$J_2 = (-1.4 \pm 1.5) \times 10^{-6},$$

a value consistent with $J_2 = 0$ to within experimental error, and

$$\beta = 0.9971 \pm .0031$$

The conclusion of Solar System dynamics then is that β has a value consistent with the value predicted by General Relativity and that the value for the solar quadrupole moment determined from solar oscillations seems to be in error.

Ronald W. Hellings
John D. Anderson
E. Myles Standish
264-664
(213) 354-3192

X-RAY CCD SPECTROMETER

Significant improvements in the detection and resolution of low-energy X rays were achieved in 1983 in JPL's continuing program for developing an X-ray charge-coupled-device (CCD) spectrometer. The instrument is being developed for use in X-ray astronomy, laboratory plasma research, and X-ray microscopy.

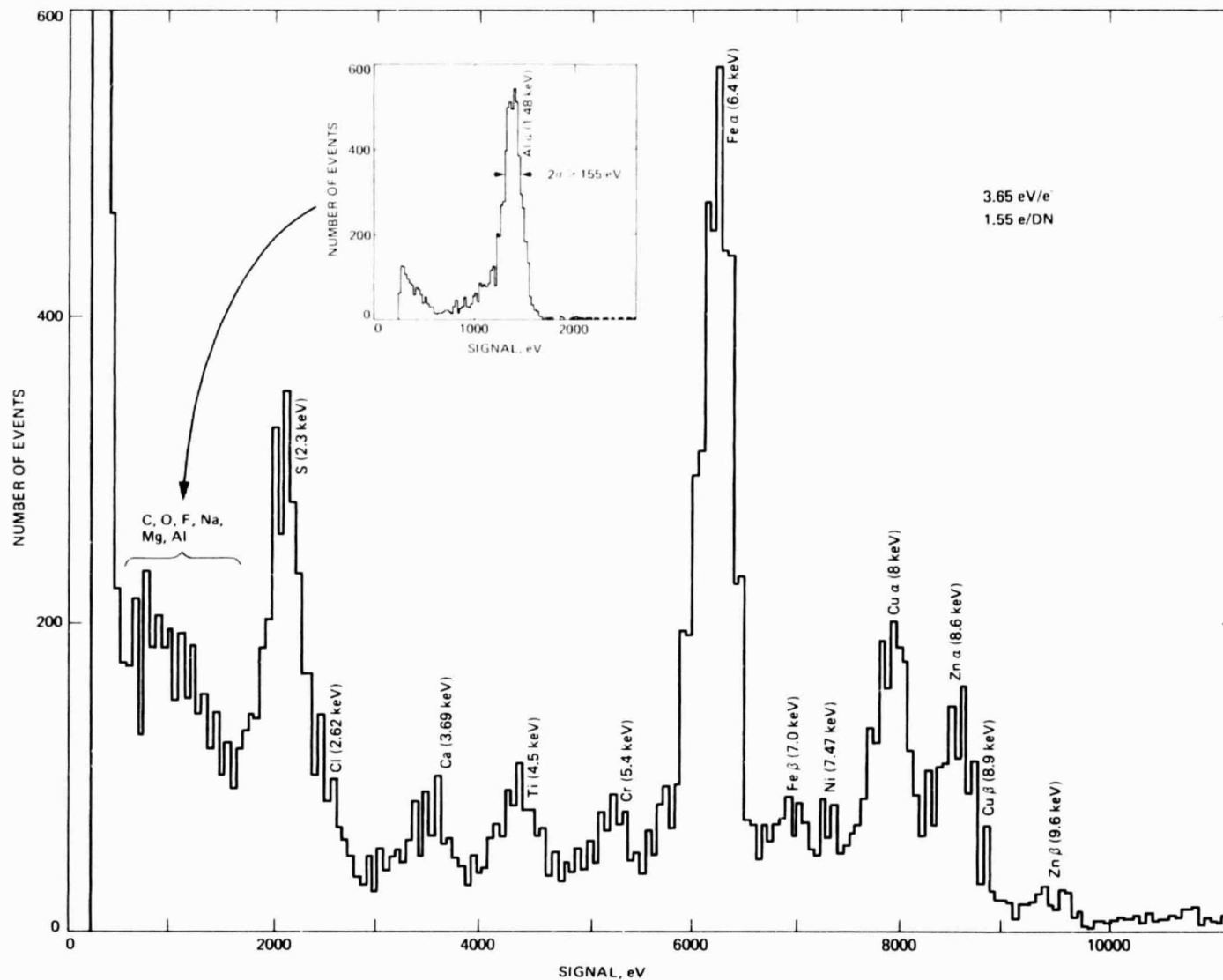
The improvements are the result of continued efforts in the optimization of the bias and drive clock for a thinned, backside-illuminated, three-phase, 800-by-800-picture-element CCD.

The X-ray CCD imaging spectrometer can provide imaging data and simultaneously identify elements by the energy they radiate. The imaging spectrometer

photographs X-ray images by "grazing" optics that deflect and focus X rays onto the CCD. Each X ray liberates a small cloud of electrons within the silicon chip. The number of electrons generated is proportional to the energy of the X ray. By measuring the signal generated where the X ray struck, the energy of the X ray and, in turn, the chemical element that produced the X ray, can be determined.

With this year's improved performance, X-ray CCDs are capable of measuring energies from 150 to 10,000 eV with an energy resolution of 150 eV. Spatial resolution is determined by the picture-element size of the CCD being used; for the 800-by-800-picture-element CCD used in this work, the spatial resolution is 15 μm .

James R. Janesick
168-222
(213) 354-7734



An X-ray spectrum was obtained by illuminating a CCD with X rays of different energies generated by fluorescing an unknown chemical composition with a source emitting radioactive alpha particles (Cm^{255}). The spectrum above plots the number of X-ray events as a function of energy. Each element that is excited emits an X ray of two possible energies (labeled $\text{K}\alpha$ and $\text{K}\beta$), shown for some elements as two distinct lines. The insert demonstrates the energy resolution that is obtainable ($\approx 155\text{eV}$) for lower X-ray energies by computer reduction of the X-ray events. Shown here is an aluminum line (1.48 keV).

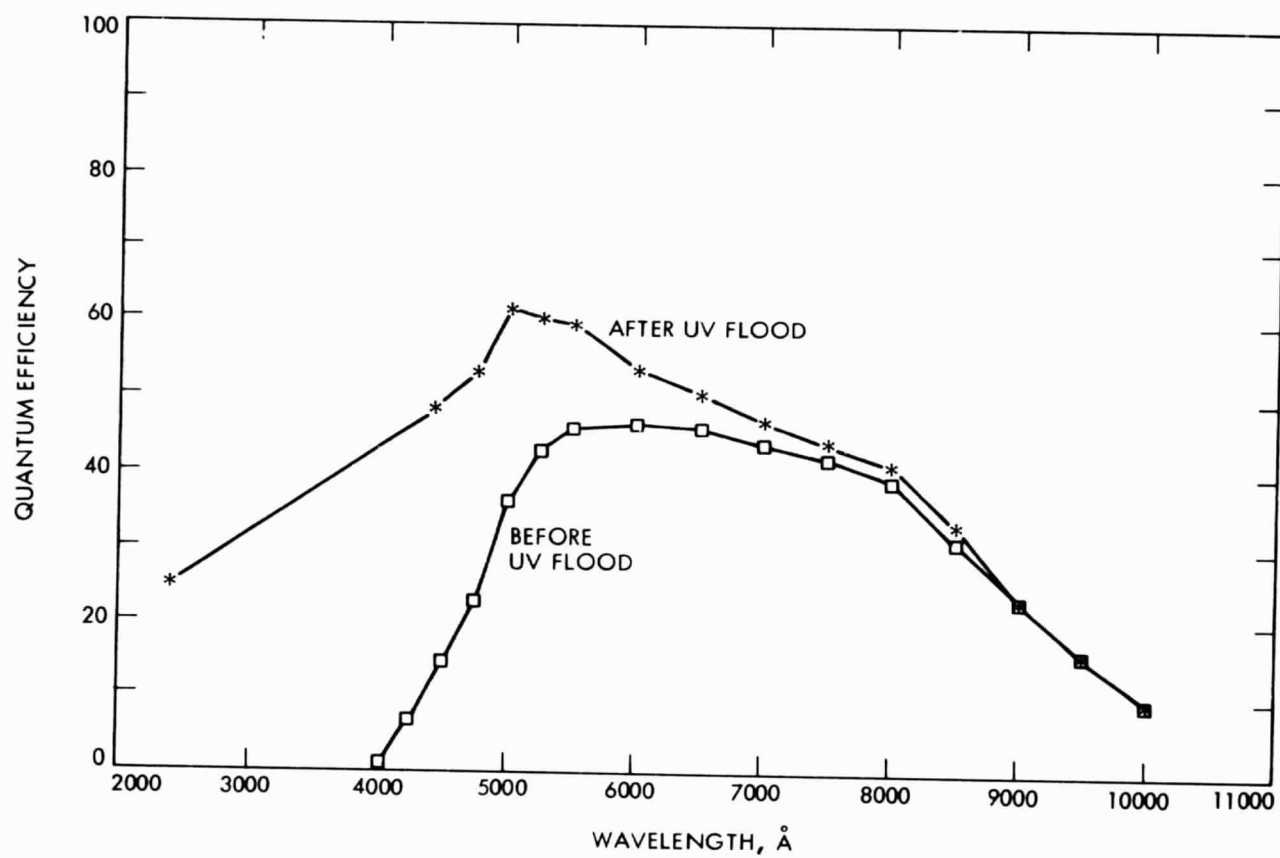
FAR-ULTRAVIOLET CCD IMAGER

A recent advance in far-ultraviolet space and science applications is the Far-Ultraviolet (UV) Charge-Coupled-Device (CCD) Imager. Charge-coupled devices have been in use for some time for imaging applications in the visible and near-infrared spectral ranges. Interest in extending the spectral response of these devices into the UV range has led to the use of phosphor coatings to convert the UV to a spectral range usable by the CCD. Although this process extends the spectral range of the CCD, the UV performance is relatively poor and nonuniform, with wavelength dependent on the spectral characteristics of the phosphor coating. Ideally, direct photo emission and collection within the CCD bulk silicon would yield the highest quantum efficiency. However, photon absorption in the UV wavelength range takes place within a depth of .01-0.1 μm in the silicon; hence, the surface layers play a decisive role and, typically, CCD devices have poor response below 4000 Å.

The improvement in extending the spectral response of the CCD well into the UV spectral range can be accomplished by simply exposing the sensor to a short ultraviolet light flood (2500 Å) before use. The attached figure shows the dramatic improvement in quantum efficiency using this procedure.

The proposed model for the physical processes involved shows that the quantum efficiency can be further improved by modification of the fabrication methods used to produce the CCD surface. (The results of initial tests on devices made with these alternate methods are very encouraging.) It is expected that the far-UV CCD imager ultimately will meet the high performance requirements associated with advanced UV astronomy observations.

James R. Janesick
168-222
(213) 354-7734



A comparative quantum-efficiency plot before and after a 2500 Å ultraviolet flood using an 800 x 800 3-phase backside-illuminated charge-coupled device.

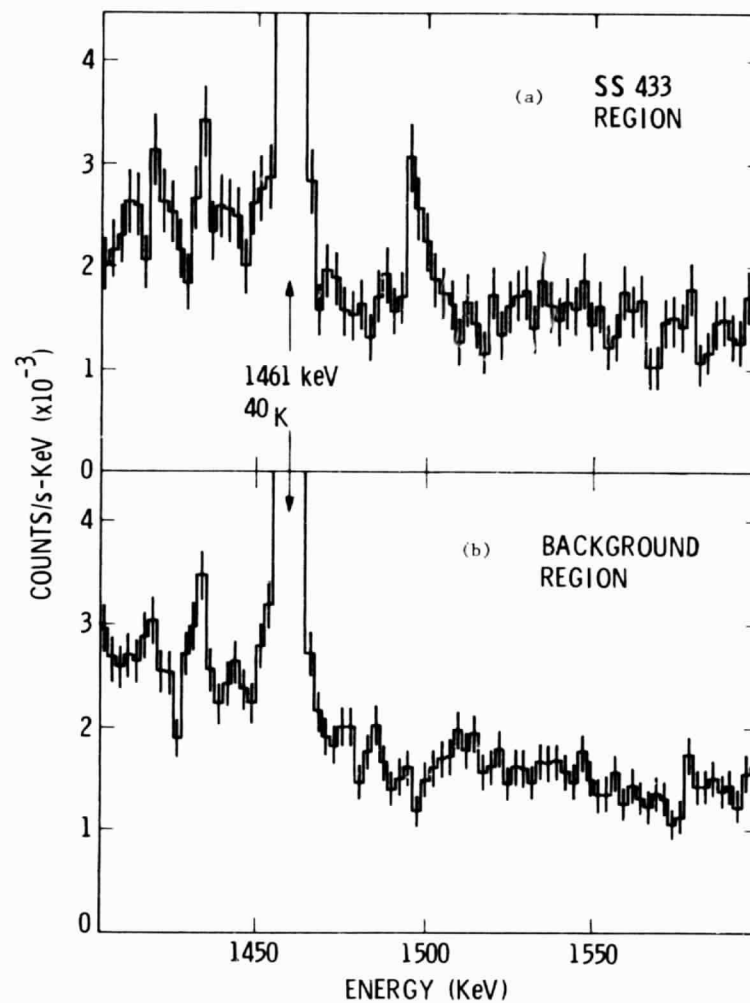
The high-resolution gamma-ray spectrometer aboard the HEAO 3 satellite has observed a strong gamma-ray line at an unexpected energy of 1.5 MeV, in the vicinity of a bizarre galactic object known as SS 433. Because of the direction of the gamma radiation, time variability which correlates with X-ray and radio variability from SS 433, and a modulation of the line energy in accordance with the pattern established for SS 433 in optical radiation, the gamma rays are identified with this source.

SS 433 is thought to be a recently formed neutron star (or black hole) around which violent high-energy processes are occurring. Previous observations of its optical radiation have indicated the presence of two oppositely directed jets of relativistic material being ejected from the central source at 26% the speed of light. The gamma rays seen by HEAO 3 are the first such observation of SS 433, and indicate that its gamma-ray luminosity is comparable to that of the strong annihilation radiation source at the center of our galaxy. The gamma rays may be from magnesium-24 in the jets. The energy of the magnesium-24 gamma-ray line is 1.369 MeV, but the jets' motion Doppler-shifts the energy seen by an Earth-bound observer. Radiation from the approaching jet is observed at 1.5 MeV. Radiation emitted at 1.369 MeV from the receding jet

should be shifted downward in energy to about 1.2 MeV, and there is evidence in the HEAO 3 data that this radiation is also seen, albeit more weakly. The gamma-ray line emission was strongest during a two-day flare in 1979. The same flare was detected simultaneously in X-rays below 2 keV by the Einstein Observatory, and in radio emission by the Very Large Array. A preliminary search for other nuclear lines has shown none as prominent as the 1.5-MeV feature.

If it is assumed that the line emission represents isotropic emission from SS 433 at a distance of 5.5 kpc, the gamma-ray line luminosity is 2×10^{37} erg/s. If the magnesium-24 identification is correct and the line is excited by collisions between magnesium-24 in the beam and other material surrounding the star, then the kinetic energy flow rate in the jets is $>10^{42}$ erg/s, a very large number and larger than most theoretical estimates. Finally, a search for nuclear line emission from other isotopes has revealed none of comparable intensity. In particular, if the material of the jets had a normal cosmic composition, we would expect lines from carbon-12 and oxygen-16 several times the intensity of the apparent magnesium-24 line. Thus the jets are apparently highly enriched in magnesium-24.

W. A. Mahoney
R. C. Lamb
J. C. Ling
G. R. Riegler
W. A. Wheaton
A. S. Jacobson
169-327
(213) 354-6606



Count rate spectra from (a) a 30-deg-wide region centered on SS 433, and from (b) a 78-deg-wide nearby background region. A strong background line at 1.46 MeV is evident in both spectra but the line at 1.5 MeV is seen only in the source spectrum.

RADIO ASTROMETRY AT THE MILLIARCSECOND LEVEL

The development of a catalogue of approximately 100 extragalactic radio sources having positional accuracy of ~ 0.005 arcseconds is one goal of the JPL/DSN radio reference-frame program. Such an accurate catalogue is required to provide a framework for the navigation of spacecraft to the planets.

The accuracy goals of the radio reference-frame program are currently set by the navigation requirements of the Galileo Project for reconstruction of the Galileo probe entry angle into the atmosphere of Jupiter. These navigation requirements have become sufficiently stringent that the reference stability and accuracy offered up to now by the stars in our own galaxy are no longer adequate. We need to reach out billions of light years to the quasars to obtain an "inertial" reference frame.

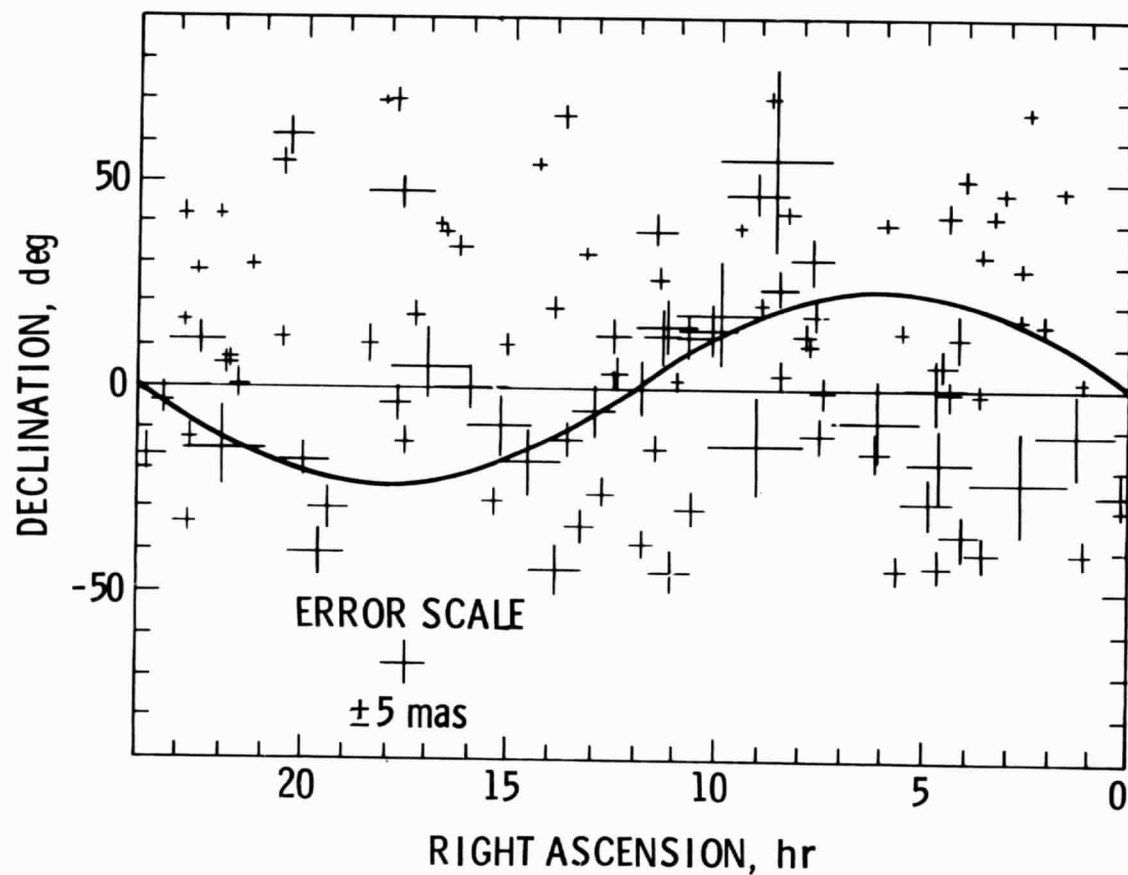
The positions of the radio sources are determined by Very Long Baseline Interferometry (VLBI) observations using the antennas of the NASA Deep Space Network on two intercontinental baselines--California-Spain and California-Australia. On each of the two baselines 16 to 24 h of data are usually obtained within a few days of each other, and since mid-1982 these pairs of observations have been made at approximately six-week intervals. From the data taken between 1978 and 1983, positions have been estimated for 120 sources well distributed in the declination range -45 to $+84$.

The formal uncertainties of these radio-source positions are 2 to 10 thousandths of an arcsecond (2 to 10 mas). As a check on the accuracy of our results we have compared them with measurements by another group which cover a smaller part of the sky, but taken at about the same time. For the 46 sources in common, the root mean square differences were found to be 4 mas in right ascension and 7 mas in declination. An ellipse of this angular size at Jupiter would have axes of 15 and 24 km. Although formally the required measurement precision exists, we are now concerned with determining the long-term stability and accuracy of the measurements.

In order for the radio reference frame to be consistent with the planetary ephemerides, the origin of right ascension of the radio-source catalogue must be related to the dynamical equinox. This is being achieved, although at a lower level of accuracy than for the source positions, by measuring, relative to the radio sources, the positions of spacecraft which are orbiting the planets Mars and Venus.

The reference frame defined by these measurements is the most accurate available. It covers such a large part of the sky that the positions will form a significant component of the next fundamental catalogue to be presented for use by the entire astronomical community.

A. E. Niell	R. N. Treuhaft
J. L. Fanelow	K. S. Wallace
B. J. Thomas	264-781
O. J. Sovers	(213) 354-4633
K. M. Liewer	



This diagram represents the celestial sphere. It illustrates the distribution in the sky of sources from the radio reference frame. The axes are right ascension and declination, and the wavy line is the ecliptic, along which most spacecraft will fly. The size of the uncertainty in position for each source is given by a cross. Note the difference in scale by a factor of about 4 million between the relative positions and the uncertainties.

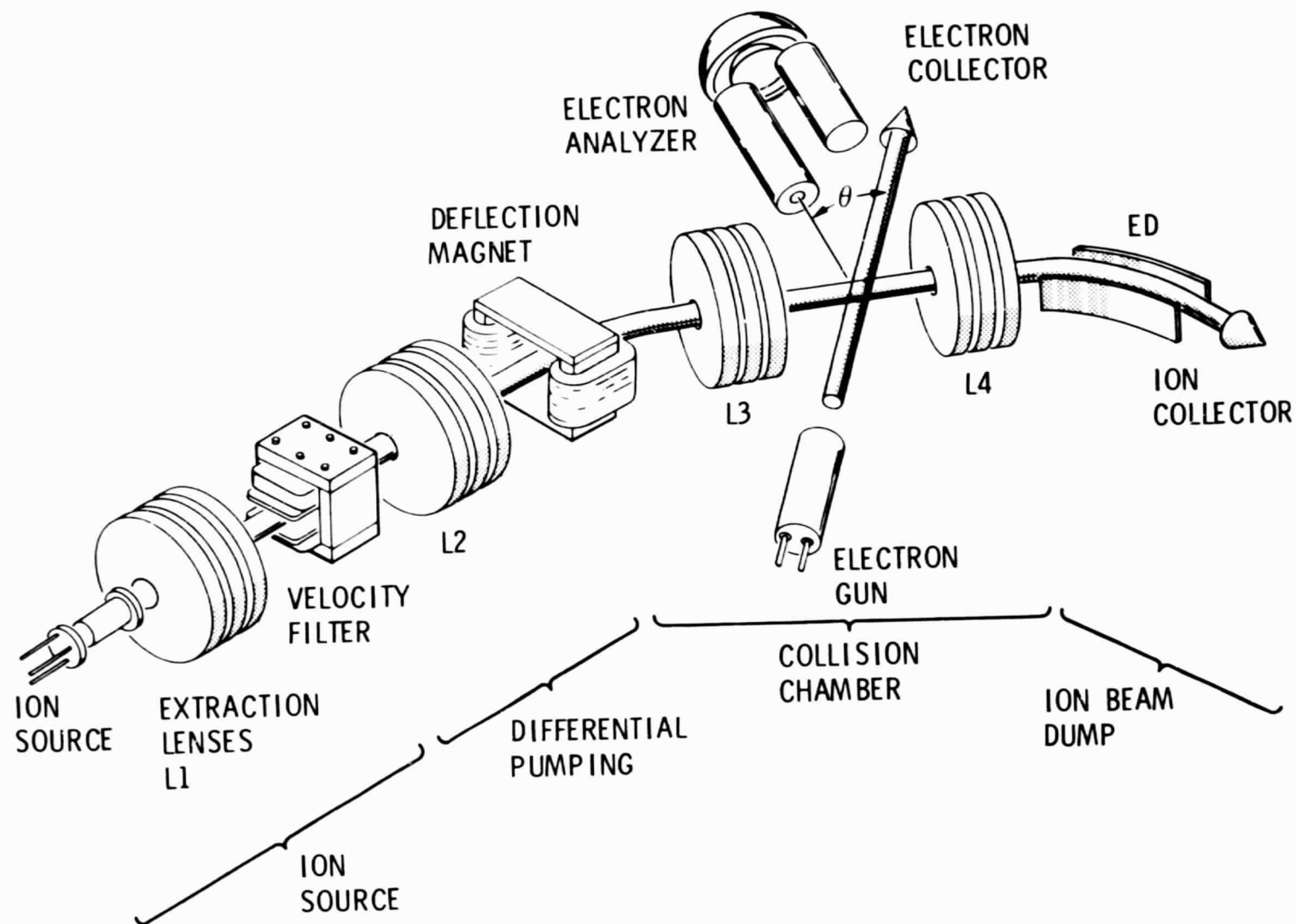
Electron-ion collision experiments carried out thus far by various research groups throughout the world have involved detection of, as the collision product, a photon (resulting from line excitations or dielectronic recombinations (DR)), an ion (from ionization, recombination, or DR), or a neutral particle (from recombination or DR). Only recently, through efforts at JPL, has detection of the scattered electron been added to this repertoire of techniques. The use of electron energy-loss methods in electron-ion collisions adds a level of versatility not possible before. For example, one may study angular distributions, intersystem transitions, resonances, and coincidences. Measured cross sections are also free of cascade contributions, and by proper choice of instrumental geometry one may detect electrons close to threshold (having very low kinetic energies) where electron-ion collision cross sections are at a maximum.

By use of a newly designed crossed electron-ion beam apparatus, measurements have been carried out at JPL in the $e\text{-Zn}^+$ and $e\text{-Cd}^+$ systems to demonstrate the energy-loss method. Spectra and angular distributions

were measured in Zn^+ and Cd^+ , and comparisons to theory and previous measurements (using photon-detection techniques) were made. Two further exciting developments in electron-ion collisions have been carried out by other research groups--the measurement of dielectronic recombination in several ions (Mg^+ , B^{2+} , C^{3+}) and the study of excitation-autoionization in multiply-charged ions.

The JPL studies have an immediate bearing on the study of high electron-temperature plasmas. Cross-section data and the study of new phenomena are required for the understanding of stellar objects such as coronae, chromospheres, supernovae, and quasars, and for the understanding of shock-heated portions of the interstellar medium and the Io-Jupiter torus. Somewhat closer to home, the development of fusion reactors such as the Joint European Torus and the Princeton TFTR requires electron temperatures of the order of 10^8 K (10 keV) for ignition to occur. At these stellar-like temperatures most ions exist in highly stripped charge states, and collisions are almost entirely between electrons and ions.

Ara Chutjian
183-601
(213) 354-7012



Schematic diagram of the JPL crossed electron-ion beam apparatus. Three-element lenses are indicated by L1, L2, L3, and L4, and the electrostatic deflector by ED. The function of the deflection magnet is to prevent ionizing photons and neutral atoms from the ion source from reaching the collision chamber. The electron scattering angle θ is shown. Length of apparatus from ion source to ion collector is 230 cm.

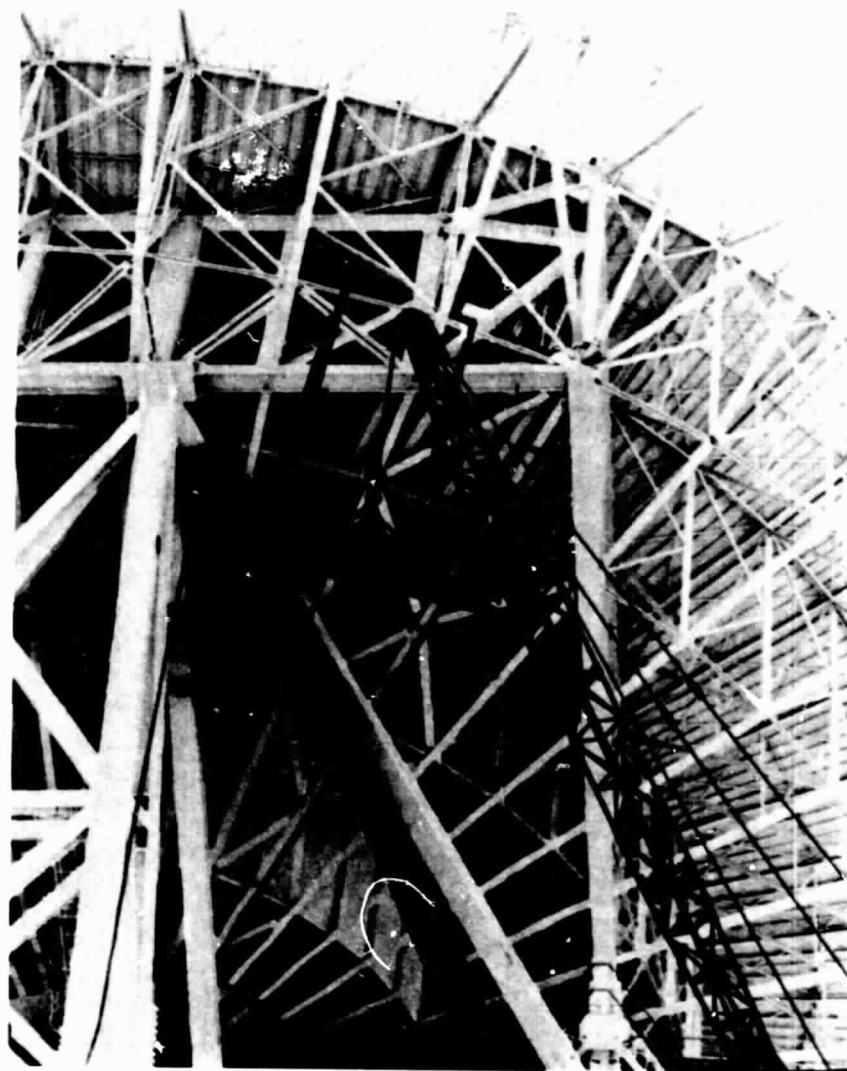
Upgrading the physical structure of the Deep Space Network (DSN) antennas increases their efficiencies and collecting area, thereby increasing the data rates obtainable and the fraction of time during which commitments can be met in severe weather. A number of significant improvements, jointly accomplished by structural, mechanical, and microwave engineers, were examined and tested during the past year. The goal is to increase the gain by about 1.9 dB at X-band frequency (8.45 GHz) for the three 64-m-diameter DSN antennas. This gain increase is part of the 64-m Antenna Rehabilitation and Upgrade Project, which, among other things, increases the diameters of the antennas to 70 m.

Supported by the large-antenna manufacturing industry, JPL is expanding the present state of the art in fabricating low-cost, precise, lightweight, mold-shaped surface panels with a less than 0.005-in. (125- μ m) tolerance. Presently, the 64-m-diameter antenna panels have an approximately 0.040-in. (1.0-mm) surface tolerance, which limits the aperture efficiency

to slightly more than 50%. The upgraded 70-m efficiency is expected to be around 67%. Initial experiments have shown that the surface contour is strongly dependent on the bond-curing temperature, the vacuum pattern, and the surface roughness of the shaping and bonding fixtures.

The new development of an automatic subreflector that focuses in the gravity-axis direction (y-axis) of the large antenna is one of several major accomplishments aimed at improving the large-antenna tipping structure, pointing precision, and reflector surface alignment at different tracking angles. The new automatic focusing feature recovers close to 0.6 dB gain otherwise lost when the antenna is at zenith. Another major accomplishment is the assessment of the potential for removing undesirable surface bumps near the elevation bearing and at the outer edges that result in an additional 50% reduction in the reflector surface tolerance at all tilt angles. Analysis of data from field observation showed encouraging agreements with the theoretical analysis.

F. L. Lansing
511-203
(213) 577-9797



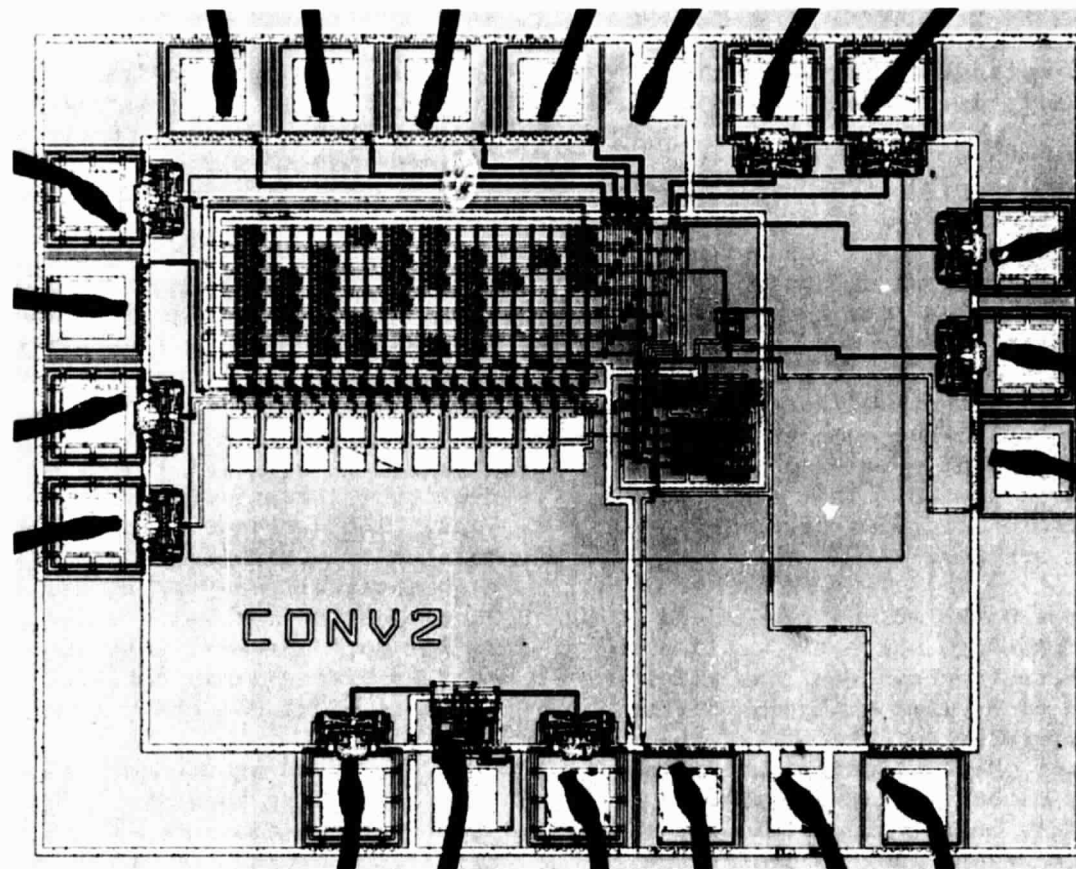
ORIGINAL PAGE IS
OF POOR QUALITY

VLSI MULTICODE CONVOLUTIONAL ENCODER CHIP

Many of the benefits of Very Large Scale Integration (VLSI) are well known. These include small size, low power, and high speed. One additional advantage is that some very complex systems can be implemented in VLSI that cannot be easily built up out of discrete parts or standard integrated circuits. These include systems consisting of many subcells, each of which must communicate with many others. The encoders and decoders that are used for error correction by the Deep Space Network are examples of such devices. VLSI offers the opportunity for increasing error-correction capability by allowing the implementation of more complex and more flexible coding

schemes. These codes can eventually reduce the required transmitter power on a spacecraft and increase the data throughput.

The first demonstration of this concept at JPL is the multicode convolution encoder chip. Although a convolutional encoder is a simple device, it does require a large number of interconnections. The chip is capable of encoding any one of four convolutional codes. It is only 2400 x 1900 μm and will handle a data rate of 1.5 million bits/s. The chip has been tested successfully and is available for generating test sequences in the laboratory.



ORIGINAL PAGE IS
OF POOR QUALITY

2.5 BITS/DETECTED PHOTON DEMONSTRATION

A demonstration program is underway at JPL to prove the viability of using for space communications optical signals with a power efficiency of 2.5 bits/detected photon. The demonstration of such a system will pave the way toward optical communications systems substantially more efficient than those previously used.

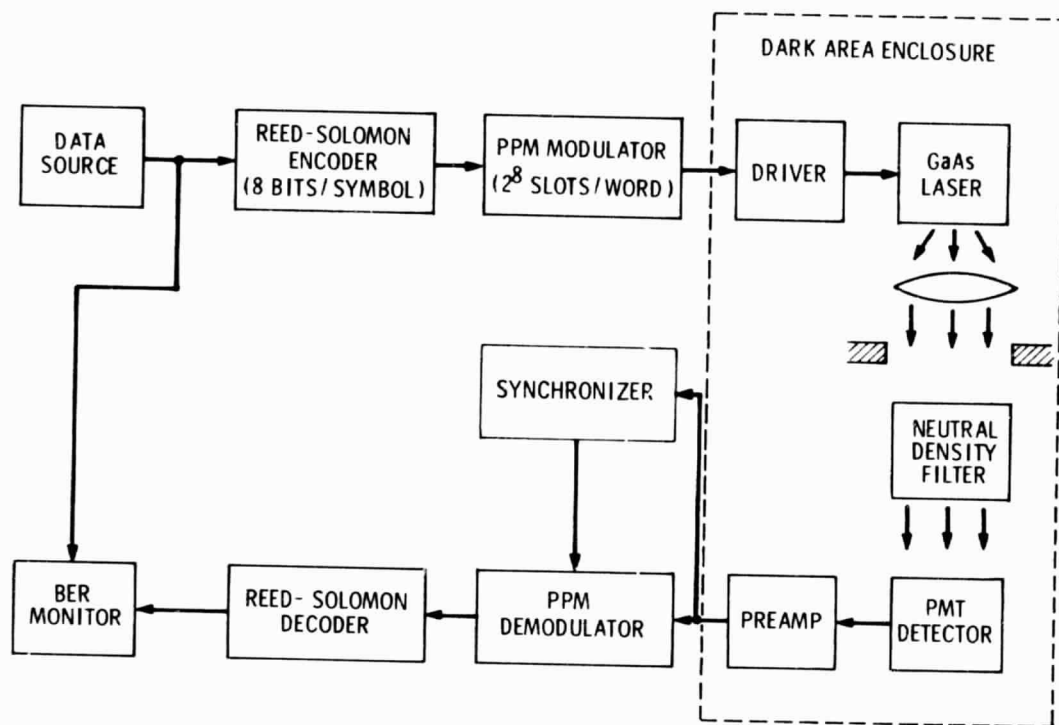
Achieving a high-power utilization efficiency is one of the necessary ingredients for viable space-to-space optical communications systems. For optical communications employing heterodyne detection techniques, the "Quantum Limit" gives rise to a communications-theoretic "Shannon Limit" of one natural unit of information (1.44 bits) per detected photon. The significance of this limit is that no (heterodyne) communication system, no matter how complex, can ever sustain the transmission of more than 1.44 bits of information per received photon. This limit was believed by many to apply to all types of optical-communications detection systems.

In the course of our work, it was recognized that the quantum limit, although correctly applied to the area of heterodyne detection systems, was being inappropriately extended to systems employing direct photon detection. By carefully accounting for the quantum radiation effects, one can derive an equivalent "Shannon Limit" for direct detection systems. This limit depends strongly on the specific communications channel characteristics, such as background light intensity, photodetector dark-current intensity and detector thermal noise, as well as the quantum-mechanical uncertainty principle. However, under reasonably favorable, but not unrealistic, conditions, this limit can be as large as 30 bits/photon.

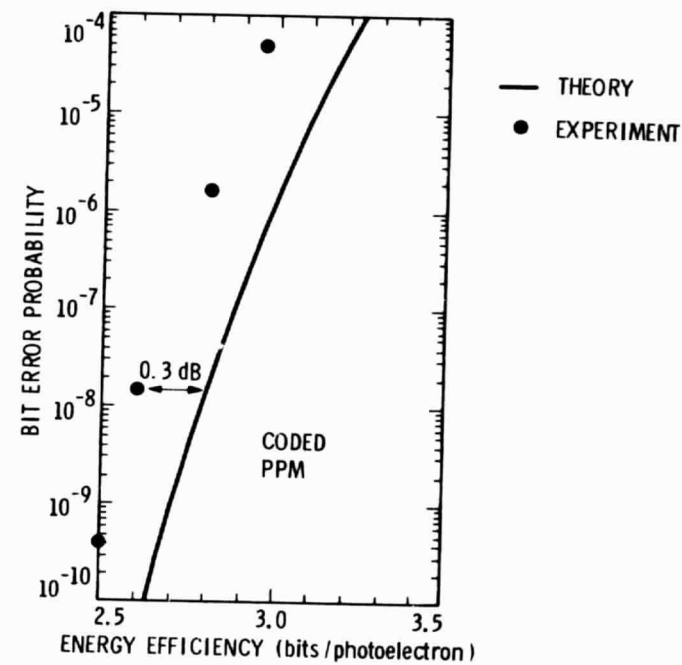
To validate the new theory, a research program was initiated to demonstrate, in the laboratory, a direct-detection optical-communications system capable of transferring 2.5 bits of information per detected photon. This goal was established because it would result in an actually implemented system whose performance comfortably exceeded the heterodyne "Shannon Limit" without placing unnecessarily difficult requirements on the research staff.

The heart of the optical portion of the system is a gallium arsenide semiconductor injection laser and a direct-detection photomultiplier tube (PMT). The GaAs laser diode is a single spatial mode device operating at $.85\text{ }\mu\text{m}$ and has the reliability and the durability characteristic of solid-state devices. The light emitted from the laser is passed through some elementary optics, followed by 70-100 dB of neutral density filters (attenuators), which simulate space loss. The attenuated optical signal is then applied to a photomultiplier tube (PMT) detector that has a high internal gain (10^6), a quantum efficiency in excess of 20% and, with moderate cooling, an extremely low dark current. All of the optical components must be placed in an extremely dark enclosure, in order to eliminate stray laboratory light.

Surrounding the optical components are modulation and coding hardware. The laser diode is driven by a 256 time-slot/word-pulse position modulator (PPM) that decides, based on an 8-bit input word, in which slot the pulse should be placed and then provides a current pulse during that slot to turn on the laser. The inverse of this process is applied to the PMT output to recreate the 8-bit word. The synchronization signal needed to operate the demodulator is



Block diagram of 2.5 bits/detected photon demonstration.



Performance curve of 2.5 bits/detected photon system.

also derived from the detected optical signal. To improve the performance of the system, an 8-bit Reed-Solomon encoder/decoder simulator is then used to surround the PPM portion of the system.

Such codes are well suited for this application because of their ability to correct erasures, which are the dominant error sources in the system. (In order to have high power efficiency, one would like to use low light intensities. However, the statistical nature of the light-generation and -detection processes results in a substantial probability of no

photons being detected. When this happens, a pulse erasure occurs.) The data streams supplied to the encoders and delivered from the decoder are then compared for an overall bit-error-rate measurement.

The goal of achieving 2.5 bits/detected photon was met and even slightly exceeded (about 3 bits/detected photons is obtainable for a bit-error probability of $\sim 10^{-4}$). The system synchronization operated down to average light intensities of 1/3 photon/pulse with less than 0.2 dB of noisy reference loss.

J. Lesh
J. Katz
238-420
(213) 354-2766

DATA ACQUISITION AND COMMAND OF PIONEER 8 FROM AN UNATTENDED STATION

The unattended Goldstone Deep Space Station used to communicate with the Pioneer 8 spacecraft is being successfully controlled from a JPL facility more than 100 miles away. Pioneer 8, launched in December 1967, is being tracked and commanded from the Network Operations Control Center (NOCC) at JPL, to demonstrate the viability and long-term reliability of operating a deep-space tracking station unattended. With the primary scientific purposes of Pioneer 8 completed, the spacecraft is being used to exercise and refine automated station procedures at the Venus Site Deep Space Station (DSS-13).

Because Pioneer 8 is close to the receiver threshold capabilities of the Venus Site 26-m antenna, it has been necessary to resort to a Fast Fourier Transform (FFT) spectrum-analysis technique to acquire the downlink. This analytic approach has proven to be as effective as conventional slow-signal searching methods.

Pointing of the antenna, tuning in of the spacecraft signal, demodulation of telemetry data, activation of the transmitter, acquiring of the spacecraft uplink, and encoding and verification of receipt of commands for the spacecraft are all coordinated by a single operator at NOCC. Because of the rich store of operator help and system operational reference displays at NOCC, it has been possible for an individual

inexperienced in spacecraft communication principles to rapidly acquire the necessary skills to control the unattended station.

Information for proper antenna pointing and spacecraft tuning are obtained from the JPL General Purpose Computer Facility for use by the remote station controller working from the NOCC. The NOCC is linked by high-speed data line to the local station controller at the Venus Site where all significant operational events are recorded on a log disk. The local station controller, communicating through the Star Switch controller, activates the various unattended station subsystems as shown. Outgoing telemetry data from the subcarrier demodulator is microwaved to Echo Site (DSS-12), where it is formatted into computer-printable telemetry for transmission by separate high-speed data line back to NOCC. Commands for Pioneer 8, carefully formulated and verified, are transmitted over an independent high-speed data line through the communications monitor and formatter (CMF), command processor assembly (CPA), and exciter, for transmission to the spacecraft.

It is expected that the experience being gained will be of significant value in meeting future Deep Space Station mission-support objectives with dramatic cost savings through the substantial reduction of station support personnel.

Conrad Foster
258-528
(213) 354-5070

MICROWAVE HOLOGRAPHIC SURFACE MEASUREMENT OF THE TIDBINBILLA 64-m ANTENNA

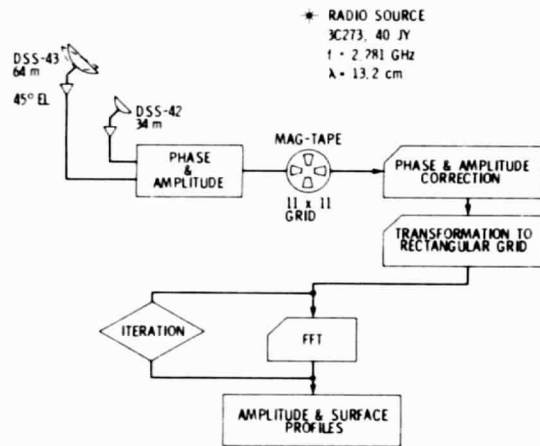
The accuracy needed in the measurement and setting of large radio antennas is at the limit of conventional survey methods. A new method, however, known as the holography technique, uses measurements of the far-field pattern of an antenna to deduce the complex illumination function across the antenna aperture. Surface deviations are manifested as phase fluctuations in the illumination function.

Initial measurements using the holography technique were successfully carried out during 1983 at the Tidbinbilla, Australia, Deep Space Communications Complex. The surface accuracy of the 64-m antenna was measured with a precision of better than 1 mm (relative to an ideal parabolic surface). The measurements were made using the real-time, two-element (34-m and 64-m) interferometer at Tidbinbilla. The 34-m-antenna element of this interferometer was used to provide the phase reference for the holography measurement during the time that the far-field pattern of the 64-m antenna was measured. The source was tracked symmetrically about transit, resulting in an elevation-angle range of about 40 to 55 deg for various sets of measurements. The sampling grid consisted of 11 by 11 points at 5.7-arcminute spacing. The measurement

schematic is shown in part A of the accompanying figure, and the reflector is shown in part B.

The sampled complex far-field pattern was Fourier-transformed to produce the complex antenna illumination function across the antenna aperture. Contour maps of the phase and amplitude functions from the first measurement grid are shown in parts C and D of the figure. The agreement of these results with the contour maps from the second measurement (at a slightly different elevation) are very good, there being differences only at or below the 1-mm level in the phase map. Although the resolution of this initial experiment is fairly coarse, several features emerge in these maps. A general surface distortion of an amplitude of about 3 mm appears to be present in the lower part of the reflector, as shown in D. Additionally, some distortion is present at about the 5-mm level in a region near the edge of the reflector. The distortion over most of the surface is below a level of about 1 mm and is noticeably less over the central region of the reflector. The unweighted root mean square surface deviation from this measurement is about 1.8 mm. Clear evidence exists in the amplitude plot for shadowing due to the subreflector quadripod support legs.

HOLOGRAPHIC MEASUREMENT PROCESS FOR TIDBINBILLA 64 m ANTENNA

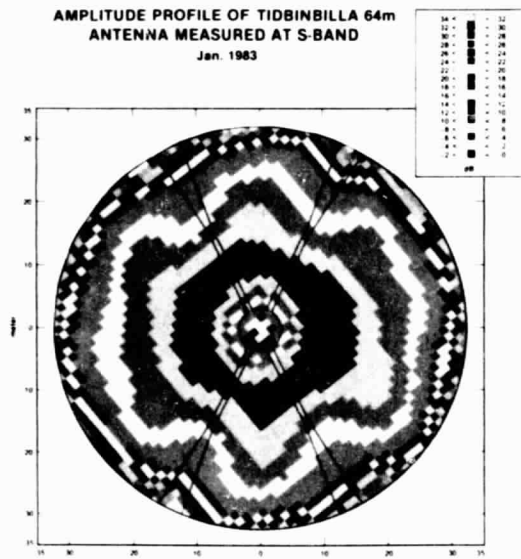


A



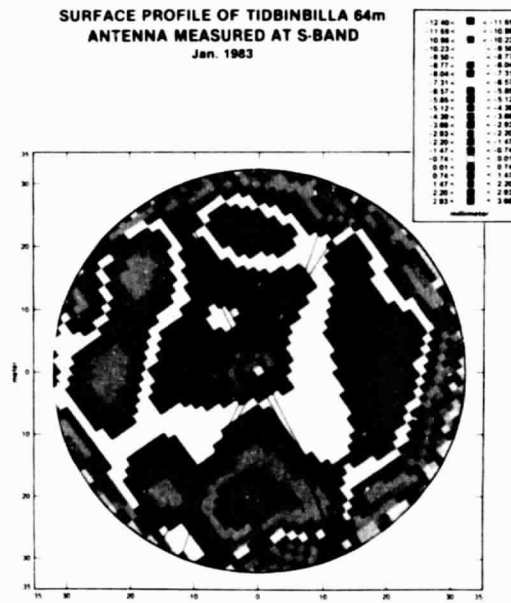
B

AMPLITUDE PROFILE OF TIDBINBILLA 64m
ANTENNA MEASURED AT S-BAND
Jan. 1983



C

SURFACE PROFILE OF TIDBINBILLA 64m
ANTENNA MEASURED AT S-BAND
Jan. 1983



D

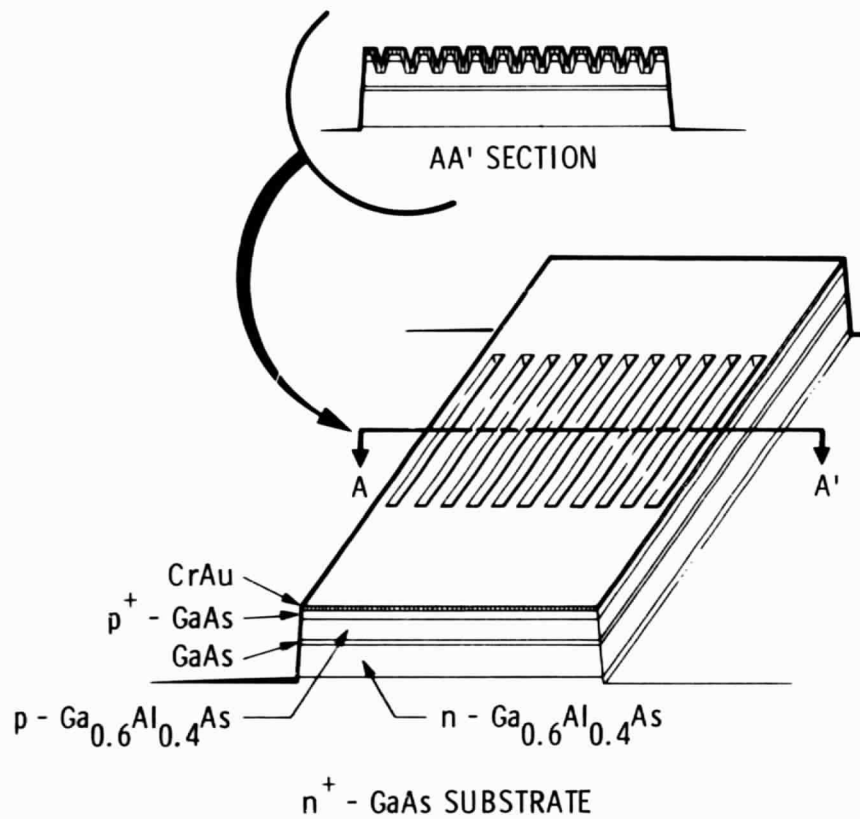
Surface diagnosis of large reflector antenna using microwave holographic metrology.

DIFFRACTION-COUPLED SEMICONDUCTOR LASER ARRAYS

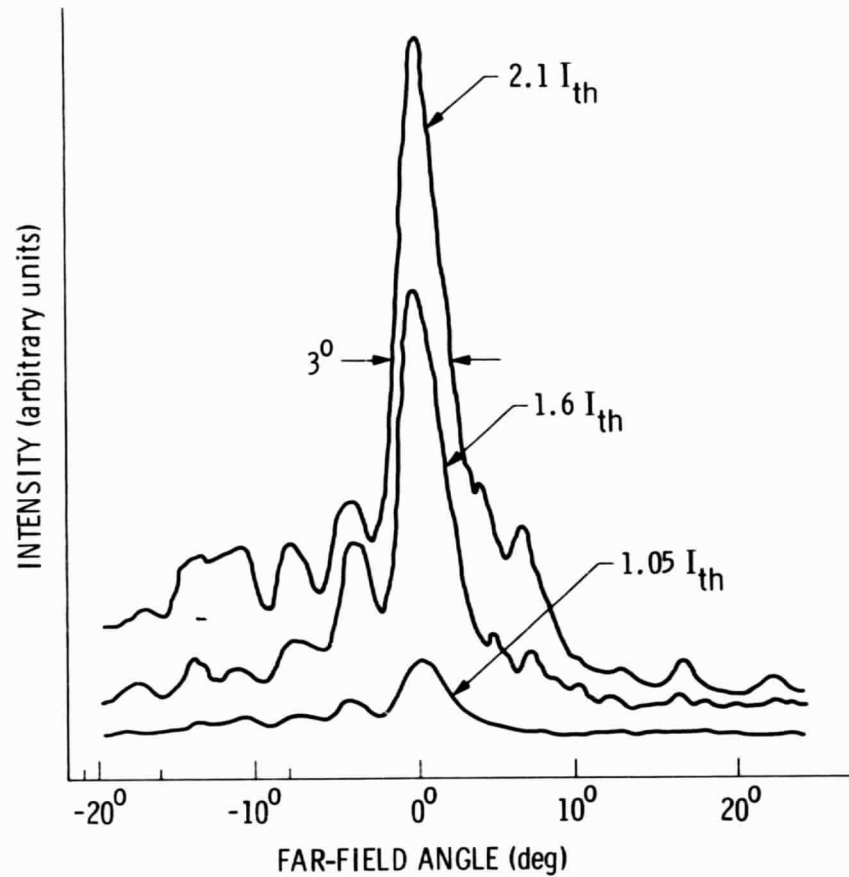
One of the necessary key ingredients for viable space-to-space optical communications systems is a high-brightness, single-mode laser emitter. Gallium aluminum arsenide semiconductor lasers are preferred mainly because of their high efficiency and reliability, which are characteristic of solid-state devices. Their one major disadvantage is that the optical power is limited to ~ 10 mW.

However, it appears that single-spatial-mode devices with power outputs of ~ 1 W can be achieved by coherently combining a number of GaAs lasers in what effectively amounts to a phased array. One way to accomplish this is by fabricating several lasers on a

common substrate in close proximity to each other. In this configuration, each laser is uncoupled from its neighbors along a part of the total resonator length, but all the lasers share a common section of the resonator in the region near the mirrors. Light from the uncoupled (waveguide) section of the laser propagates in the common resonator section, where it diffracts. Upon reflection from the resonator mirror, some of the light is reflected back into the waveguide section, as is the case in any laser. However, fractions of this field are also reflected back into the adjacent lasers, thus constituting the dominant coupling mechanism. Peak output powers of up to 1.1 W were obtained in low-duty-cycle operations.



Diffraction-coupled laser array.



Diffraction-coupled array far-field beam pattern.

PROPERTIES OF RESIDUES FROM SUBLIMED DIRTY ICE: COMET AND MARS APPLICATIONS

The properties of freeze-dried dilute dispersions of dust in water are of considerable interest in studies of comet nucleus mantles and the polar regions of Mars. In both environments the formation of a "rind" residue due to the sublimation of water ice containing various amounts of clay may be an important process.

We have attempted to simulate on the surface of ice-dust mixtures the development of ice-poor regoliths as the result of preferential ice sublimation. Such phenomena may occur as the result of seasonal or long-term sublimation of dirty ice caps on Mars and as the result of sublimation of cometary ices.

We have studied the development and disruption of this rind and, in the case of comets, its subsequent levitation by water-vapor flow. These simulations were achieved by a variety of experimental approaches, including the simultaneous spraying of 100- μ m water droplets and 0.1- μ m montmorillonite grains into liquid nitrogen and the fine spraying of various concentrations (10%, 1%, and 0.1%) of the same silicate in liquid water into liquid nitrogen. Sublimation of the nitrogen and the water produced ice-poor rinds which were disrupted and ultimately levitated by subsequent ice sublimation. In those experiments, which we believe to be the closest to a realistic simulation of natural conditions, the most striking result was the development of large cohesive agglomerates of individual clay particles, and in some cases a continuous cohesive crust. Scanning electron microscope (SEM) observations reveal that the material formed by

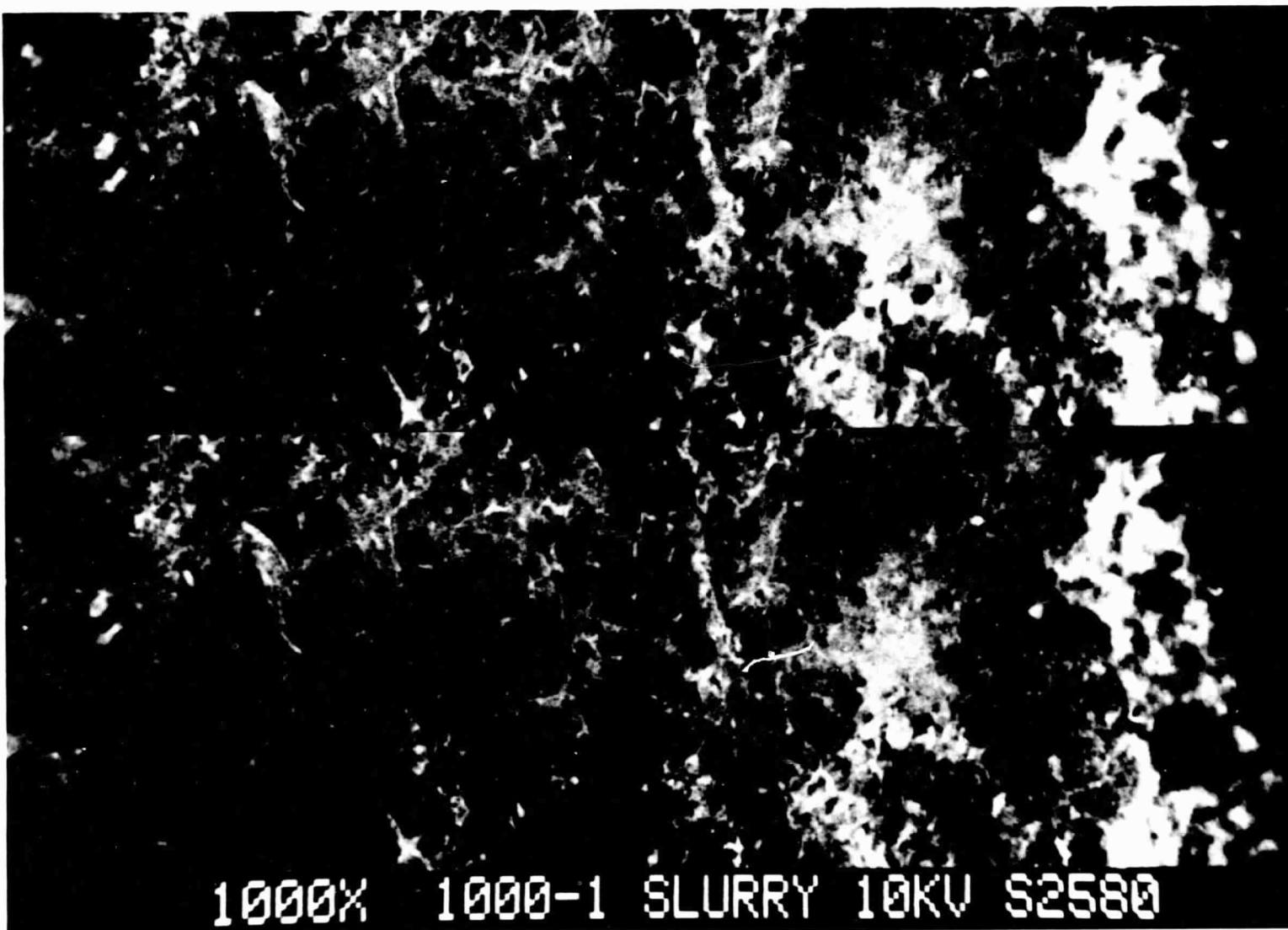
freeze-drying the 0.1% solution does not retain the original spherical shape of the sprayed droplets; instead it consists of a filamentary network, as shown in the SEM stereo photographs.

The results of the control experiments show that formation of these agglomerates or crusts does not require the occurrence of "trivial" cementation processes involving the leaching of salt and their subsequent redeposition between soil particles. Instead, strongly cohesive and even elastic structures can apparently be made simply as the result of the flow of cold water vapor around individual clay grains and the subsequent assemblage of these grains into tough, fibrous structures. One, as yet unproven, hypothesis is that the flow of water vapor can cause enough electrical charging to cause the clay particles to assemble into such filamentary structures. Once assembled, however, retention of charge or water does not appear necessary to the survival of these agglomerates, since they were examined at length under the SEM and yet persisted as tough and pliable structures.

These results suggest that such structures might be assembled on Mars during ice-cap sublimation. This may explain the origin of the sand-like material comprising the extensive Martian circumpolar dune fields.

On comets these processes could play a major role in creating the grain size distribution of silicates launched from the comets and observed in their tails.

R. Stephen Saunders
J. Stephens
B. Banerdt
183-501
(213) 354-3372



ORIGINAL PAGE IS
OF POOR QUALITY

SEM stereo photo showing filamentary network resulting from the freeze-drying of a 100- μ m droplet of 0.1%-dispersion montmorillonite.

PALOMAR ASTEROID SEARCH PROGRAM

The JPL Asteroid Search Program yielded an Apollo, 1983 LC, an Earth-crossing Amor, 1982 XB, an Amor, 1983 LB, a deep Mars-crosser, 1983 PA, and several inner-belt asteroids. These asteroids were discovered with the 0.46-m and the 1.22-m Schmidt telescopes at Palomar Observatory from December 1982 to August 1983. A crucial recovery observation of the unusual Amor, 1982 YA, was also obtained with the 1.22-m Schmidt.

1982 XB was discovered on the night of 13-14 December with the 0.46-m Schmidt, which detected the asteroid's unusual prograde motion of a rapid 4 deg per day. Other observatories were immediately alerted, and within only 2 days after the initial discovery, the asteroid had been observed photometrically at visual and infrared wavelengths by four different observatories. 1982 XB was found to be an Earth-crossing Amor, and on its discovery apparition made an exceptionally close approach to Earth (0.03 AU). The close cooperation of these astronomers in observing this asteroid made 1982 XB the most fully investigated near-Earth asteroid during its discovery apparition. 1982 XB was characterized by various physical observations as a 300-m-diameter silicaceous body with a rotational period of 9 h. Mission analysis shows 1982 XB to be one of the four best mission candidates in terms of delta-V to rendezvous. The low delta-V is primarily due to its low orbital inclination (3.9 deg) and its exceptionally close perihelion distance (1.01 AU).

Apollo 1983 LC and Amor 1983 LB were discovered on a single plate taken with the 1.22-m Schmidt on the

night of 12-13 June. The discovery of two near-Earth asteroids on the same plate, only 3 deg apart, is unprecedented. 1983 LC crosses the Earth's orbit to within 0.77 AU of the Sun at perihelion, with a low inclination of 1.5 deg. Its orbit is quite eccentric, however, carrying it to an aphelion distance of 4.5 AU. 1983 LC passed within 9.5 million km of Earth on 7 July as it approached perihelion, moving about 8 deg per day. 1983 LB has a highly inclined orbit ($i = 25.0$ deg) and reaches perihelion at a distance of 1.19 AU from the Sun. At discovery, its apparent motion was 1.4 deg per day, 50% faster than 1983 LC.

The deep Mars-crosser, 1983 PA, was discovered 7-8 August with the 0.46-m Palomar Schmidt. It is a bright [$B(1,0)=14$], high-inclination object which has escaped detection until now because of a nearly 10:3 commensurability between its orbital period and that of Earth.

The successful recovery of 1982 YA, an Amor asteroid discovered in France, was accomplished using the 1.22-m Palomar Schmidt. Only two observations from 21 and 23 December 1982 were available from the discoverer, and hence no definitive orbit could be computed. Recovery plates were taken in early January, two weeks following discovery, but the asteroid was not detected until recently, when correspondence and prints were exchanged with the discoverer, F. Dossin. With more information and details of the discovery, a careful reexamination of the recovery plates revealed the elusive image of this near-Earth asteroid, which otherwise would have been lost.

Eleanor Helin
Scott Dunbar
183-501
(213) 354-4606



Photograph of 1982 XB exposed on a IIIa-F emulsion with the 1.22-m Palomar Schmidt, 3 weeks after its discovery with the 0.46-m Schmidt and 2 weeks after its closest approach to Earth at a distance of 4.8 million km.



Discovery photograph of 1983 LC, from a IIIa-J plate taken on the 1.22-m Palomar Schmidt. The faint trail in the center consists of two components because the exposure was *gated* (40 min open, 15 min closed, 10 min open) to reveal the direction of motion without the necessity of taking a pair of plates.

ORIGINAL PROCESS
OF POOR QUALITY

RADAR DETECTION OF COMETS

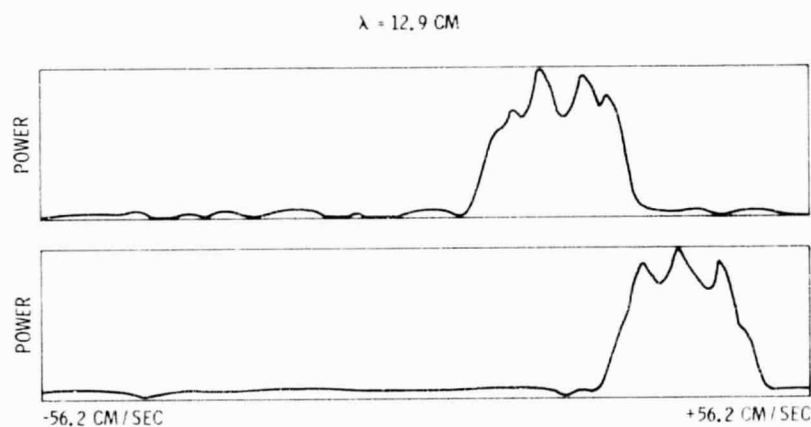
The discovery of two new comets that approached Earth closely enough for the details of their nuclei to be studied by radar astronomy techniques caused considerable excitement among the scientists at JPL and elsewhere who specialize in cometary studies. Normally, the glow of ionized gasses and light scattered by dust particles would completely obscure nuclei details even if they could be resolved by Earth-based optical telescopes. Radar provides new ways to achieve resolution based on precise measurements of the energy in the Doppler-shifted spectra and by resolving the object in time delay. In the case of the comets IRAS-Araki-Alcock (IAA) and Sugano-Saizusa-Fujikawa (SSF), only Doppler spectroscopy was used. Comet IAA arrived at closest approach on May 11, 1983. Two short periods of observation were scheduled for May 11 and May 14. Three days of radar observation were scheduled just prior to the time of closest approach of SSF. Comet IAA yielded a series of very strong spectra while no echoes were seen in the SSF spectra. Analysis has been concentrated on the IAA comet.

Comet IAA was observed near its closest approach and again on May 14, 1983, at which time its distance had about doubled. Distance is the most important parameter for radar detection, as it comes into the detectability equation as the inverse fourth power. Thus, we expected the comet to be about 16 times weaker for the second observation period. We compensated

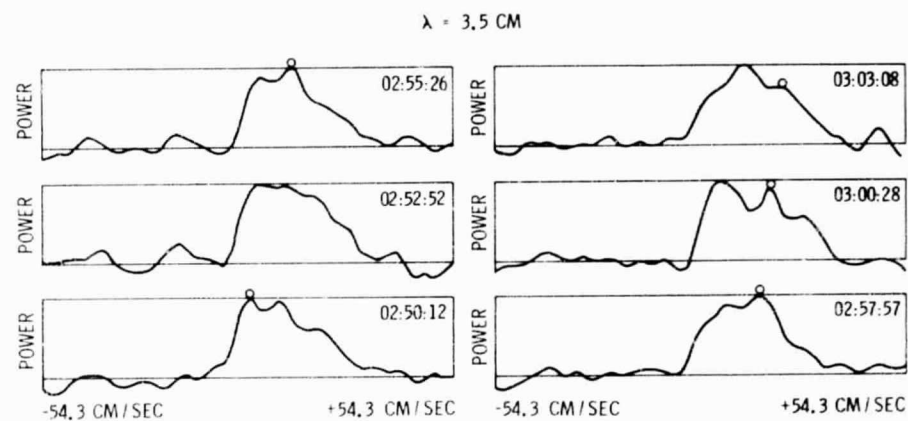
partially for this, however, by using the more sensitive X-Band radar system for the second observation period. This radar is roughly four times more sensitive than the S-Band radar, primarily due to its shorter wavelength, which yields a greater antenna gain from the 64-m-diameter antenna.

The experiments were carried out by transmitting a 400-kW continuous-wave monochromatic signal toward the comet until the entire volume of space between Earth and the comet was filled by either signal or echo. Then the transmitter was turned off, so that the receiver could catch the incoming echoes. During the first observation period, this duration was only 30 s, making this comet the closest natural object ever observed by radar astronomy other than the Moon. The radar echo was immediately observed in the JPL 65,000-channel digital RFI spectrum analyzer, which was able to determine the frequency of the echoes accurately. The transmitter frequency was then shifted to bring the echo within the observing range of our high-resolution radar spectrum analyzer. The resulting spectra were so strong that the noise was barely discernible on the real-time display.

Most of our analytic effort has been devoted to determining the spin-axis direction, the rotation rate, and the size of the nucleus. These quantities are all interrelated and influence the width of the



A pair of typical S-Band spectra; note the complex structure in the spectrograms.



A longer sequence of spectra from the second observing period, during which the polarization properties were measured to determine the major mechanisms active in backscattering the echoes. The polarization ratio and the spectral shape indicate that the surface is very rough on scale sizes much larger than the wavelength and less rough on scale sizes near the size of the wavelength. Complex multiple scattering similar to that observed for the Galilean moons is ruled out.

spectra. The rotation rate may be estimated from the motion of features in the spectra. Currently, two theories are under study. The first is the possibility that the comet rotates slowly (less than once a day), in which case its size would be a few km in radius and its surface reflection properties little different from many asteroids that we have observed. The second theory is that a rapid rotation rate (roughly 1.6 h) is indicated by the motion of features

in the spectra. This rapid rate requires a small radius to match the spectral widths. The small radius implies a highly reflective surface to match the power observed in the echoes. A possible model that can explain this observation requires a swarm of loosely orbiting particles near the comet. The large physical cross section of the swarm could provide the apparent high reflectivity without increasing the spectral widths. Both hypotheses are under further study.

R. Jurgens
R. Goldstein
238-420
(213) 354-4974

II. Information Systems and Space Technology Development

HYDRIDE-ABSORPTION CRYOGENIC REFRIGERATOR

A new method of refrigeration that can generate cryogenic temperatures of 20 K (-253°C), without the use of electricity and with almost no moving parts, has recently been tested at JPL. Since the system has no wear-related parts, other than very long-life check valves, and since it can be powered entirely by heat from the Sun or by any low temperature "waste" heat, it is ideal for cooling cryogenic equipment on very long-life space missions.

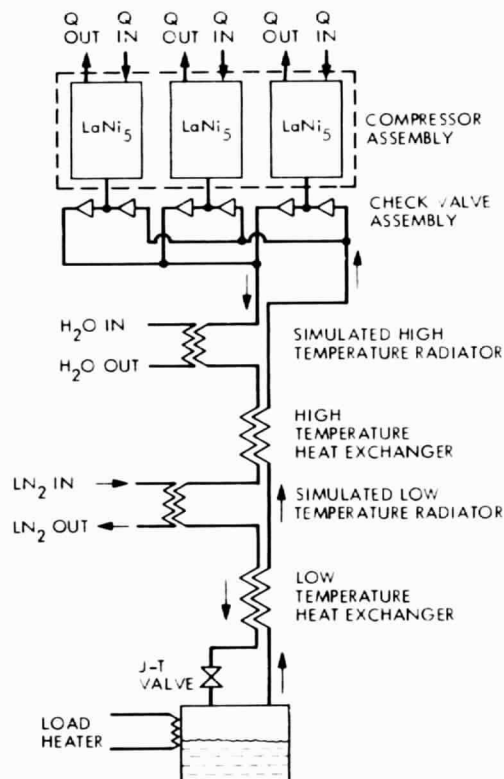
A critical milestone was accomplished recently when a three-compressor, continuously operable breadboard model was successfully tested for 300 continuous hours, while being powered solely by low-level heat. Longer tests are expected in the near future. The three cylindrical compressors are filled with a metallic powder, LaNi_5 . The powder has the peculiar property that it absorbs a tremendous amount of hydrogen gas at room temperatures and pressures, but greatly compresses the gas with only moderate increases in temperature. The three breadboard compressors are cooled by flowing water in the surrounding water jackets. After a nearly full charge of hydrogen gas has been absorbed, electrical resistance heaters on the canisters are activated. The hydrogen gas is then compressed from 60 psi at 40°C to 600 psi at 100°C . By alternately heating and cooling the units, a continuous supply of high-pressure hydrogen is

forced through a heat-exchanger/expansion-valve loop. Expansion of the hydrogen gas to 60 psi causes liquefaction at 29 K (-244°C), or at a lower temperature if a lower saturation pressure is selected. In effect, then, the system does the work of a compressor, but is powered only by heat and has almost no moving parts.

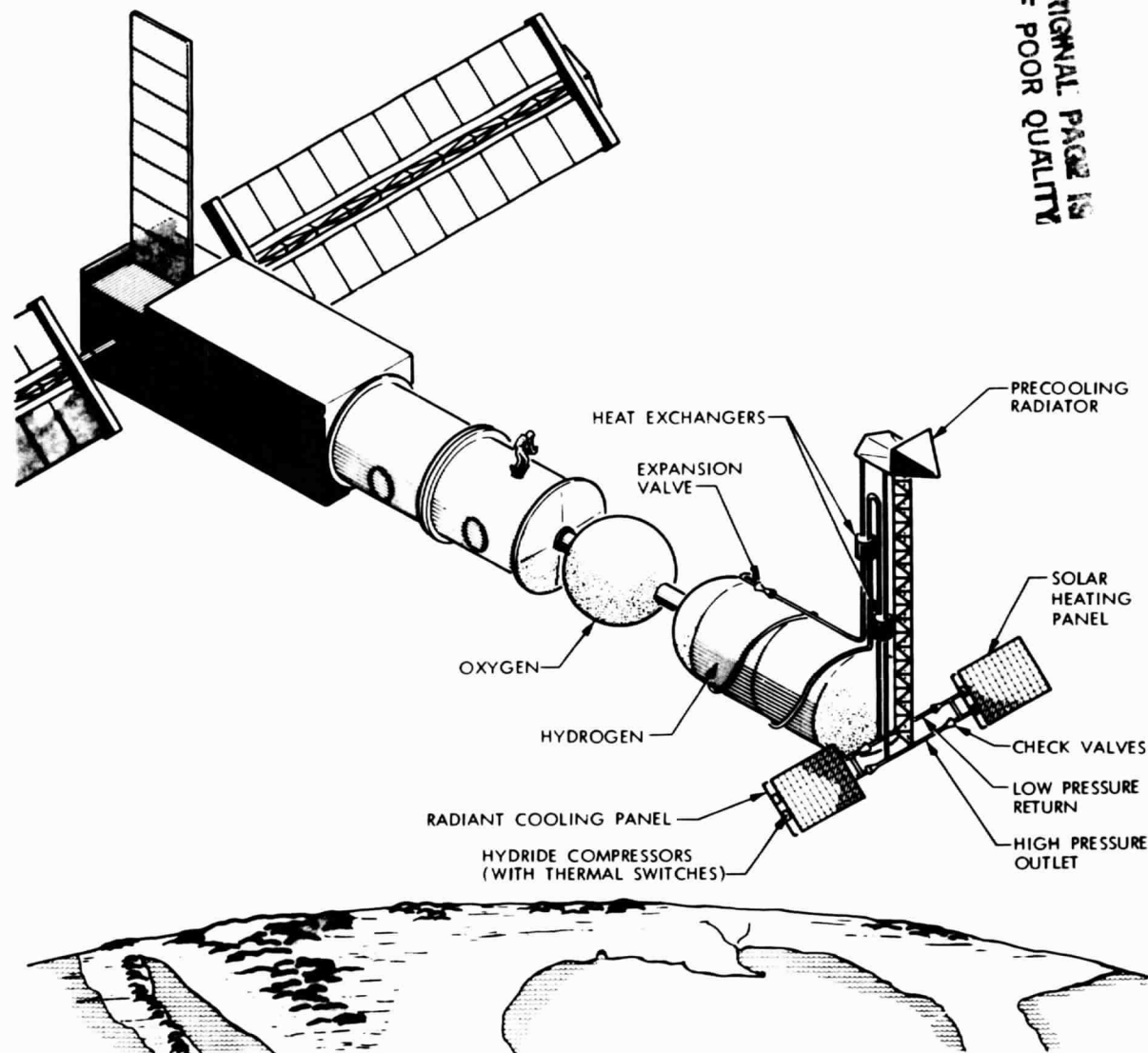
In space, the hydride refrigerator could extend the life of future space station refueling ports by cooling the large liquid-hydrogen fuel tanks likely to be in service. It could also greatly increase the useful life of orbiting systems such as the Infrared Astronomical Satellite (IRAS). Since a liquid-hydrogen-cooled shield would greatly reduce the boil-off of IRAS's liquid-helium coolant, the useful life of IRAS could be extended from one year to three years or more. The hydride refrigerator is also ideal for cooling infrared sensors during missions to the outer planets, which may take 10 years or more to complete. It could operate by using only the abundant waste heat put out by the nuclear power sources typically used on such long-lived missions.

In future application on Earth, the hydride refrigerator system could be used to liquefy hydrogen fuel, cool hydrogen-powered cars and planes, and cool superconducting motors and computers.

J. A. Jones
157-102
(213) 354-4717



This operational schematic illustrates a JPL refrigeration system in which hydride compressors are being used to cool cryogenic equipment.



Tomorrow's hydride refrigerator may be used to cool large liquid-hydrogen propellant tanks in possible future space station re-fueling ports. Powered only by heat from the Sun, the refrigerator would keep the liquid hydrogen tanks cold, thus preventing hydrogen boiloff. Since the system has no wear-related parts, it could potentially operate for decades without maintenance.

PARTICULATE CONTAMINATION ENVIRONMENT OBSERVED ON STS-3

During the STS-3 mission, a significant number of particles were observed being released from the orbiter. The observations occurred while the orbiter was flying in a tail-to-sun attitude. The flight crew sighted the particles through the aft flight-deck window and recorded the event with the rear-facing payload-bay TV cameras.

A midflight experiment was proposed to mission control to observe these particles more intensively in the one and only remaining tail-to-sun attitude period. The proposed experiment was accepted, and further measurements were made with the rear-facing payload-bay TV cameras. The two cameras were used as a stereoscopic pair, with the scene recorded on a split-screen format in an attempt to obtain camera-to-particle distances. In addition, the planet Venus and the Moon were recorded as brightness standards. The goal of both of these refinements was to resolve the apparent size ambiguity of the observations (true size vs. distance).

The JPL Image Processing Lab analyzed the videotape recording, obtaining the number of particles in the field of view and their apparent size. The trajectories of selected particles were also obtained.

Analysis of these trajectories demonstrated the effect of drag due to the residual atmosphere at orbital altitude. This effect provided another means for the determination of particle size.

The results of the analysis, which was funded by the Air Force Space Division, indicate a significant number of particles (typically 60 in a 4° half-angle field of view) with sizes in the range 0.5 to 5 cm. These particles arise from a source or sources near the aft end of the orbiter and the payload bay.

The shuttle user community in general, and investigators employing optical or IR instruments in particular, share a grave concern regarding the in-flight particulate environment. Sunlight scattered from nearby particles can severely contaminate low-light-level measurements in an unknown manner. Sunlight will also warm these particles to a temperature of about 280 K, so that a similar contamination problem arises for all IR observations. In both cases, experiment data could be rendered useless by this contamination.

This new information will significantly aid in understanding the problem.

C. R. Maag
J. Barengoltz
F. D. Kuykendall
157-507
(213) 354-6453



ORIGINAL PAGE IS
OF POOR QUALITY

An image processing and analysis system for flow-field diagnostics has been developed for the Department of Transportation, the Federal Aviation Administration, and the U.S. Army. Built upon a basic software package developed by JPL for the analysis of planetary imagery, the system has been further developed for basic experimental fluid mechanics and combustion research.

The system has been successfully applied for the analysis of aircraft fuel sprays, both for combustion and fuel-mist flammability studies. Recognition, size measurements, and tabulation of fuel drops were carried out by digital techniques. Sharp imaging of fuel drops with velocities up to 100 m/s and diameters as small as 5 μm was accomplished with very-high-resolution film and a pulsed-laser light source. No a priori information on the drop size distribution, nor on system response to various drop sizes, is required. The wide dynamic range, insensitivity to drop optical properties, and lack of a priori information assumptions concerning drop shape are some of the unique features of this technique which are not available in a single currently available drop-counting method.

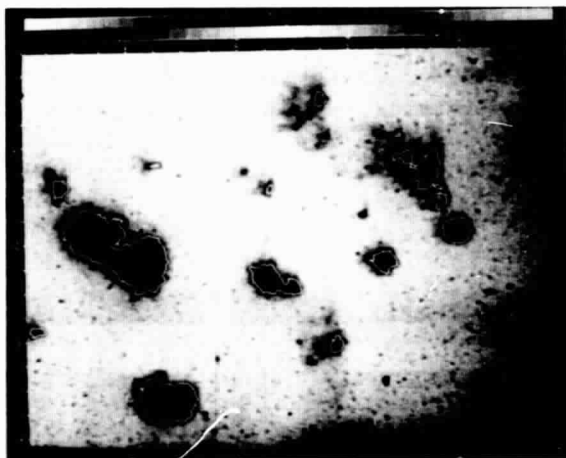
Automated measurements of fireball size and growth rate have also been accomplished with the image processing system. High-speed movies of full-scale aircraft crash tests were digitized and analyzed on a frame-by-frame basis. These measurements provide the

only quantitative flammability data for large-scale studies where more direct conventional techniques cannot be used.

Digital image processing has been applied to the analysis of a shadowgraph motion picture of a helium-nitrogen mixing layer in order to characterize the coherent vortex structures in the flow. Both the primary streamwise coherent vortices and the secondary spanwise ones were considered. Pattern recognition algorithms were designed to measure the characteristics of the vortices and their temporal evolution.

Simultaneous velocity measurement at a large number of points in a flow has been the subject of another experimental effort. To enhance our understanding of physical processes associated with complex flows, there is a great desire to know, at an instant, velocity vectors at many independent points in the flow fields so that processes such as entrainment, mixing, vorticity distribution, etc., can be accurately determined. A combined application of digital image processing techniques and the use of particles with luminescent properties can provide such information. Because of this property, they do not need a continuous illumination. Therefore, it is possible to determine both module and direction of the velocity vector by knowing the coordinates where the particles were excited with a laser. The photographic shuttering time provides a calibration for the time coordinate.

Virendra Sarohia
M. Hernan
67-201
(213) 354-6758



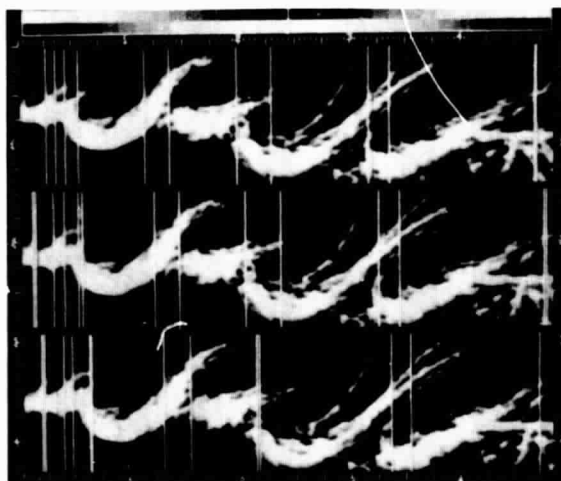
Fuel droplets—shape analysis.



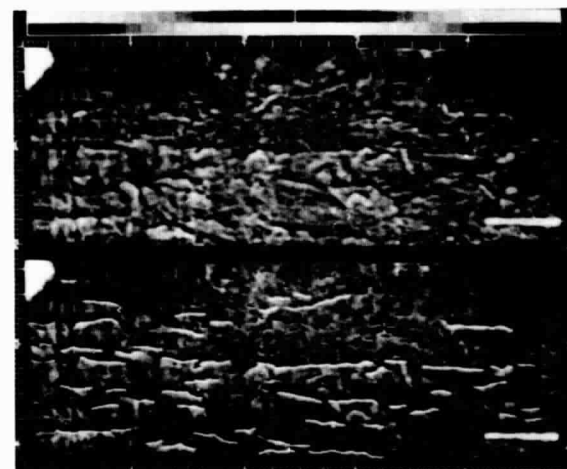
Full-scale aircraft crash test.



Shadowgraph mixing layer.



Primary vortices detection.



Secondary vortices detection.

ORIGINAL PAGE IS
OF POOR QUALITY

COMPUTER-VISION AND ROBOTICS RESEARCH

Research and development tasks in robotics and machine intelligence in 1983 included a pilot demonstration illustrating the utility of a computer-vision and robotics-control system performing real-time tracking and grappling to halt a moving object.

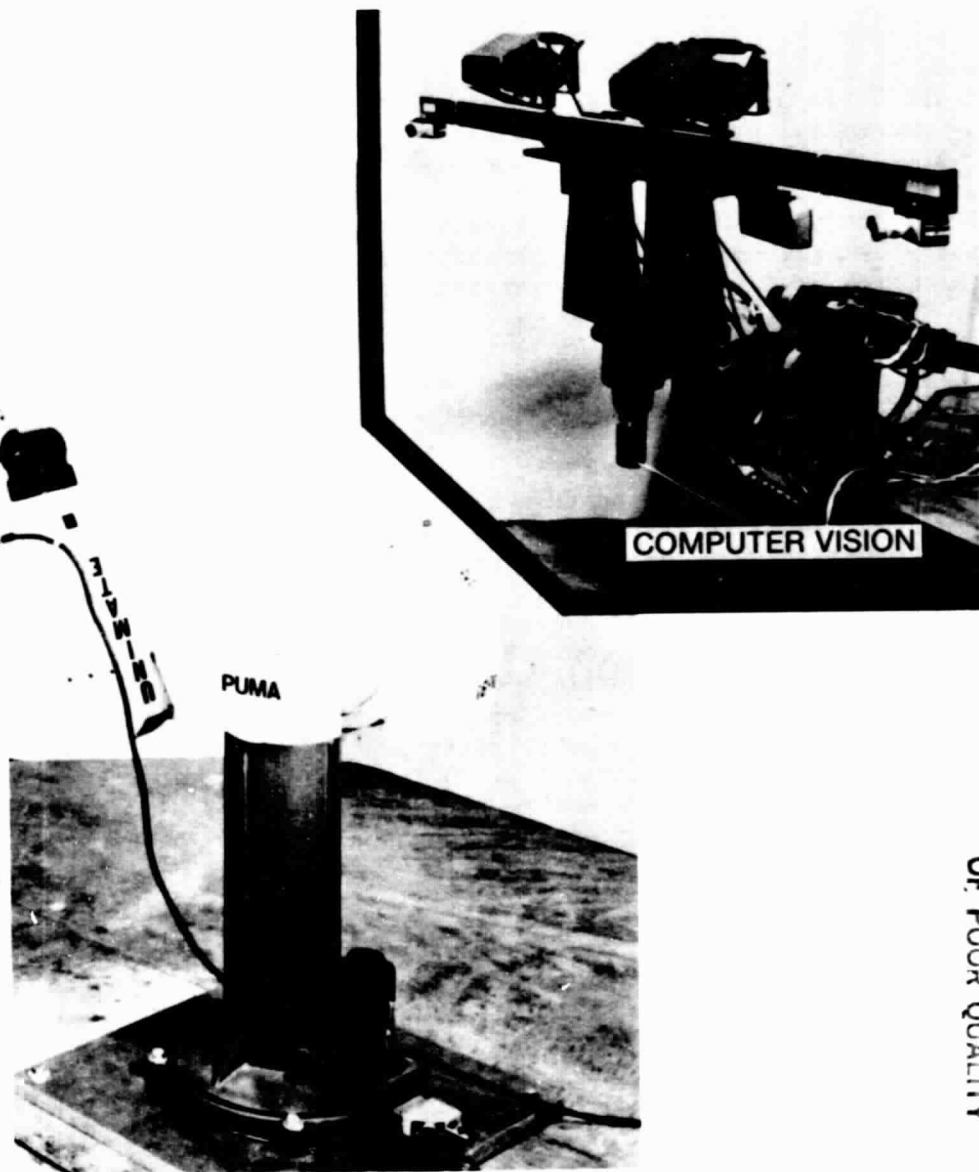
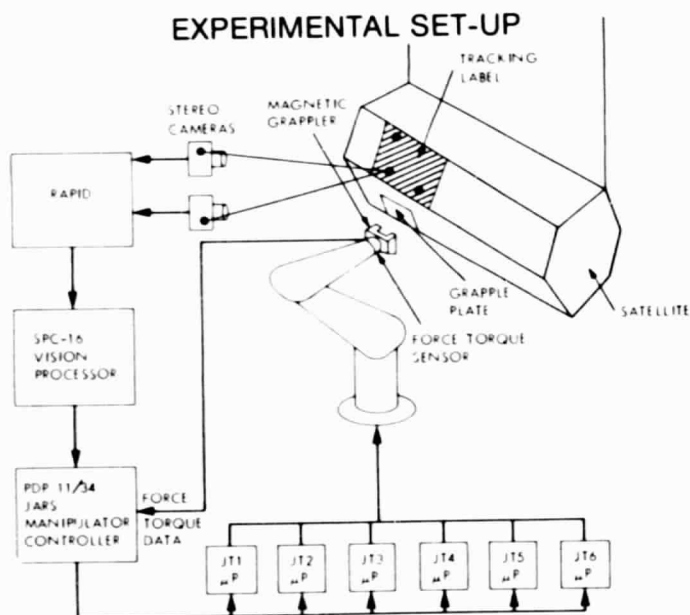
The work is a significant achievement in computer vision and robotics control applicable to spacecraft and space station systems.

The pilot demonstration involved a system similar to the space shuttle remote manipulator system (RMS), which can track and grapple a tumbling satellite in space, as characterized by the STS-7 RMS/SPAS experiment. Comparison between the two technology baselines reveals at least an order of magnitude improvement in manipulation capability and autonomous operation, using computer vision and robotics control.

Vision algorithms for performing automatic object acquisition were developed that will be integrated with the robust complex-object tracker developed in FY'82. These programs are being developed and converted for a VAX11/750 minicomputer, which is part of JPL's advanced vision system. This laboratory system architecture consists of industry-compatible hardware, and will include a VLSI vision-algorithm preprocessor, the programmable image feature extractor (PIFEX), that will replace and improve the current IMFEX.

Current achievements and continuing research toward an integrated computer-vision and robotics-control system have demonstrated the utility, often driven by necessity, of using this technology in space and factory-level automation. Its applicability to space operations is being realized and its implementation in future missions is being actively pursued.

E. P. Kan
T-1201
(213) 354-2726



Robotic satellite tracking and grapping experiment.

ORIGINAL PAGE IS
OF POOR QUALITY

IMPROVED-PERFORMANCE SHUTTLE-NOZZLE TEST

JPL's Propulsion Systems Section has completed a highly successful program that evaluated nozzle ablative materials as candidates for improving the performance of shuttle solid-rocket booster motor (SRM) nozzles. The program was the culmination of a series of subscale-nozzle materials development and evaluation programs conducted at JPL over the past five years.

The NASA Marshall Space Flight Center has been sponsoring an extensive subscale-nozzle materials evaluation program at JPL since 1978. The objectives of this program have been to identify and evaluate improved nozzle materials and to qualify alternate suppliers of candidate materials. The early part of the program involved extensive screening and evaluation of nozzle materials, employing two different subscale motors. A total of 42 successful tests were conducted with a motor that contained approximately 230 lb of shuttle solid propellant and that had a 2.2-in.-diameter nozzle throat. This motor had a burn time of 12 s at an average chamber pressure of 750 psia. The second motor contained 3,175 lb of propellant, had a 4.0-in.-diameter nozzle throat, and burned for 46 s at a higher chamber pressure, approximately 900 psia. Six nozzles were successfully tested with this larger motor.

Based on the test results from the 2.2- and 4.0-in.-throat nozzles, a test of four nozzles was carried out to evaluate the polyacrylonitrile (PAN) and pitch carbon cloths. An existing 48-in.-diameter heavyweight motor at JPL was redesigned to accommodate a scaled-down (9.5-in.-throat) version of the shuttle

flight nozzle. This motor contains 10,300 lb of propellant and burns for 32 s at an average chamber pressure of 650 psia, and an average thrust of 75,000 lb-f.

The 9.5-in.-throat nozzle was designed jointly between MSFC, JPL, and Morton Thiokol, Wasatch Division.

The first 9.5-in.-throat subscale nozzle was fabricated from the SRM-nozzle baseline material, Rayon carbon cloth. This was to provide a direct comparison of subscale- with fullscale-nozzle rayon carbon-cloth material tests and thereby provide a baseline for the evaluation of the following three subscale nozzles.

All four subscale-nozzle test firings were completely successful. The nozzle-throat erosion measured in this fourth test was 7.8 mils/s, which translates to a 24.5% decrease in erosion from that of the first 9.5-in.-nozzle test, the nozzle containing the baseline Rayon carbon-cloth materials. Nozzle number N-4 contained several different materials; however, the throat section was fabricated from continuous-filament polyacrylonitrile (C-PAN) obtained from two different suppliers. The forward section of the throat was fabricated with material from Polycarbon, Inc., while the aft section of the throat was made of C-PAN from Stackpole Corporation. In addition to the lower erosion rate of these new materials, there was also a considerable decrease in the density of the materials. The combined benefits of these improvements in the nozzle materials translate into a substantial projected payload gain for the shuttle by incorporating this new nozzle design into the full-scale SRB nozzle.

Floyd Anderson
125-224
(213) 354-3167



ORIGINAL PAGE IS
OF POOR QUALITY

Test-firing of a 9.5-in.-throat nozzle.

GASEOUS OXYGEN/HYDROGEN THRUSTER TECHNOLOGY

As interest in a space station mission has increased, NASA technology programs have been directed toward development of the needed technologies. The gaseous oxygen/hydrogen thruster has been identified as one of the prime candidates for providing drag makeup and attitude control for a future space station. Space station propulsion technology trade studies done by JPL indicate that from a life-cycle cost standpoint it is necessary to develop simpler, lower-cost gaseous oxygen/hydrogen propulsion systems in order to justify this high-performance system for the space station application.

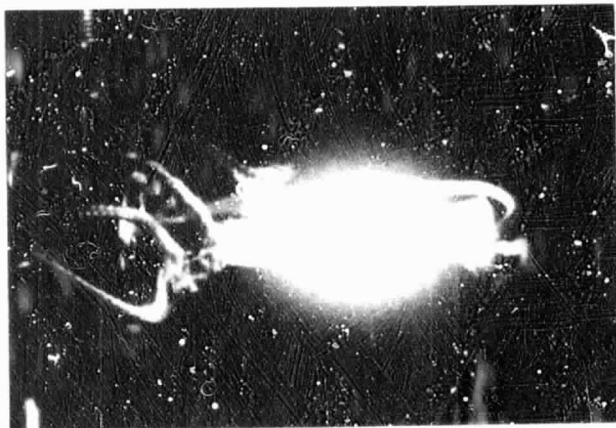
During FY'83, JPL has been working on a NASA-OAST propulsion-technology program to identify and evaluate the critical technologies required for advanced high-performance gaseous oxygen/hydrogen thruster designs in the 25- to 100-lbf thrust range for space station use. The program emphasizes the development of a radiation-cooled gaseous oxygen/hydrogen thruster (45-lbf thrust), which will permit the use of a simpler, lower-cost propulsion-system design concept. Rhenium was selected as the thrust-chamber material, since it can be operated at the temperatures (3500°F) necessary for high performance. Rhenium fabrication techniques were developed earlier

on the JPL Fluorine/Hydrazine High-Energy Propulsion-System Development Program.

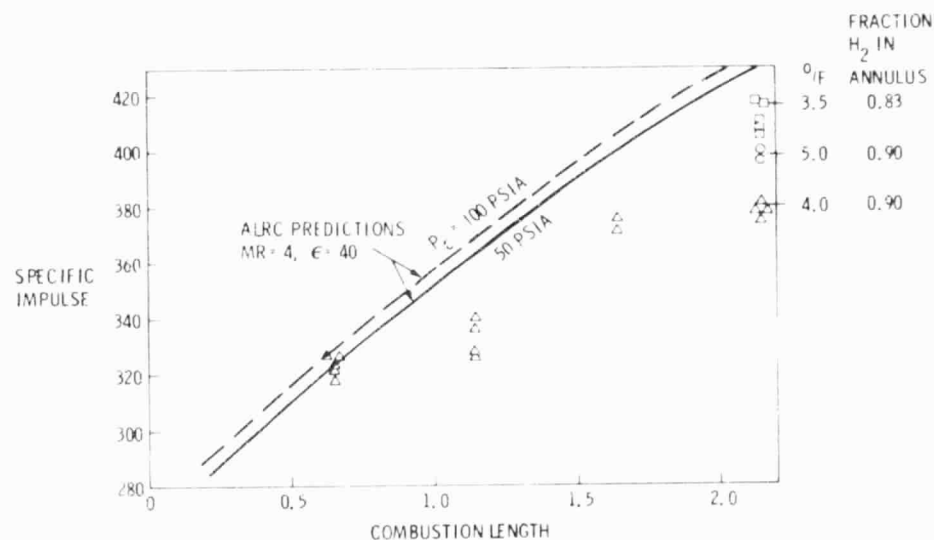
At typical thruster operating temperatures, rhenium material suffers severe structural degradation when exposed to oxidizing environments. Both oxidation-resistant coatings and gas-barrier surface protection methods have been evaluated as a means of protecting the rhenium. Vacuum tests of a subscaled (0.5-lbf) rhenium thruster have successfully demonstrated that properly designed gas-barrier techniques can provide adequate protection. Hydrogen gas is directed by a sleeve to flow along the surface of the rhenium chamber to form a gas barrier. The subscaled thruster has been run in both the steady-state and pulse modes for a total run time of sixty min, providing much higher performance when compared to Earth-storable bipropellants (about 310 lbf-s/lbm) and monopropellants (about 235 lbf-s/lbm). Steady-state specific impulses achieved were in the range of 400-420 lbf-s/lbm. Rhenium surface temperatures reached about 3200°F in the steady-state operating mode.

Results of the subscaled thruster tests were used in the design of the 45-lbf thrust unit which is now under evaluation.

Mack W. Dowdy
125-224
(213) 354-2182



SUBSCALE O_2/H_2 THRUSTER



HIGH PERFORMANCE, RADIATION-COOLED, RHENIUM THRUSTER CAN REDUCE DDT&E COSTS

- ONE HOUR CUMULATIVE RUN TIME
- MEASURED SPECIFIC IMPULSE $417 \text{ LB}_F\text{-SEC/LB}_M$
- GREATEST SINGLE RUN DURATION - 30 MIN
- MAXIMUM WALL TEMPERATURE 3500°F

Subscale rhenium thruster demonstrates feasibility of radiation-cooled gO_2/gH_2 thruster.

ORIGINAL PAGE IS
OF POOR QUALITY

HYBRID TOPOLOGY DEVELOPMENTS

Two main components are required for photovoltaic energy systems--the solar array, which converts sunlight into dc electric power, and an inverter, which subsequently converts dc to standard 60-Hz ac power. At present, the major obstacle such systems face is the array cost. However, as array cost continues to fall, inverter cost increases in relative importance.

Furthermore, inverter efficiency is important, independently of array cost, because the energy delivered is proportionate to inverter efficiency.

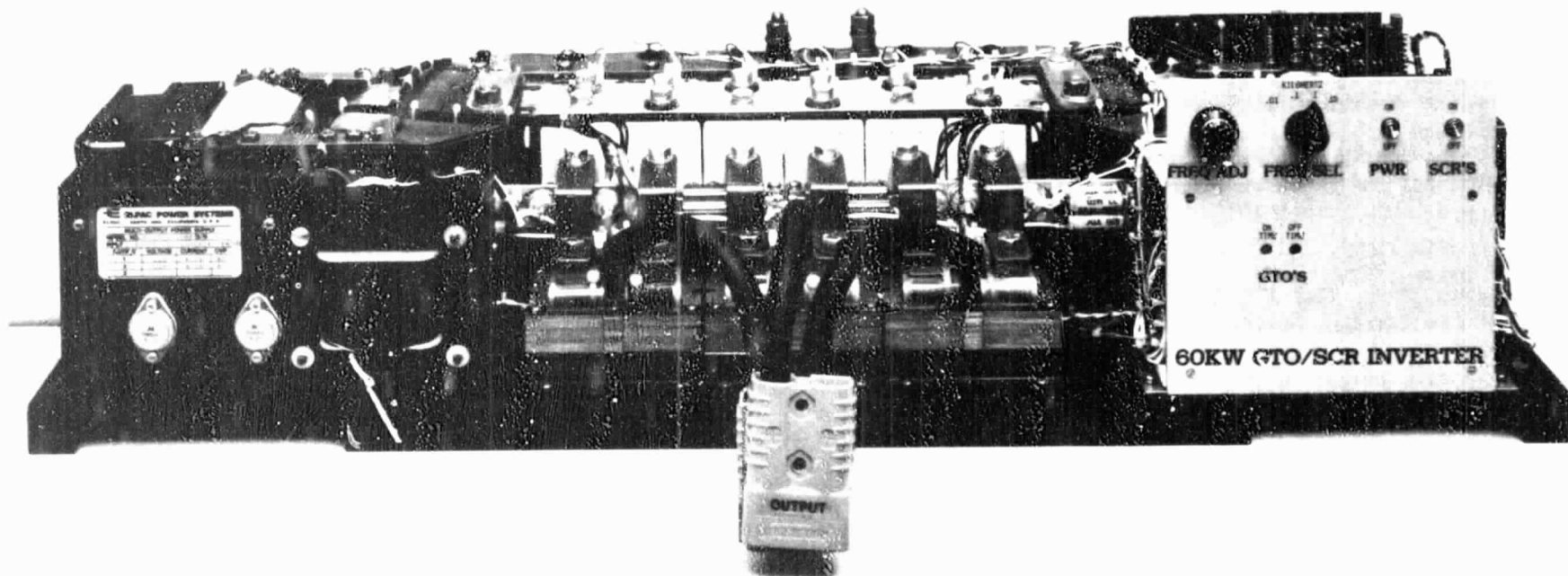
A new inverter concept has been developed within JPL's Advanced Power Concepts and System Analysis Group whereby cost and efficiency are simultaneously improved. The concept involves the combining of diverse power semiconductor devices in such a way that the strengths of one compensate for the weaknesses of another.

One embodiment of this concept is a scheme wherein a single Gate-Turn-Off Thyristor (GTO) pro-

vides commutation for the six main thyristors of a bridge circuit. Since GTO costs and on-state losses are considerably higher than those of conventional thyristors, the hybrid scheme offers both efficiency and cost advantages over conventional pure-GTO schemes. With presently available components, it appears the hybrid scheme offers simultaneous cost and loss reductions of 25% to 50%.

Development of a 60-kW three-phase proof-of-concept GTO/SCR inverter was funded by Sandia National Laboratories. Objectives of this effort were to confirm the predicted cost and efficiency improvements and to identify unforeseen technical problems. While testing and evaluation of the inverter are ongoing, preliminary results indicate efficiencies above 96% for power levels between 6 kW and 60 kW, with efficiency above 97.5% at 30 kW. A conventional inverter would have efficiencies ranging between about 90% and 94% for the same test conditions. Results of this effort are particularly gratifying in that applications to other areas such as electric vehicles and space power systems seem well suited.

Willy E. Rippel
507-207
(213) 577-9121



ORIGINAL
OF POOR QUALITY

THE VLSI DESIGN CENTER

The Very Large Scale Integration (VLSI) Design Center achieved full operation during 1983. Its function is to provide facilities for teaching and practicing design and layout of LSI/VLSI custom chips, and for the development of software and hardware (the "design tools") to support these activities. It contains a classroom with display terminals, a user area with design terminals, and a VAX 11/780 computer, the "LSI VAX". In addition to the terminals in the Design Center, the LSI VAX supports remote access by terminals located elsewhere on the Laboratory (through short-haul modems at 9600 baud), by dial-up telephone lines at 300 and 1200 baud, and by the ARPAnet. The LSI VAX is a research machine, with about 60% of its support coming from VLSI work, which includes development of the design tools, use of the system for circuit-design projects, and use of the system for test-chip design in the Product-Assurance Program. The balance of the support comes from other JPL research projects.

During 1983, the JPL VLSI design course was taught at the Design Center to about 50 employees. The special skills required to design custom circuits on silicon are taught in this course. It concludes with the submittal of a design file for fabrication, with the completed and packaged chip returned to the

designer (or the team of designers) for testing and evaluation.

The JPL design course was also taught at JPL to 11 NASA and DoD employees. About half of the class completed chip designs and submitted them for fabrication by the end of the class; others took their designs with them for later completion and submittal for fabrication through JPL. The JPL design-tool programs were given to the participants on magnetic tape for installation in their own facilities. JPL will provide patches and updates for these programs; the users will provide bug reports to JPL.

The design tools implemented during 1983 and currently available on the LSI VAX include ART, a geometrical layout language embedded in Pascal; CRAYON, an interactive graphics editor; NPADS, an interactive program for making bonding-pad connections; CIFPLOT, a graphics checkplot program; MOSSIM and MOSPATCH, switch-level logic simulators; and EXTRACT, a program that reconstructs a transistor diagram from a geometrical layout.

The VLSI Design Center provides support for the NASA/DARPA Product-Assurance Program and the DSN design-tools task. It also provides JPL with access to the ARPAnet.

Tom Griswold
198-231
(213) 354-7163

PULSED PLASMA THRUSTER IGNITION SYSTEM LIFETIME

With JPL research assistance, a one-milli-pound pulsed plasma thruster (PPT) is being developed by the Air Force Rocket Propulsion Laboratory (AFRPL) to provide long-term station-keeping for satellites. One of the major limitations of the pulsed plasma thruster has been the lifetime of the ignition system, which is composed of a spark-gap igniter plug and its associated trigger circuit. A carbonaceous deposit was found to accumulate on the igniter plug during thruster operation, thereby limiting thruster lifetime.

An effort to increase lifetime experiments was initiated at JPL in conjunction with the AFRPL PPT development and testing program in order to understand and improve the ignition system. During these experiments, plume velocity, plug erosion characteristics, ignition modes, and energy utilization efficiency of the ignition system were determined.

The JPL research effort led to several conclusions. It was found that the amount of carbonaceous deposit accumulated on the igniter plug could be controlled by changing the resistive coupling element, used to couple the igniter plug cathode to the thruster cathode, to an inductive one. Further improvement was demonstrated by using a fast-rise-time, high-current trigger pulse. It was also possible to determine the dynamic impedance of the plug discharge so that a trigger circuit could be developed with an impedance matched to that of the igniter plug.

The results of the tests were a factor-of-5 increase in thruster lifetime (life tests were conducted at the Fairchild Republic Corporation), and suggest other modifications (by generating a shorter and more energetic ignition discharge) that could result in further increased lifetime benefits by another factor of 3 in the future.

Kenneth L. Atkins
198-220
(213) 354-6293

DEVELOPMENT OF SAFE, HIGH-ENERGY LITHIUM CELLS FOR NASA APPLICATIONS

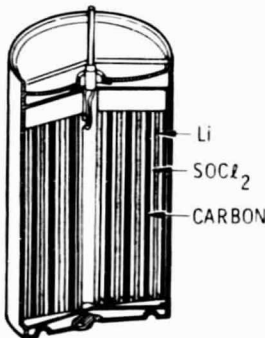
With the resolution of specific thermal and chemical problems in the lithium-thionyl chloride (Li-SOCl_2) electrochemical couple, it is now possible to develop safe, high-energy (up to 600 Wh/kg), and long-life (up to 10 years) Li-SOCl_2 cells for a variety of NASA applications.

The primary reason these batteries have not been employed to date to any large degree by NASA is that they have been reported on occasion to vent and to even explode. Further, the causes for these phenomena are not completely understood. For these reasons NASA has sponsored efforts to understand and resolve thermal and chemical safety problems in these cells.

The thermal issue arises from the fact that the Li-SOCl_2 cell, like most other cells, generates heat internally during discharge. Under certain conditions, especially at high rates, the heating effects may cause the internal temperature to rise beyond a critical limit (such as 179°C , the melting point of Li) where known exothermic reactions can take place. For this reason a portion of the investigations have been directed towards understanding the thermal behavior of these cells.

Based on calorimetric measurements, an equation was developed to correlate heat generation, Q , with operating conditions, V , I , and T . Subsequent thermal modeling and experimental testing established that operating temperatures can be predicted with relatively good accuracy. In turn, this permits the establishment of safe operating limits, such that cell temperatures remain below the upper unsafe limit. On this basis the thermal problem is manageable.

The chemical issue takes into account the fact that during discharge and reversal there may be several intermediate species that may be formed in the process of the overall reaction, from reactants to end products. Further, it is possible that one or more of these intermediates may be a high-energy, unstable species that may decompose with release of sufficient energy to explain the venting or, alternatively, to trigger the chemical Li-SOCl_2 reaction. For these reasons a considerable effort has been made to identify the species involved in the discharge and reversal processes. This work has been carried out by a coordinated technology and research effort involving chemical and spectroelectrochemical investigations on both laboratory- and hardware-type Li-SOCl_2 cells.

THE CELL	SAFETY ISSUES RESOLVED
 <p>ENERGY: TO 600 Wh/kg LIFE: TO 10 yrs</p>	<ul style="list-style-type: none"> • INTERNAL HEAT GENERATION <ul style="list-style-type: none"> - UNDERSTOOD AND MANAGEABLE • FORMATION OF HAZARDOUS COMPOUNDS? <ul style="list-style-type: none"> - NONE FOUND DURING NORMAL DISCHARGE ($V > 1.5$) - NONE FOUND DURING REVERSAL ($V < 0$) OF ANODE LIMITED CELLS - SOME FOUND DURING REVERSAL ($V < 0$) OF CATHODE LIMITED CELLS
	CONCLUSION
	<ul style="list-style-type: none"> • Li-SOCl₂ CELLS SHOULD BE MADE WITH ANODE LIMITED DESIGN

Safety of Li-SOCl₂ primary cells.

- INTERNAL HEAT GENERATION
 - INTERNAL HEATING CAN RAISE CELL TEMPERATURE TO EXCESSIVE LIMIT
 - HEAT GENERATION RATES MEASURED AND CORRELATED WITH OPERATING CONDITIONS
 - CAN NOW SPECIFY SAFE OPERATING LIMITS BY THERMAL ANALYSES
- FORMATION OF HAZARDOUS COMPOUNDS
 - SOME SPECULATION THAT HAZARDOUS COMPOUNDS CAN BE FORMED IN CELLS
 - DURING NORMAL DISCHARGE ($V > 1.5$) NO HAZARDOUS COMPOUNDS FOUND IN BOTH ANODE AND CATHODE LIMITED CELLS
 - DURING REVERSAL ($V < 0$, AND ELECTRICALLY PREVENTABLE) NO HAZARDOUS COMPOUNDS FOUND IN ANODE LIMITED CELLS AND SOME FOUND IN CATHODE LIMITED CELLS
- CONCLUSION
 - HIGH ENERGY (10 TIMES GREATER THAN ALKALINE) Li-SOCl₂ CELLS CAN BE PRODUCED AND OPERATED IN A SAFE MANNER PROVIDED THEY ARE MADE WITH AN ANODE LIMITED DESIGN

Resolution of safety issues.

Results have elucidated the very complex cell chemistry and have been used to formulate detailed mechanisms for the reactions that occur within these cells. Through these mechanisms it was possible to establish a complete accounting of cell chemistry and thereby reach practical conclusions regarding cell safety. These conclusions were that, at ambient temperature: a) there are no hazardous species formed for the condition of normal discharge ($V > 1.5$) and for anode limited reversal ($V < 0$), and b) some

hazardous combinations of materials are formed for the condition of cathode limited reversal ($V < 0$). Therefore, the cell must be designed to avoid the condition of cathode limited reversal.

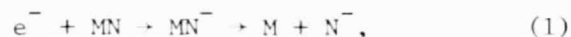
With resolution of these issues safe, high-energy, and lightweight Li-SOCl₂ cells can now be developed and advantageously employed in a variety of NASA applications.

Gerald Halpert
Boyd Carter
198-220
(213) 354-5474

III. Technology Applications

MEASURING TRACE AMOUNTS OF CONTAMINANTS PRESENT IN A GASEOUS ENVIRONMENT

In many situations there is a need for detecting and measuring with high sensitivity contaminants present in an ambient environment. For example, one would like to measure trace amounts (≈ 1 part per billion or less) of CH_3Cl , CF_2Cl_2 , CFCl_3 , CH_3CCl_3 , CCl_4 , NH_3 , etc., present in Earth's atmosphere, or to detect low levels (of the order of 500 parts per million) of H_2 and O_2 in an atmosphere of N_2 , or to monitor the presence of hydrazine (N_2H_4) in the space shuttle environment. An instrument which can perform these measurements should have high sensitivity of detection, have fast response times (within a few seconds), and be simple. At JPL we have developed techniques which serve as the basis for a laboratory instrument called the Negative Ion Contamination Monitor, which meets these requirements. The instrument relies upon the process of dissociative electron attachment, which can be represented by the following reaction:



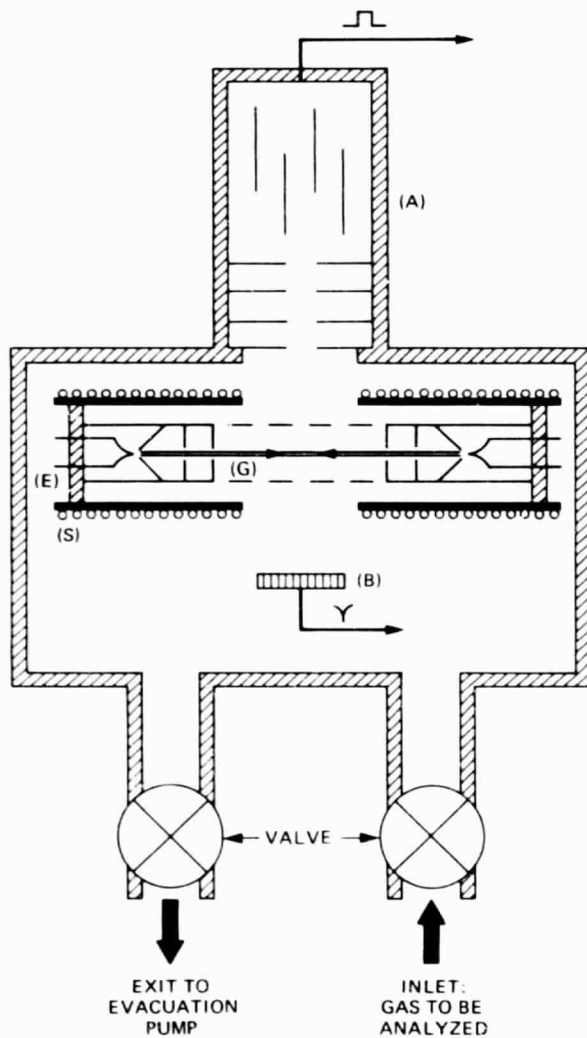
where MN is an attaching molecule, MN^- is a temporary negative ion, and M and N^- are the neutral and negative ion fragments, respectively. This reaction takes place only for certain fixed values of kinetic energies of incident electrons (e^-). Therefore, it is a resonance process, and the electron energies at which attachment takes place are known as "resonance energies." Each molecule has its own set of resonance energies. Thus, a molecule can be distinguished from others by simply measuring: (a) the mass of N^- , (b)

the resonance energy at which N^- is produced, and (c) the intensity of N^- signal. For certain molecules, such as halogenated hydrocarbons present as trace amounts in dry air, the probability of reaction (1) taking place is many orders of magnitude higher than the probability of this reaction occurring for air molecules. Therefore, these molecules can be detected even at concentrations of the order of 1 part per billion or less.

In operation, the quadrupole mass spectrometer is set to detect the negative ion of interest (e.g., H^- produced from H_2O), the kinetic energy of incident electrons is varied from 0 to 20 eV, and the resulting negative ion signal is then recorded as a function of electron energy in a multichannel analyzer. Each negative ion is individually counted as an event by means of a charged-particle detector placed at the exit of the mass spectrometer, together with pulse-counting circuitry.

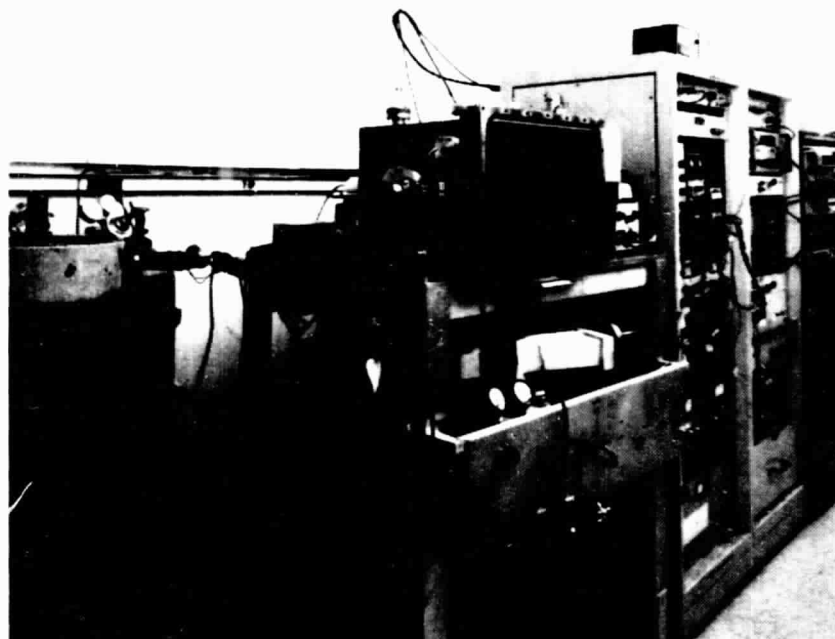
The contamination monitor has been tested by measuring trace amounts of CH_3Cl present in dry air, a sample of which was provided by the National Bureau of Standards (NBS). This contained 340 parts per billion of CH_3Cl in dry air. Our measurements, which utilized preconcentration techniques, yielded a concentration of 346 parts per billion, which is in excellent agreement with the NBS value. We are currently developing a compact and portable version of the instrument for flight applications.

S. K. Srivastava
O. J. Orient
183-601
(213) 354-3246



- (A) - MASS SPECTROMETER DETECTOR
- (B) - CHARGED PARTICLE DETECTOR
- (E) - ELECTRON GUN
- (S) - SOLENOID FOR PRODUCING AN AXIAL MAGNETIC FIELD
- (G) - NEGATIVE ION EXTRACTION GRID

Schematic diagram of the Negative Ion Contamination Monitor.



First laboratory version of the Negative Ion Contamination Monitor.

ORIGINAL PHOTOGRAPH
OF POOR QUALITY

METAL SHELL TECHNOLOGY AND ITS APPLICATIONS

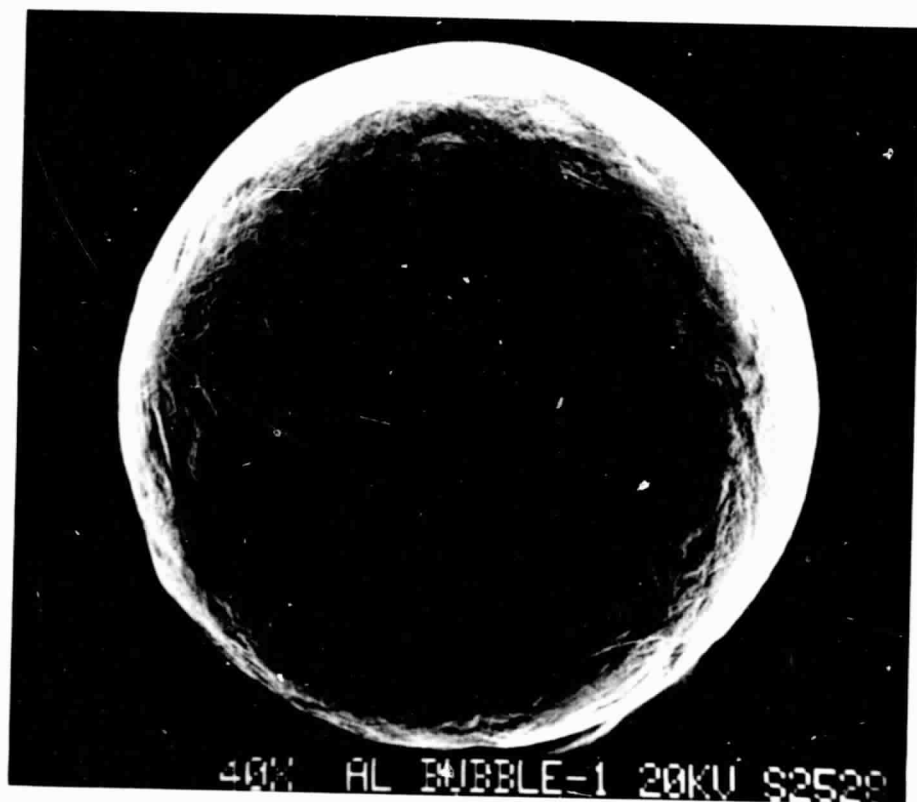
Metal shells of various materials, sizes, and aspect ratios (radius/wall thickness) can have many useful and novel applications. For instance, high-quality shells of metallic-glass materials can be used as DT fuel containers for laser fusion. There are other potential applications as well. Chemicals having high latent heat of fusion at a well-defined phase-transition temperature can be contained inside the metal shells and serve as a heat-exchanging medium with a minimum amount of temperature excursion. Metal shells can also be used as containers for hazardous materials. In addition, by controlling the density of the metal shells, a neutral-buoyancy condition can be achieved with a prescribed carrier fluid so that the shells can be used as efficient surface-catalytic agents. As a low-density material, metal shells can be sintered together to provide structural strength and geometric flexibility potentially applicable to future structures in space.

In the past year, the Physical Acoustics and Containerless Science Group has developed an extensive program to investigate various aspects of metal-shell formation, such as the promotion and generation of high concentricity, gravitational effects, techniques for forming encapsulated shells, sintering techniques, and material considerations.

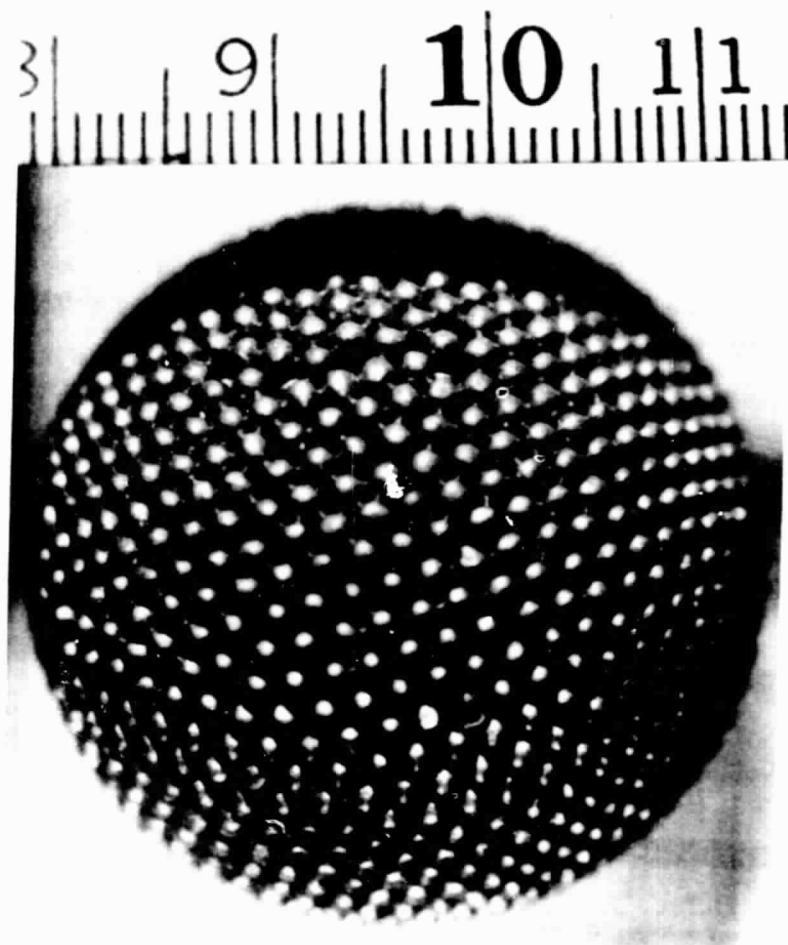
Aluminum shells of sizes ranging from 500 μm to 2 mm have been formed using a technique developed by J. Kendall of JPL.

These shells have been successfully sintered together using a liquid phase technique. In order to increase bonding strength, other sintering methods are being considered. These include electric-discharge, ultrasonic, volume-diffusion, and composite-material methods.

Mark C. Lee
Wesley M. Akutagawa
Taylor G. Wang
169-327
(213) 354-4795



Aluminum shell with a diameter of 2 mm and an aspect ratio of 5.



Liquid phase sintered aluminum shells using silicon powder.

ORIGINAL PHOTOGRAPH
OF POOR QUALITY

HYDROCEPHALUS SHUNT

Hydrocephalus, a condition most often affecting growing children, is characterized by an abnormal pressure on brain tissues. This results in abnormal brain development, leading in many cases to severe retardation.

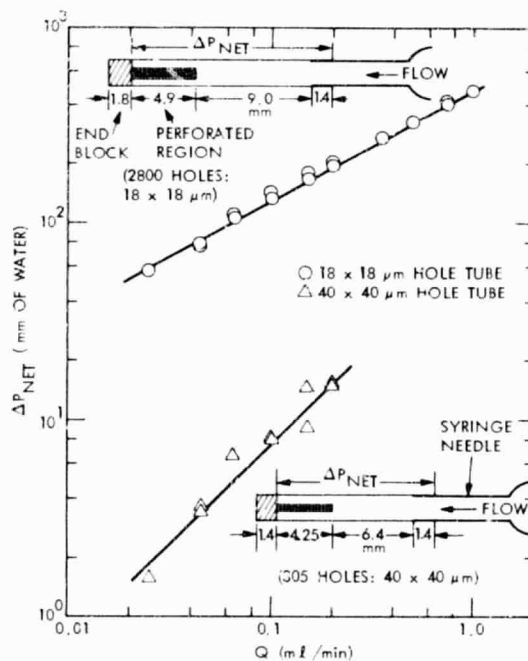
Treatment for hydrocephalus is, in theory, simple: a perforated tube (shunt) is inserted into the affected cavity to drain off the excess fluid. Existing shunts, however, are less than satisfactory due to blockage by cellular debris or ingrowth of choroid plexus cells. Blockage by debris has more or less been solved by valves which allow back-flushing. However, blockage by cellular ingrowth appears to be the major problem with existing shunts. Shunt replacement is therefore required on the average of once every year. By replacing the handful of 1-mm holes in standard shunts with thousands of micron-sized holes, it is hoped to prevent cellular ingrowth.

JPL is applying its expertise in "drilling" the holes and in the study of the fluid flow through the

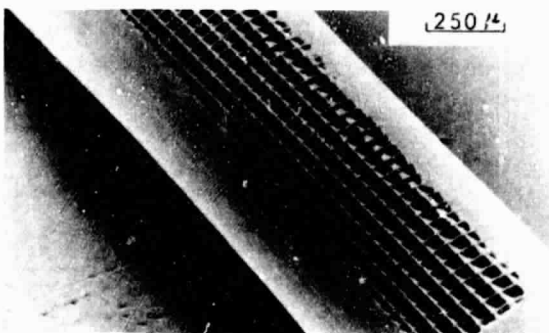
perforated tubes. JPL skills in flow mechanics are being applied to both the accurate measurement of the low flow rates involved and to the development of a model for the fluid flow through the very small perforations.

Ion-beam technology developed for advanced electric-propulsion systems is being applied to "drill" perforations of sizes and configurations calculated to prevent clogging of the shunt and to permit appropriate drainage rates. Several techniques have been developed at JPL to produce high-quality perforations with a high degree of reliability. These include water-cooling to prevent thermal damage, mechanical mounting and ion-beam collimation to assure good hole definition, and a mandrel inserted into the tube to indicate when all the holes have been "drilled". Thus, JPL is providing both the design specifications for an improved shunt and the technology necessary to implement them.

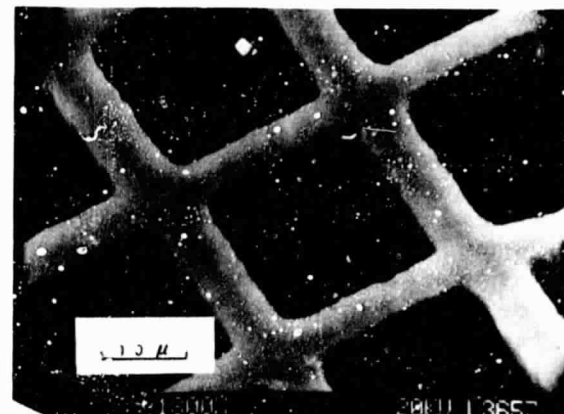
Stephen B. Gabriel
Charles E. Garner
Lloyd Back
Young I. Cho
186-118
(213) 354-6850



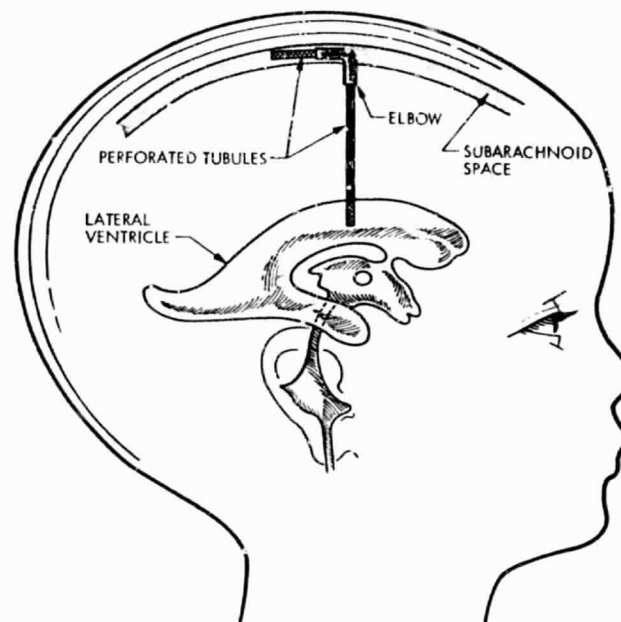
Pressure difference vs. flow-rate measurements. By changing the size of the hole region and/or the size of the holes in the shunt, clinically observed values for cerebrospinal fluid flow rates of 0.30 to 0.56 ml/min at pressures of 80-200 mm water could be achieved.



Sputtered section of a microtubule showing the hole pattern obtained by bombarding the microtubule with an argon ion beam.



$\sim 20 \mu m$ holes "drilled" in $\sim 626\text{-}\mu m$ -diameter Teflon tube.



Shunting of cerebrospinal fluid from the lateral ventricle to the sub-arachnoid space using sputter-perforated microtubules.

ORIGINAL PAPER
OF POOR QUALITY

PRESSURE DISTRIBUTION AND FLOW SEPARATION IN ARTERIAL BRANCH CAST AND MODELS

There is ample precedence for suspecting that local flow disturbances at arterial bifurcations and branches are implicated in the localization of atherosclerosis in these areas. This localization occurs in two areas, suggesting quite different flow structures --that is, probable high-shear locations and probable sites of separation or stagnation, both of which are known to exist at branches. What is required is to map discrete hydrodynamic flow behavior at sites that are lesion-susceptible and sites that are lesion-resistant in the vascular tree during the disease process.

This investigation was undertaken to acquire a better understanding of the fluid dynamics in branch regions of actual arteries by flow-testing hollow vascular replicas made from primary casts of human cadavers and Plexiglas models.

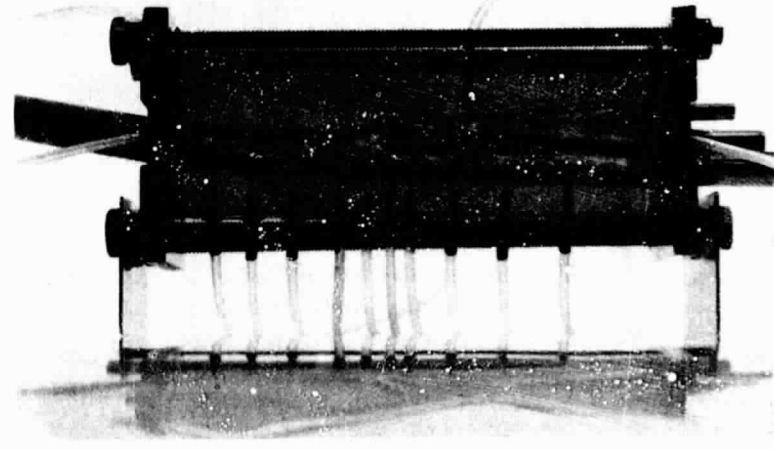
A polyurethane casting of the deep femoral branch of a cadaver was obtained from the USC School of Medicine. This casting has been fitted with end plates and tubes for connection to the flow bench-test system in the Biomedical Fluid Dynamics Laboratory at JPL. In order to obtain pressure measurements at a number of locations in the parent vessel and in the branches, a number of pressure tap holes were made in the main lumen as depicted in the femoral arterial-casting picture. A multichannel differential-pressure transducer

system was built with valving and manifolding. Instantaneous flow rates were determined with flow cuffs, each connected to an ultrasonic Doppler flowmeter.

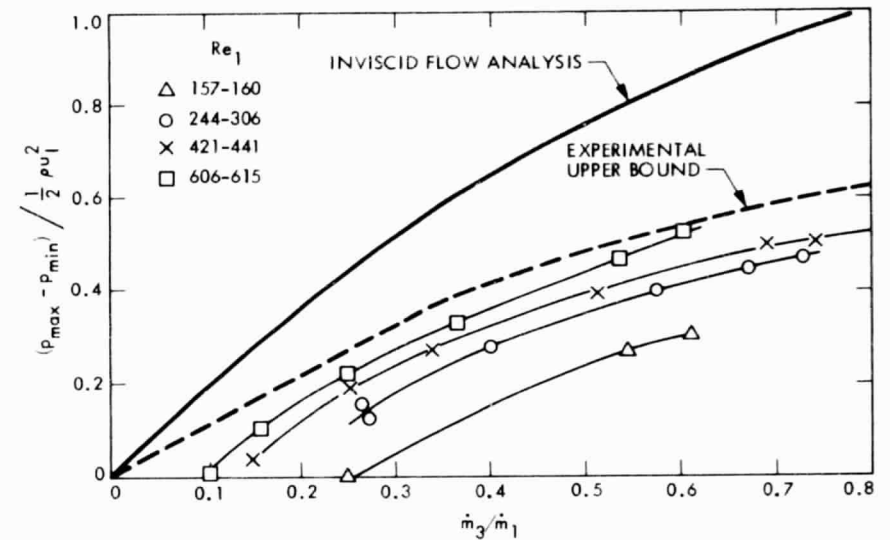
Pressure rise in steady flows through branch junctions in arteries was simulated by a flow through a Plexiglas model and flow visualizations were conducted. For a branch flow rate to main lumen flow rate ratio, \dot{m}_3/\dot{m}_1 , greater than about 0.4, flow separation occurred along the wall opposite the branch. Hydrodynamic interpretation of the flow separation and reattachment processes is as follows: Local increases in pressure along the wall are coupled to local decreases in blood velocity which, when large enough, lead to separation of the flow in the momentum-deficient shear layer along the wall. The separated flow reattaches to the wall distal to the separation location, forming a reverse flow region. In the reattachment process, that part of the flow that does not have enough momentum to overcome the pressure rise associated with the reattachment is turned rearward to form the reverse flow or separation region.

An inviscid analysis was able to explain the pressure rise near branch junctions. Flow separations tend to occur in such regions of rising pressure, and this seems to be intimately associated with atherosclerosis.

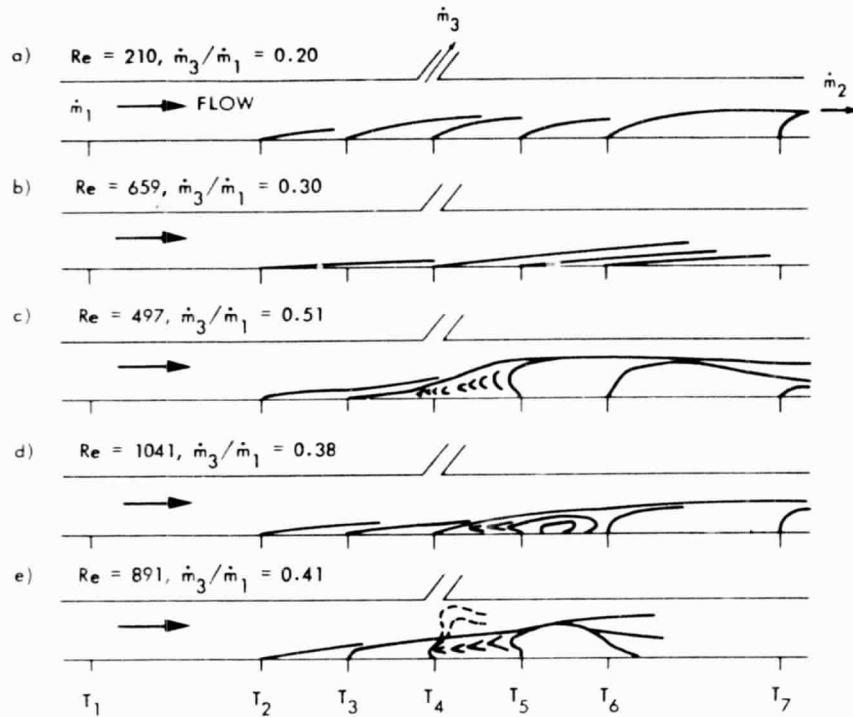
Lloyd H. Back
Young I. Cho
125-159
(213) 354-3537



In vitro, steady flow in a casting of the femoral artery branch of a human being was studied by measuring pressure difference in the main lumen and also in the branch over a Reynolds number of 200 to 1600. Effects of viscous and inviscid flows in this branch were demonstrated quantitatively.



Pressure measurements along the main lumen of the 60-deg branch model were conducted by varying branch flow-rate ratio (\dot{m}_3/\dot{m}_1) and Reynolds number (Re_1). Inviscid flow analysis using the Bernoulli equation provided a hypothetical upper bound for the pressure rise.



Flow-visualization studies using dye injected at many locations along the wall revealed very complex, three-dimensional fluid motions associated with the flow-separation process; a 60-deg Plexiglas branch model was used.

ORIGINAL PAGE IS
OF POOR QUALITY

ANALYSIS OF INDIVIDUAL BIOLOGICAL PARTICLES BY MASS SPECTROMETRY

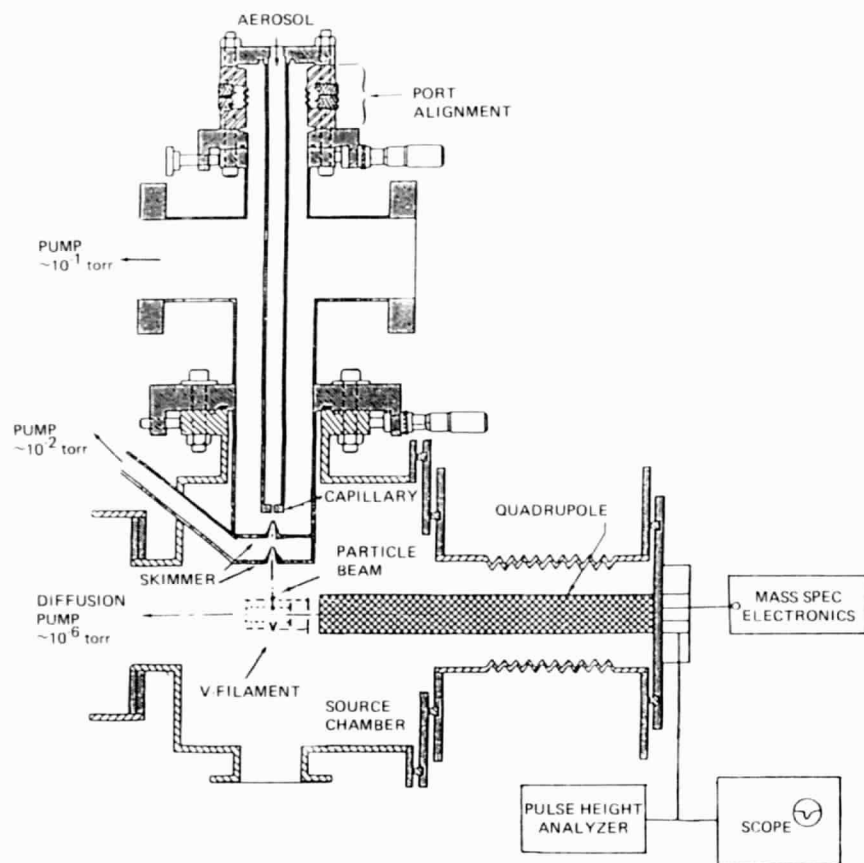
The technique of analyzing particles through mass spectrometry, developed at JPL, has been successfully applied to the analysis of single biological particles in the aerosol form. This technology involves a combination of the methods of particle-beam generation and mass spectrometry, and can aid in the differentiation and identification of microorganisms. Two major milestones that have been achieved in this work on bioparticle analysis are the preparation of a beam of bacterial particles from aerosols for their direct introduction into the mass spectrometer, and the measurement of their mass spectra.

The bacterial aerosols are generated by nebulizing their bacterial suspensions in ethanol. A beam of particles is then produced by the expansion of the aerosol through a capillary nozzle into a vacuum. Because the particles are heavier, compared to the carrier gas molecules, they remain confined to the beam axis and are led efficiently into the ionizer of a quadrupole mass spectrometer. Here they impinge on a resistively heated filament and are volatilized. The resulting vapor plume from an individual particle is then ionized by electron impact in an in situ fashion.

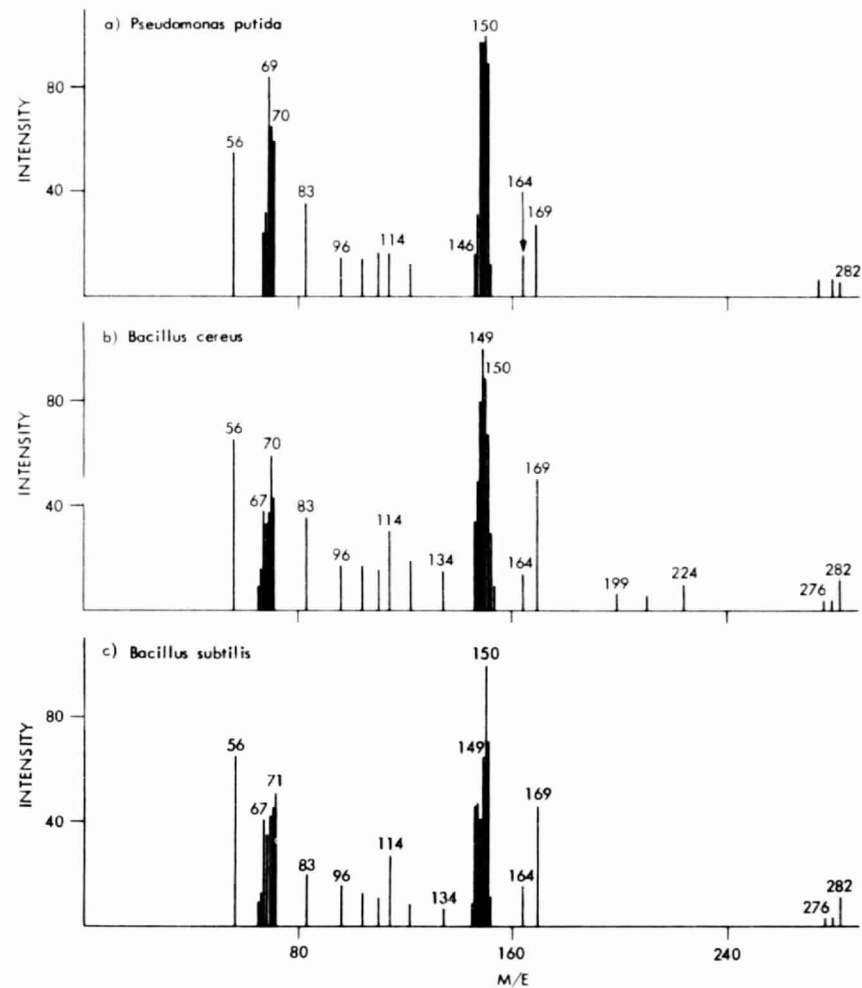
A burst of ions thus produced from individual cell particles has a pulse of about 100 μ s, which

necessitates the manual scanning of the mass spectrometer, monitoring one mass peak from each cell. The charge under each ion pulse is measured by integration, and a proportional output voltage is used for determining the pulse-height distribution. The average intensity of a mass peak is obtained from the pulse-height distribution of about a thousand ion pulses from different particles.

Pseudomonas putida, Bacillus subtilis, and Bacillus cereus bacteria have been used in the present studies. Signals were observed at several masses throughout the spectrometer mass range of 30-300 amu. A common set of more than 30 mass peaks was selected for intensity measurements. Characteristic mass spectral features were seen, and the similarity between them is believed to be due to the fact that the microorganisms have essentially the same major chemical building blocks. The important points of differentiation between the spectra, however, lie in the relative intensities of various peaks. For example, the intensities of mass peaks at 69, 114, 134, 169, and 282 amu relative to the intensity at 149 amu is higher in the spectrum from Bacillus cereus than those derived from Pseudomonas putida. Such analysis of intensities can aid in the differentiation and identification of microorganisms.



Schematic of PAMS system.



Mass spectra of bacteria particles.

The detection and identification of biological particles in air on a continuous, real-time basis by using this technique is thought to have many applications, including monitoring a protected environment such as a clean room. The technique may find clinical applications when fully developed.

A limitation on the current technique is that a large number of particles must be measured. The problem can be overcome by using a focal-plane mass spec-

trograph (nonscanning), which could then permit all the ions of different masses from a particle to be monitored simultaneously. One such miniaturized mass spectrograph (Mattauch-Herzog type), with an ultra-sensitive electro-optical ion detector covering the entire focal plane, has been developed and built at JPL. The mass-spectrometer particle-beam generator is planned to be interfaced with this system and should provide a complete mass spectrum from individual particles.

M. P. Sinha
L. E. Giffin
11-116
(213) 354-6358

IV. Energy and Energy Conversion Technology

LOW-COST POLYCRYSTALLINE SILICON-PROCESS DEVELOPMENT

The utilization of photovoltaic solar cells for terrestrial applications requires a drastic reduction in the cost of the solar arrays. The Low-Cost Solar Array Project, managed by JPL for the Department of Energy, was initiated in March 1975 to develop the overall technology to achieve the national solar-energy cost-reduction goal.

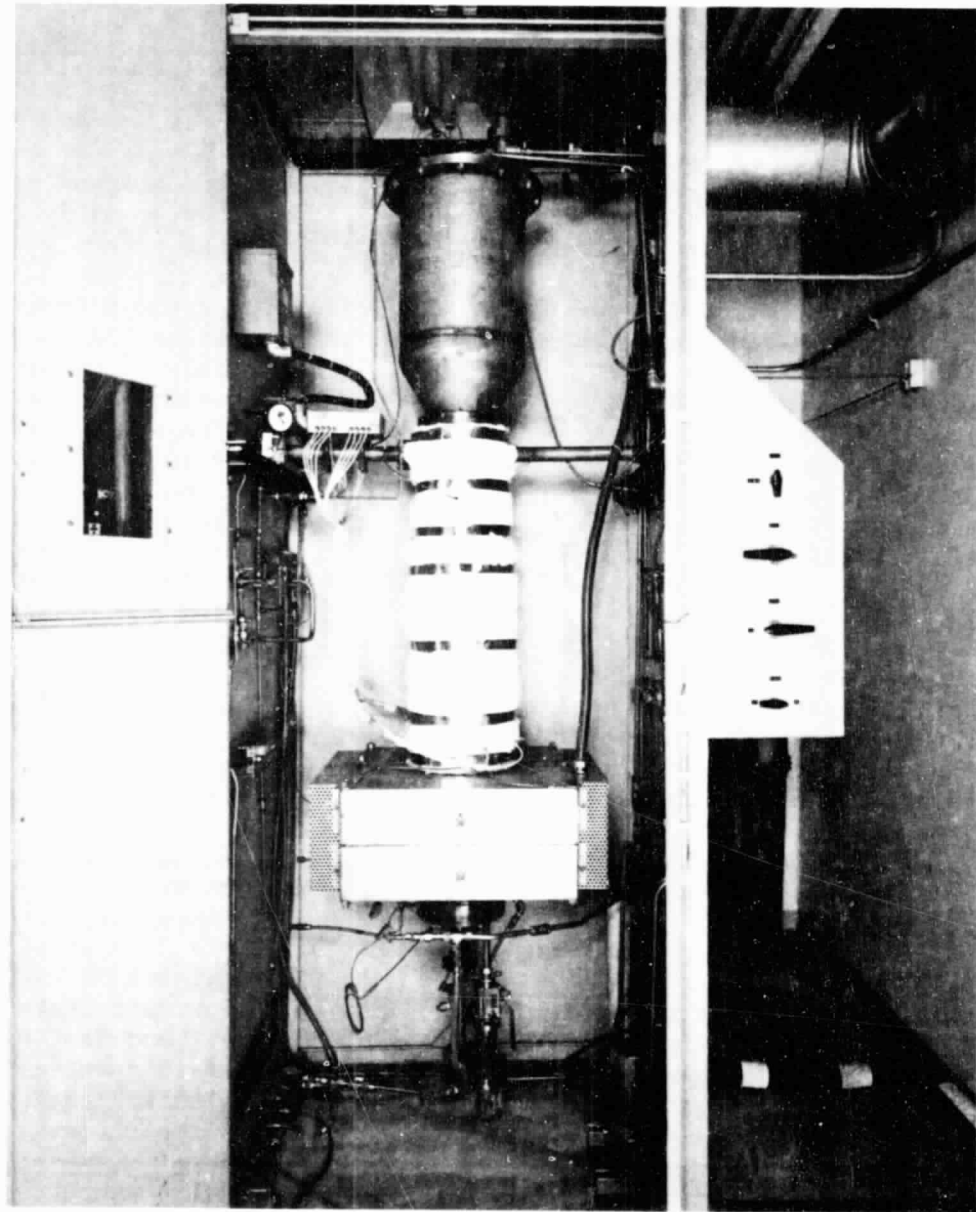
One responsibility is to develop the technology for a chemical process capable of producing semiconductor-grade polycrystalline silicon at a price of less than \$14/kg; the present market price is about \$50/kg. The most successful approach has been the development of the low-cost silane process, in which highly pure silane, produced from impure metallurgical-grade silicon, is converted to semiconductor-grade silicon. This development is nearing the stage of a practical demonstration as a result of an extensive JPL/DOE research and development program, which has included efforts at Union Carbide Corporation to carry out the primary chemical-engineering development and design tasks; at JPL to provide intensive research on fluidized bed technology; and at several universities and industrial laboratories to provide supporting research for solving chemistry and chemical-engineering problems.

The installation, checkout, and operation by Union Carbide of a 100-t/yr pilot plant in Washougal, Washington, represents a major achievement. A large-scale production plant with a 1200-t/yr capacity, based on the design of the pilot plant, is being installed. This plant incorporates the technology, developed under JPL/DOE contracts, for generating

ultrapure silane. The plant currently depends on the use of proprietary silicon-deposition reactors. The silicon product has the purity specifications of <0.2 ppma carbon or oxygen, <0.1 ppba phosphorus, and <0.01 ppba boron. Although this process using the proprietary reactors has the capability of producing the highest-purity silicon presently available commercially, it lacks the potential for meeting the goal of being low cost.

To achieve this goal, efforts to develop a fluidized-bed reactor technology for the conversion of silane to silicon at high volume and low cost have been underway at JPL and Union Carbide, with supporting research being done at Oregon State University and Caltech. Calculations showed that the low-cost goal could be met if a fluidized-bed reactor could be operated with at least 10% silane. The silane concentration seemed to be a major obstacle since the operation of other types of reactors had been limited to silane concentrations of about 2%, due to a gas phase reaction that produced very fine, unusable powder. However, the use of much higher silane concentrations has been demonstrated in carefully designed and controlled experiments in fluidized-bed reactors at JPL and Union Carbide. In fact, at JPL successful fluidized-bed reactor runs were made at 20, 40, 60, 80, and 100% silane, while avoiding the formation of unusable fine powder in worrisome quantities. These results have been explained with a theory involving aerosol and particle-scavenging phenomena. The concurrent collaborative studies at Union Carbide are mainly directed toward defining the design and operating conditions for steady-state production.

Ralph Lutwack
238-343
(213) 354-7648



JPL 6-in.-diameter fluidized-bed reactor for silicon deposition.

ORIGINAL PAGE IS
OF POOR QUALITY

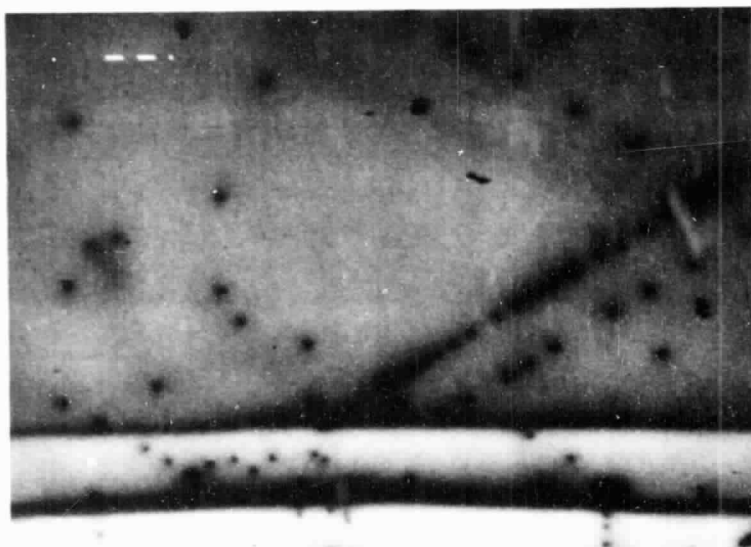
Material characterization is an integral part of the work to develop new low-cost silicon-sheet and solar-cell technologies. In comparison with single-crystal silicon, which is commonly used for transistors and integrated circuits, the new low-cost silicon materials that are under development might contain more impurities, larger residual stresses, and/or a higher density of structural defects. For the success of the program, it is necessary to understand the properties of these imperfections. Under sponsorship of the Department of Energy, JPL's Flat-Plate Solar Array Project has made significant contributions toward developing better characterization tools and improving our understanding of the effects of imperfections in the new materials. Highlights of the JPL work include:

- (1) Measuring electron-beam-induced current in silicon samples at a wide range of temperatures in a scanning electron microscope is an effective way to electrically characterize active defects in silicon that are detrimental to solar-cell performance. For example, recent results from low-temperature experiments on dendritic-web silicon ribbons, a low-cost high-quality material developed for terrestrial solar-cell applications, have revealed for the first time the existence of electrically active defects that delineate the traces of two different $\{111\}$ glide planes (surfaces along which atomic layers slip when crystalline material is subjected to stress). The observation suggests that the defects are dislocations introduced in the material by plastic deformation during the cooling

process, a manifestation of thermal stress. The density of these dislocations is found to be position-dependent, providing a new method to study the thermal-stress problems during ribbon growth.

- (2) The grain boundary is one of the major structural defects in the new silicon material. Because of lattice mismatch, the boundaries can act as potential barriers for majority carriers, recombination centers for minority carriers, trapping sites for impurities, as well as sinks and/or sources for lattice defects. The structural defects and impurities at the boundary give rise to the electronic localized states and, consequently, create the characteristic electrical properties. The localized states can be considered a bridge connecting structural defects due to lattice mismatch to the electrical properties important to polycrystalline solar-cell performance.

The recent study of $[100]$ and $[221]$ tilt boundaries using deep-level transient spectroscopy at JPL has demonstrated (a) that there is a general trend where the density of states at the boundary increases as the electronic state becomes deeper in the energy band gap, with maximum densities of 10^{11} - 10^{12} $\text{cm}^{-2}\text{eV}^{-1}$, and (b) that the spatial distribution of structural defects and impurities responsible for the formation of these states at boundaries with similar macroscopic electrical properties



Electron-beam-induced-current image of two parts of dendritic-web silicon-ribbon sample taken at 100 K. The dark spots represent plastic-deformation-induced dislocations. The lines of dislocations are the intercepts of $\{111\}$ planes with the surface. These dislocations are not observable at room temperature.

ORIGINAL PAGE IS
OF POOR QUALITY

is not often uniformly distributed throughout the boundary plane at the microscopic scale.

- (3) The crystal lattice mismatch at a grain boundary creates a strain field. As a result, the behavior of foreign atoms at the boundary can be altered, as demonstrated by the observation, reported years ago, of enhanced phosphorus diffusion at silicon grain boundaries. Recent JPL studies on cast-polycrystalline photovoltaic materials

(Wacker, HEM, and Semix) have shown that the enhancement of phosphorus diffusion for the three materials is the same, indicating that the properties of the boundaries are similar, even though the host materials are grown by different techniques. The results also reveal that grain boundaries showing the enhanced diffusion always have strong minority-carrier recombination activities. These results significantly increase our understanding of the nature of the new low-cost materials.

V. Earth Observational Systems

THE NEW AIRBORNE THERMAL INFRARED MULTISPECTRAL SCANNER

A new airborne Thermal Infrared Multispectral Scanner (TIMS) proposed by JPL investigators was completed in the summer of 1982 by Daedalus Enterprises, with six bands between 8 and 12 μm .

The instrument has been designed to explore the use of thermal infrared multispectral remote sensing of Earth. From laboratory spectral work and from previous remote-sensing experiments, we anticipated that significant geologic information could be extracted from TIMS data. Silicate rocks exhibit a broad, deep decrease in transmission between 8 and 11 μm due to Si-O stretching vibrations. The depth and position of the band are related to the structure of the constituent minerals and are especially sensitive to the quartz content of the rocks.

The TIMS was installed in the National Space Technology Laboratories Lear Jet and flown over several JPL test sites in August 1982, including Death Valley, California. Data from these flights were processed at JPL's image processing laboratory.

Despite some noise in the data, it is readily apparent that they contain significant geologic information.

In the enhanced image of Death Valley, silica-rich rocks were easily separable from the nonsilicates. The Eureka and Stirling Quartzites (red on the image) stood out in sharp contrast to the other Ordovician and Cambrian metasediments (blue and green), and Tertiary volcanic rocks (magenta) were easily separable from both. Also clearly distinguishable were various age units in the fan gravels (red, pink, blue, green), their separability apparently related to source material, differential weathering, and the development of desert varnish on the surfaces of exposed pebbles.

This instrument is viewed as an important tool to extend into the thermal infrared our capability for remote sensing of surface materials. Data in this wavelength region complement data from the visible and near infrared available from several other scanners, and add significantly to our ability to identify geologic materials remotely. We will continue our research directed toward a shuttle TIMS.

Anne Kahle
183-501
(213) 354-7265

Figure (opposite page): TIMS image of Death Valley, California. The valley floor (green and yellow in this image) lies above center. The eastern edge of the Panamint Mountains can be seen at the bottom of the image, with large alluvial fans draining to the valley floor.

ORIGINAL PAGE
COLOR PHOTOGRAPH



AIRBORNE IMAGING SPECTROMETER: FIRST USE OF IMAGING SPECTROMETRY IN EARTH REMOTE SENSING

Images acquired in as many as 128 spectral bands by the Airborne Imaging Spectrometer (AIS) promise to usher in a new era in Earth remote sensing. Through the application of new technologies in infrared detector arrays and image processing, direct identification of Earth surface materials is now possible--a capability that had been predicted from laboratory measurements but never before demonstrated.

AIS is the first of the new generation of Earth remote-sensing instrumentation and represents the first known use of an infrared area array in a scientific application. Operating in the pushbroom mode, AIS passes light from the ground through a slit and into a grating spectrometer where it is dispersed and focused on a 32- x 32-element detector array, forming one line of a spatial image 32 pixels wide in 32 contiguous spectral bands. As the aircraft flies down track, successive lines are acquired, building up a two-dimensional image in many narrow spectral bands. AIS operates in the 1.2- to 2.4- μ m range and by tilting the grating through four positions in one instantaneous field of view, images in 128 spectral bands

can be acquired. The spectral bandwidth is about 10 nm.

The detector array was developed for JPL by the Rockwell International Science Center. It is an infrared detecting device consisting of a mercury cadmium telluride (HgCdTe) chip mated to a silicon charge-coupled device (CCD), which acts as the multiplexer for reading out the signal. By specifying the ratio of Hg to Cd in the HgCdTe chip, the cutoff wavelength can be tailored as desired.

A more advanced airborne instrument, the Airborne Visible and Infrared Imaging Spectrometer (AVIRIS), is currently under development. It will extend the spectral coverage from 0.4- to 2.5- μ m in contiguous bands. Images generated by AVIRIS will be some 5600 pixels wide. Finally, a Shuttle Imaging Spectrometer Experiment (SISEX) has been proposed to NASA as a logical step toward an eventual free-flying or space-platform instrument. Each of these instruments will have a profound effect on Earth remote sensing by making the long-sought goal of direct surface-material identification a reality.

A. F. H. Goetz
Gregg Vane
183-501
(213) 354-3254

DEVELOPMENT OF RELIABLE EXCIMER LASER SOURCES FOR SPACEBORNE ACTIVE REMOTE SENSING

Ultraviolet (UV) excimer lasers are considered ideal sources for remote sensing of atmospheric parameters and constituents because of their high-energy tunable output. However, early excimer devices exhibited low efficiency (less than 1%) and short lifetime (less than 10^6 discharge cycles, especially for the electrical components) under repetitively pulsed operation. This has prevented their use on platforms such as the space shuttle and meteorological balloons.

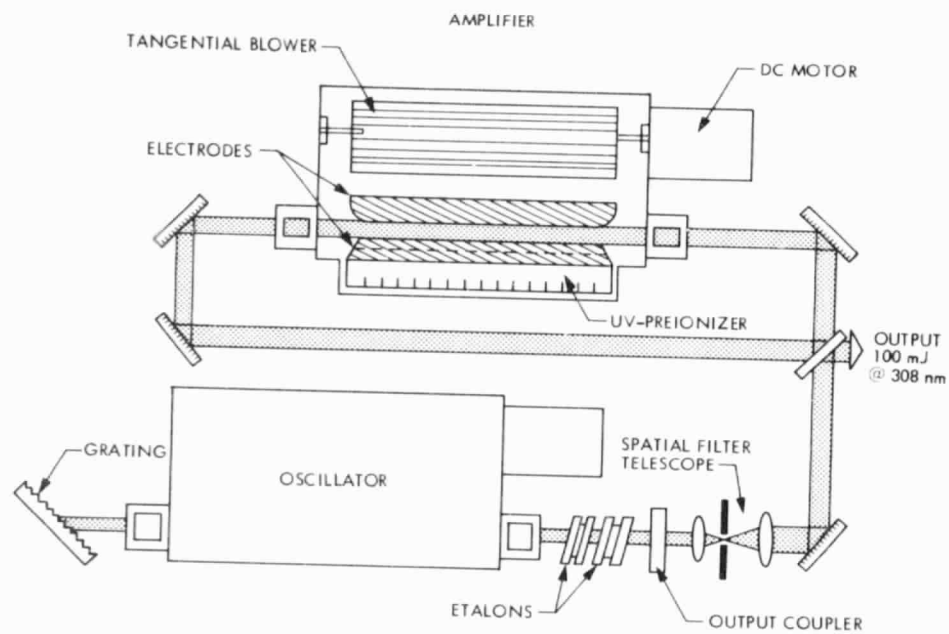
However, recent developments in the application of magnetic-switch technology to pulsed excimer lasers, as patented by the Laser Physics and Chemistry Group at JPL, have demonstrated that laser efficiency greater than 2% and component lifetimes greater than 10^8 pulses can be achieved for high-pressure gas lasers such as excimers or CO₂.

The incorporation of the magnetic-switch technology has been demonstrated for the first time in a repetitively pulsed XeCl tuned oscillator-amplifier excimer system. In addition to increased system reliability and efficiency, the magnetic switches also permit longer optical pulse-width operation from UV excimer lasers, a feature required for the tunable narrow-spectral-bandwidth operation necessary for remote sensing. Laser linewidths from XeCl of <200 MHz (0.0005 Å) have been achieved using the magnetic-switch technology on a JPL XeCl excimer laser.

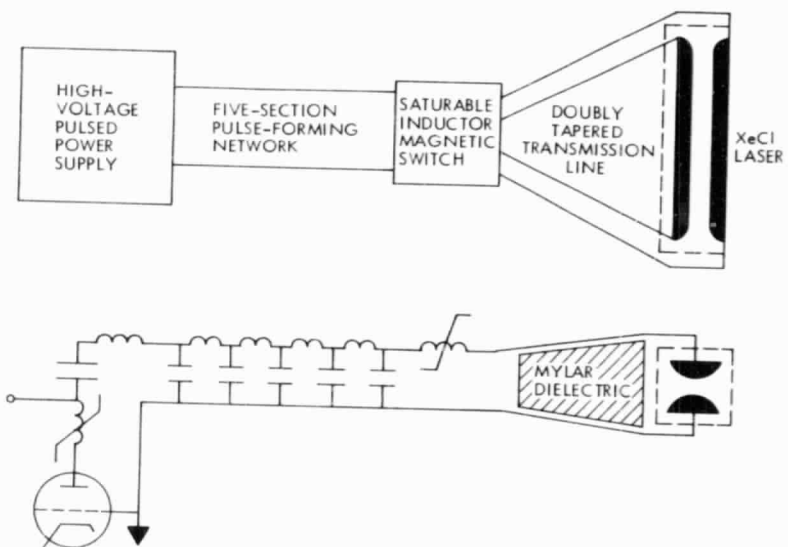
The significance of those demonstrations is that it foreshadows the development of a vastly improved class of high-power gas lasers that can be used for long-term, unattended operation such as might be required for spaceborne remote-sensing instruments. Also, the Navy has expressed strong interest in the use of a magnetically switched XeCl laser for the satellite-submarine communication blue-green laser system. The magnetic-switching concept is essential to longevity for satellite-based laser systems.

The improved tunability and spectral narrowing obtained from this configuration of the excimer laser has permitted high-resolution measurements of OH radicals using laser-excited fluorescence in laboratory experiments. Sensitive detection of trace levels of NO in atmospheric air samples was also demonstrated in the laboratory, using an in situ excimer laser-based two-color ionization method. The demonstration of narrow spectral linewidths from the magnetically switched excimer laser would also permit a wind measurement to be accomplished in conjunction with a narrow-band etalon filter. The increased backscatter from the atmosphere at the shorter wavelengths makes this technique competitive with proposed IR CO₂ laser methods, which require considerably higher-energy laser pulses as well as more stringent bandwidth requirements.

J. B. Laudenslager
183-601
(213) 354-2259



Magnetically switched P.F.N interfaced to XeCl laser using tapered transmission line.



Schematic of the JPL XeCl UV laser for lidar applications.

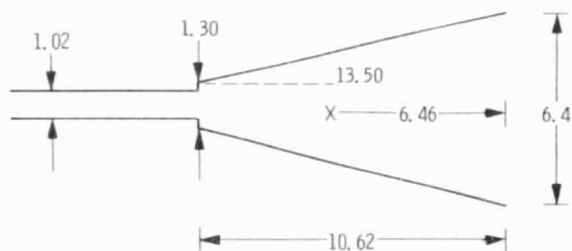
A DUAL-MODE HORN FOR SUBMILLIMETER WAVELENGTHS

An improved design for a microwave feed horn has been developed for radiometric applications in atmospheric remote sensing and astronomy. The advantage of the horn is that it is simple to construct but has the symmetric patterns and low sidelobes required for remote sensing applications at wavelengths near one millimeter. The horn may also be useful at longer wavelengths when an inexpensive, high-performance horn is needed.

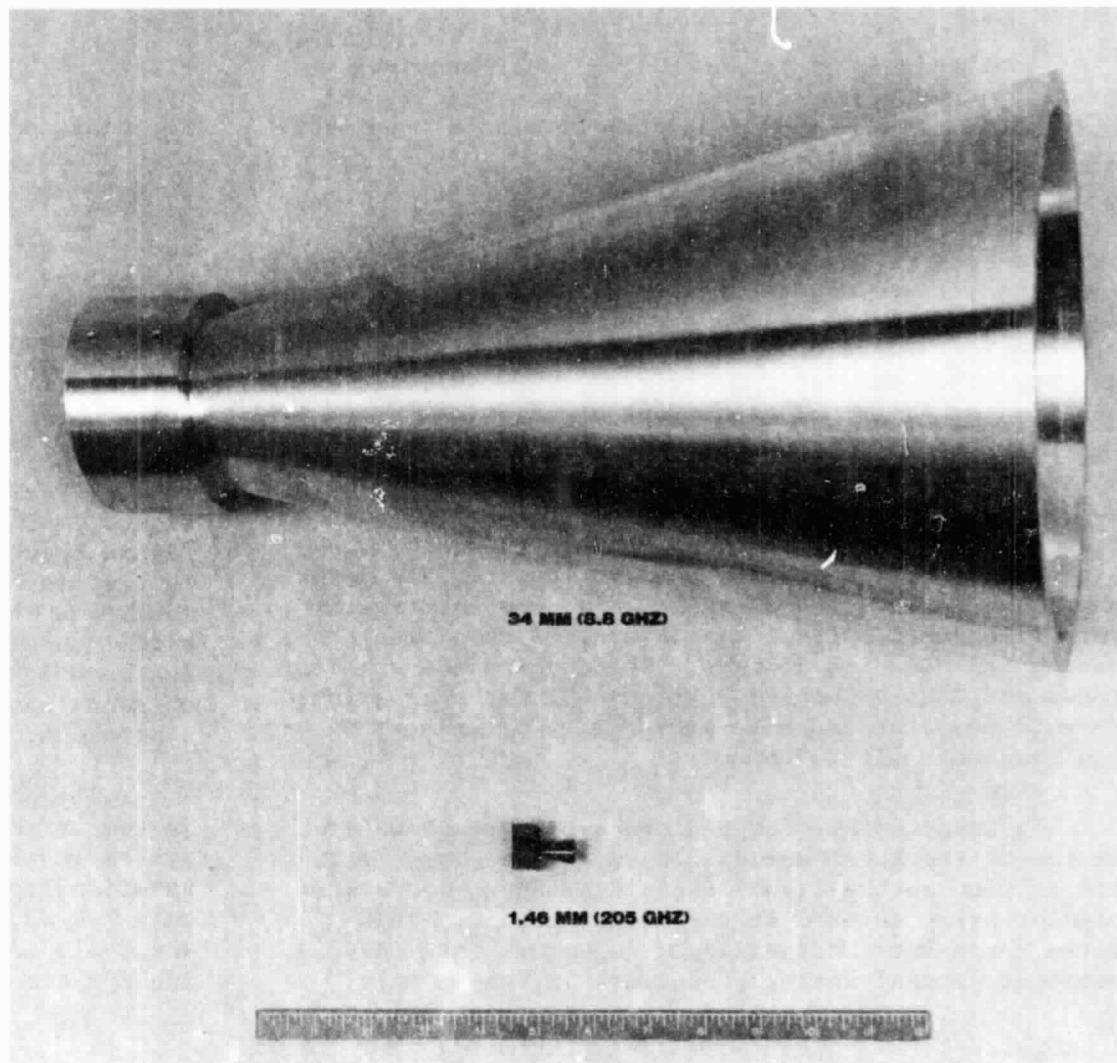
The horn is conical in shape and has evolved from an earlier design by P. D. Potter of JPL. The new design is simpler to construct and is almost a factor of two shorter than the original Potter design.

The horn design has been constructed and tested for four different wavelengths between 0.5 mm and 34 mm. It has a beamwidth of 6-deg half angle at the 3-dB points, and has a well-defined phase center. The measured radiation pattern is comparable in quality to Scalar feed horns which are conventionally used in applications where low sidelobe patterns are needed. The Scalar feed horn requires fabrication of many small grooves in its wall, a task which becomes impossibly difficult as the wavelength gets shorter. The advantage of the new design over the Scalar feed horn and the earlier dual-mode design by Potter is in the simplicity of construction. This new design is being utilized in radiometers on the Upper Atmospheric Research Satellite (UARS).

Dr. H. Pickett
168-314
(213) 354-6861



Horn cross-sectional diagram, with dimensions in units of the design wavelength.



Dual-mode horn.

HYBRID SAR DATA PROCESSOR

Synthetic Aperture Radar (SAR) data requires very intensive computer processing to produce images, and rapid growth in the use of SAR has created a huge backlog of data to be processed into imagery. It is expected that the use of imaging radar will increase greatly in the future.

Specialized digital systems are currently under vigorous development to solve the data-processing bottleneck. However, such systems are large, heavy, and very power hungry (requiring 10 to 20 kW), and are thus limited to ground processing applications.

Recent developments in electro-optic technology have made possible digitally controlled optical analog processors with several orders of magnitude advantage in computational capability per unit power. SAR data processing is one natural application for such systems since film-based optical analog systems have been processing SAR data for decades. The development of laser diodes and Charge-Coupled-Device (CCD) detector arrays has made possible moderate-performance processors requiring very little power.

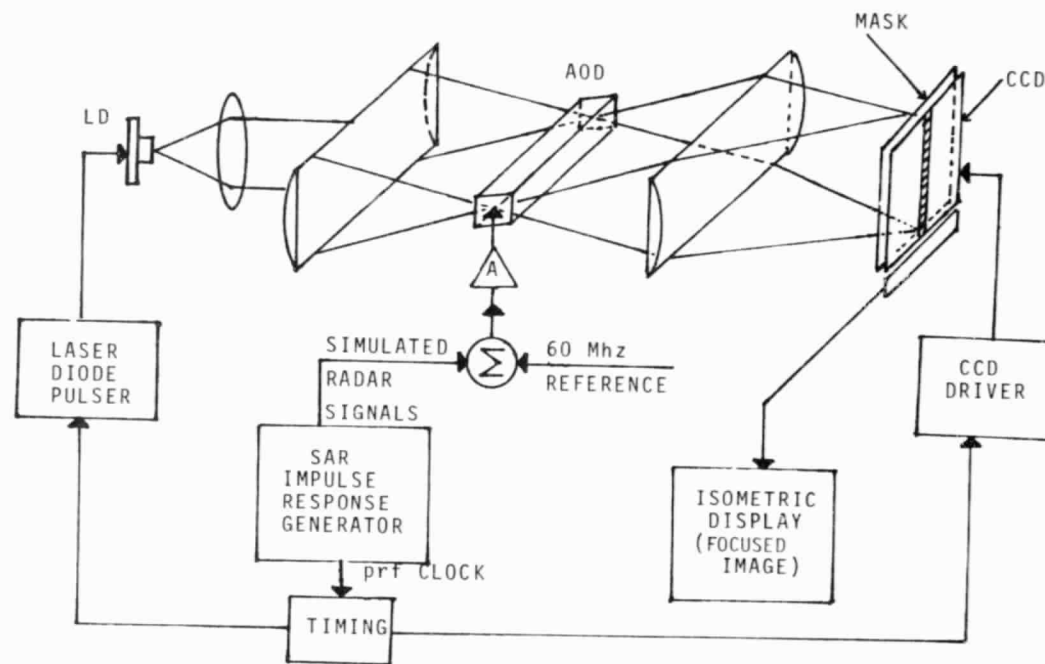
An architecture for SAR processing is shown at the top of the accompanying figure. An acousto-optic cell is used as the signal input transducer and a CCD detector array is used as the output device. This system represents a significant departure from conventional optical analog processors in two aspects.

First, both input and output are electro-optic (instead of film-based) and can occur in real time. Secondly, conventional analog SAR processors compress both dimensions spatially at the same time; the acousto-optic/CCD system compresses first in range, spatially, then in azimuth, temporally. This technique permits two-dimensional processing with a one-dimensional input device. While two-dimensional input devices are under active development, they are currently significantly behind the maturity of the acousto-optic cells in one-dimensional performance.

The basic concept has been demonstrated in a collaborative experiment between JPL and Professor Dimitri Psaltis of Caltech, who developed the technique. The bottom three parts of the accompanying figure show (a) the point target signal synthesized to test the system, (b) the azimuth reference-function mask, and (c) the CCD detector output. The test-signal input range bandwidth was 20 MHz and the Doppler bandwidth was about 40 Hz. The compression ratio obtained was on the order of 100 to 1 in both dimensions.

The potential of this technique is very great: in comparison to a real-time digital processor, the system exhibits about a factor of twenty less in computational performance, but the power consumption is only 2 W as opposed to 20 kW. Additionally, this system could be implemented in integrated optics, reducing the size to a few cubic inches.

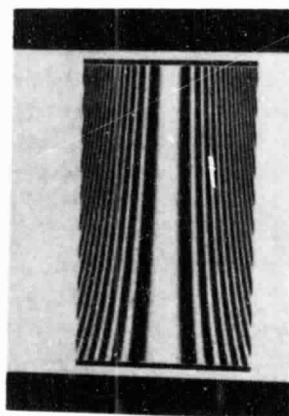
Tom H. Bicknell
183-701
(213) 354-2523



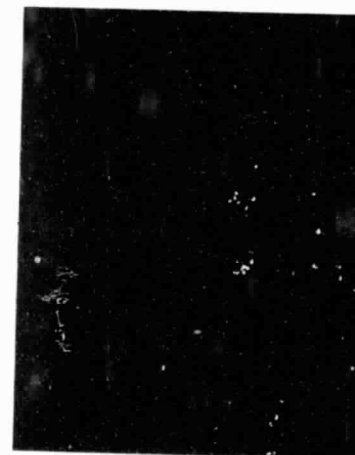
ACOUSTO-OPTIC/CCS SYSTEM



a. Point Target Signal



b. Reference Function Mask



c. Compressed Signal

Hybrid SAR data processor.

PILOT OCEAN DATA SYSTEM

In response to the need for more effective access to satellite-data sets by scientific investigators, the Pilot Ocean Data System is being developed to demonstrate techniques for the management and analysis of large satellite-data sets for the ocean sciences. The complete geophysical data sets from the GEOS-3 altimeter and the Seasat altimeter, scatterometer, and microwave radiometer have been compressed and stored in an on-line data system that provides rapid, selective access to data subsets selected by sensor, time, and location. A flexible, self-guided menu interface provides the casual user access to a growing inventory of data-management and data-analysis tools. An investigator can interactively examine a data-set catalog, search an on-line bibliography, browse through sample data sets, or apply assorted analysis tools to rapidly find a candidate data set and evaluate its utility for a specific application. Graphics workstations, connected to the Pilot Ocean Data System via a commercial communications network at 1200 bits/s, have been provided to investigators at several major universities and research institutions.

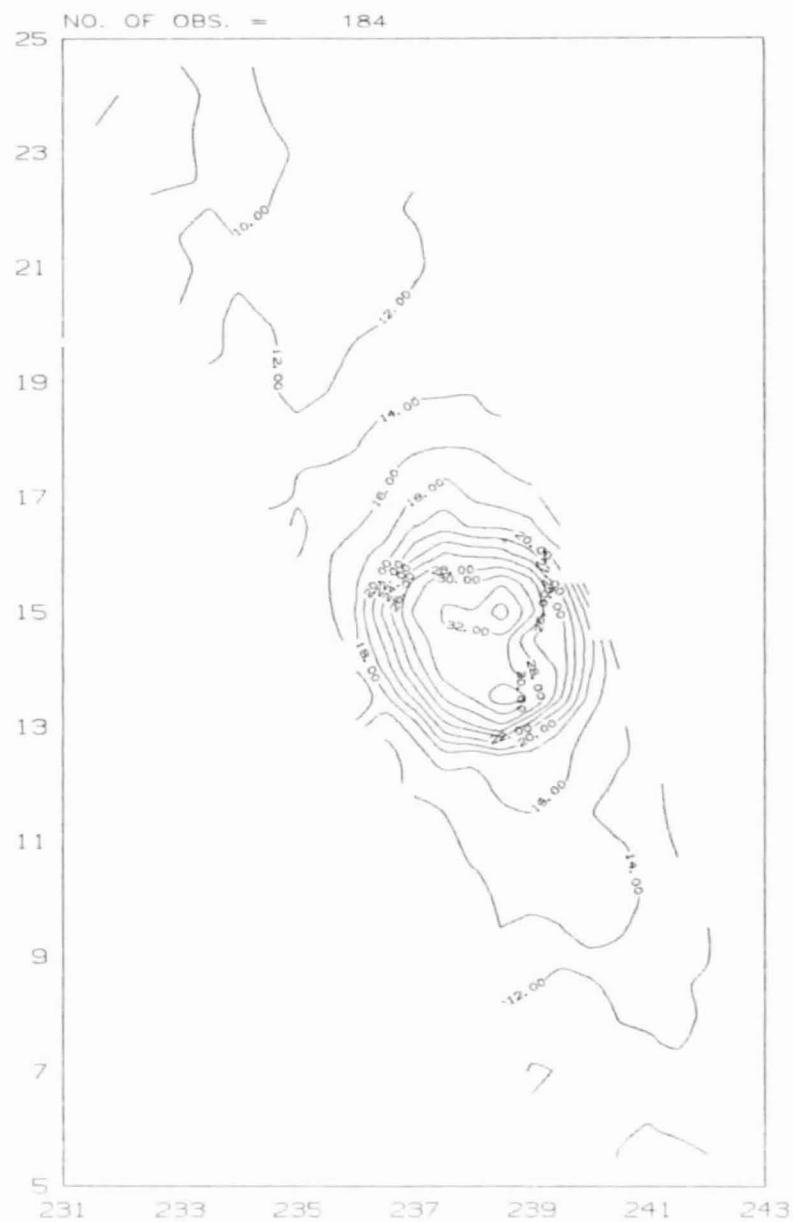
Currently available GEOS, Seasat, and correlative in situ data amount to approximately 700 megabytes on-line and about 50 gigabytes on tape. Plans call for the acquisition of new data sets such as the NIMBUS Coastal-Zone Color Scanner, the TIROS Advanced Very-High Resolution Radiometer, and the DMSP Microwave Imager. Some data sets will have a temporal coverage of five or more years, allowing investigators to study annual and interannual variability of meso-scale and large-scale oceanic features. By the mid-1980s the Pilot Ocean Data System is expected to be

supporting an on-line data base of 20 to 50 gigabytes, by making use of digital optical-disk storage.

Satellite-data access is provided by combining an algorithm for determining intersect times of sensor fields of view with specified regions on Earth's surface, with a relational data-base management system that manages the indexes into the very large satellite-data files. Access to any desired segment of satellite data can be obtained in minutes. The data-base management system manages the in situ data directly, as the volume is more modest. Data output is in the form of magnetic tapes, printed listings, or tabular and graphic displays at the user's terminal. Paper or magnetic-tape output products are shipped to investigators within 24 hours of generation via an express shipping service.

During 1983, the PODS facility was improved by redesigning the on-line bibliography as a relational data base, by completing the multi-user version of the Relational Information Management System (RIM), and through the addition of a powerful and easy-to-use graphics capability and supporting image-processing hardware and software. These capabilities supported such activities as two sea-surface temperature workshops and the production of a prototype ocean color and temperature time series of the California Current. Also during this year, contacts were initiated with the National Snow and Ice Data Center in Boulder, Colorado, to plan for the transfer of PODS technology for the purpose of archiving polar ice and snow data expected from the SSM/I microwave radiometer to be launched in 1985 on a DMSP satellite. Finally, the GEOS-3 altimeter data set, covering the years 1975-1978, was added to the archive holdings.

A. Zygielbaum
171-209
(213) 354-3494



Pilot Ocean Data System: SMMR winds—Hurricane Fico.
(Data time: 78:07:14:13:34:39 - 78:07:14:13:40:28)

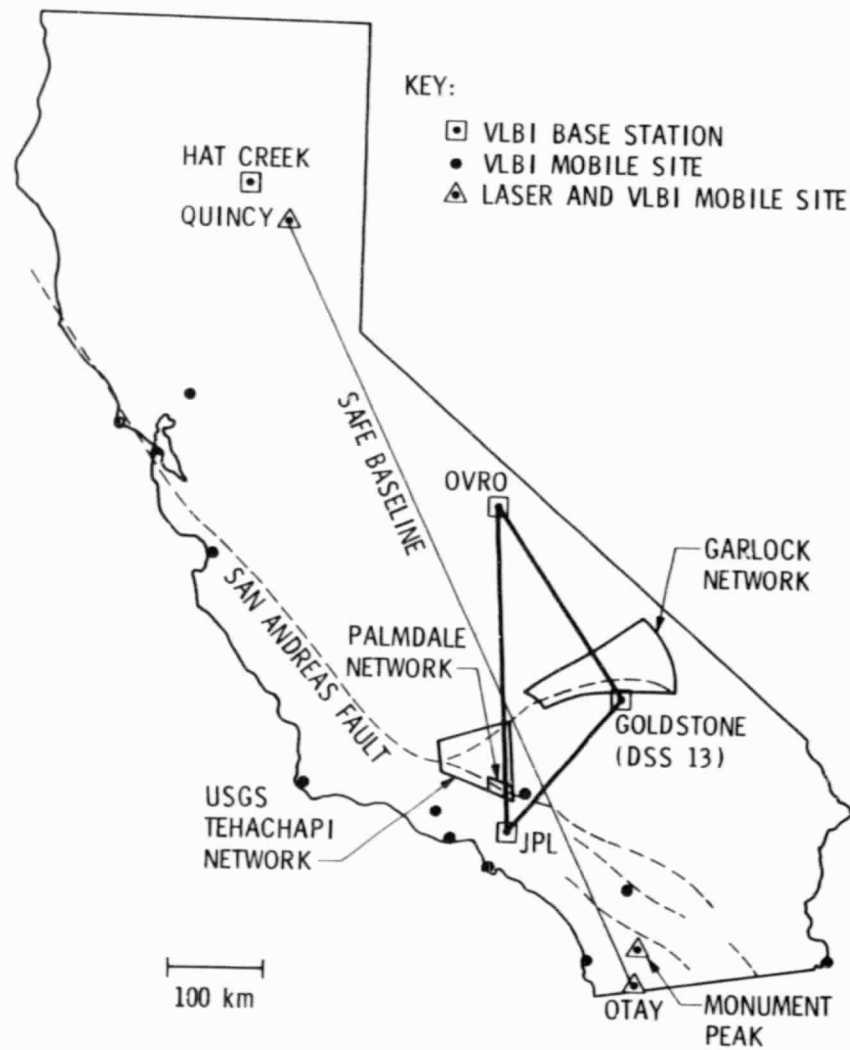
RADIO INTERFEROMETRIC MEASUREMENT OF THE JPL/OWENS VALLEY/GOLDSTONE BASELINES USING THE MOBILE VLBI SYSTEMS

The Mobile VLBI Systems developed at JPL have been deployed in the Western United States in a campaign to obtain geodetic measurements of regional deformation. These measurements will add significantly to the knowledge of plate tectonics and crustal deformation near plate boundaries. Eventually, such measurements could contribute to deeper understanding of the earthquake mechanism and lead to earthquake-hazard reduction by the identification of regions with a high probability of earthquake occurrence.

We are now completing the analysis of results from the Mobile VLBI campaigns of 1980-1982. The most frequently measured baselines in this period are the three formed by the 40-m telescope of the Owens Valley Radio Observatory near Big Pine, California, the 26-m Deep Space Station 13 (DSS 13) telescope of the NASA Goldstone Tracking Complex near Barstow, California, and one of the Mobile VLBI stations located at JPL. Twenty-four separate measurements were made of one or all of these baselines in the period 1980-1983.

Linear least squares fits to these data indicate that there is no statistically significant motion in the horizontal plane above the level of 1.7 standard deviations, with upper limits generally on the order of 1- to 2-cm/yr. These rates are smaller than might be naively inferred from USGS laser-geodimeter network-strain measurements and from the satellite laser ranging SAFE experiment. Both of these show a compression in approximately the north-south direction of 1.0 to 1.5×10^{-7} /yr. In addition, the long-term average motion along the North American/Pacific plate boundary (the San Andreas fault) is about 5.6 cm/yr in a right-lateral sense, which would also imply a compression of the north-south JPL/Owens Valley baseline of about 1.0×10^{-7} /yr. The results from the Mobile VLBI measurements, on the other hand, are consistent with rigidity of the JPL/Owens Valley/Goldstone triangle, with possibly a small (but not statistically significant) expansion of the JPL/Owens Valley baseline of 0.2 ± 0.8 cm/yr or $0.05 \pm 0.2 \times 10^{-7}$ /yr. The reason for this difference may arise from the facts that the tectonics of the region are complex and that the four results are a disparate set, both spatially and temporally.

John M. Davidson
264-748
(213) 354-7508



Crustal Dynamics Project-Mobile VLBI site locations.

SERIES GPS RECEIVER

The initial engineering test phase has been completed for the SERIES (Satellite Emission Range Inferred Earth Surveying) task. This technology has been developed at JPL to meet the need for high-precision, cost-effective geodesy, and to complement the Mobile VLBI (Very Long Baseline Interferometry) System for earth surveying.

The heart of the SERIES geodetic system is a novel receiver designed to utilize the signals broadcast from the GPS (Global Positioning System) satellites. The receivers have been shown to produce high-precision geodetic measurements and provide high-accuracy calibration of the ionosphere.

The GPS used by SERIES will consist of a constellation of 18 operational NAVSTAR satellites by the late 1980s. This system has been developed by the DOD primarily for navigation, and makes use of pseudonoise sequences. The navigation accuracy (nondifferential) of the GPS system using conventional GPS receivers is about at the 10-m level.

During the last four years, the SERIES team at JPL has developed a novel type of GPS receiver. These receivers do not require knowledge of the exact

sequences being used by the GPS satellites. In addition, when two SERIES receivers are used differentially to determine a baseline, accuracies of a few cm can be obtained. The original SERIES implementation was to use the GPS satellites as RF noise sources for VLBI terminals. However, it was realized that the periodic structure in the GPS signal can also be used to provide ranging information, even without sequence knowledge. By exploiting the periodic structure of the GPS signal, bandwidths were collapsed and data acquisition and subsequent data processing were greatly simplified.

Two proof-of-concept SERIES stations have been constructed. These stations each have a 1.5-m-diameter prime-feed parabolic dish antenna. These antennas provide 23-dB gain in the GPS signal. The receiver has been constructed from off-the-shelf components wherever possible. The receivers contain a locally generated test signal for self-calibration. Data are recorded on either floppy disks or 9-track tapes.

These proof-of-concept stations have been tested on baselines up to 171 km long during the last 1.5 yr. Baseline vectors determined with the current stations have demonstrated the few-cm measurement accuracies for baselines of a few tens of km.



ORIGINAL PAGE IS
OF POOR QUALITY

Portable GPS system at Mammoth Lake measuring baseline between Mammoth Lake and the Owens Valley Radio Observatory.

An additional feature of the SERIES technique is the ability to synchronize clocks at different sites by receiving common GPS satellite signals. This was demonstrated on a 21-km baseline when clock offsets, measured by the SERIES stations, were compared with simultaneous independent measurements made by an atomic clock carried between the two stations. The agreement between the two techniques was within 1 ns for each of the two demonstrations performed. The

SERIES technique for clock synchronization is expected to give accuracies of 10 ns for stations separated by intercontinental distances.

Improvements are currently being made to the SERIES receivers to further increase measurement precision. A SERIES spin-off, SERIES-X, is under development as the basis of a precision navigation system for the TOPEX satellite.

C-2
L. E. Young
264-737
(213) 354-5018

INDEX OF NATIONAL AERONAUTICS AND SPACE ADMINISTRATION
SPONSORING PROGRAM OFFICES

OFFICE OF SPACE SCIENCE AND APPLICATIONS (OSSA)

Deep Space Exploration

Planets and Their Satellites

CCD Imaging of the Outer Planets	4
Plasma Physics at Saturn	6

Astrophysics

Infrared Astronomical Satellite	8
Testing Relativity With Solar System Dynamics	11
X-Ray CCD Spectrometer	12
Far-Ultraviolet CCD Imager	14
Gamma-Ray Line Emission From SS 433	16
Radio Astronomy at the Milliarcsecond Level	18
Electron Impact Excitation of Ions From Energy-Loss Spectra Measurements	20

Small Bodies--Asteroids and Comets

Properties of Residues From Sublimed Dirty Ice:	
Comet and Mars Applications	34
Palomar Asteroid Search Program	36
Radar Detection of Comets	38

Information Systems and Space Technology Development

Hydride-Absorption Cryogenic Refrigerator	42
Particulate Contamination Environment Observed on STS-3	44
Flow-Field Diagnostics Using Digital Imaging Techniques	46
Computer-Vision and Robotics Research	48
Improved-Performance Shuttle-Nozzle Test	50
Gaseous Oxygen/Hydrogen Thruster Technology	52
Hybrid Topology Developments	54
The VLSI Design Center	56
Pulsed Plasma Thruster Ignition System Lifetime	57
Development of Safe, High-Energy Lithium Cells for NASA Applications	58

Technology Applications

Measuring Tract Amounts of Contaminants Present in a Gaseous Environment	62
Metal Shell Technology and Its Applications	64
Hydrocephalus Shunt	66
Pressure Distribution and Flow Separation in Arterial Branch Cast and Models	68
Analysis of Individual Biological Particles by Mass Spectrometry	70

Earth Observational Systems

The New Airborne Thermal Infrared Multispectral Scanner	80
Airborne Imaging Spectrometer: First Use of Imaging Spectrometry in Earth Remote Sensing	83
Development of Reliable Excimer Laser Sources for Spaceborne Active Remote Sensing	84
A Dual-Mode Horn for Submillimeter Wavelengths	86
Hybrid SAR Data Processor	88
Pilot Ocean Data System	90
Radio Interferometric Measurement of the JPL-Owens Valley/ Goldstone Baselines Using the Mobile VLBI Systems	92
SERIES GPS Receiver	94

OFFICE OF SPACE TRACKING AND DATA SYSTEMS (OSTDS)

Deep Space Navigation and Communication

Technology Upgrade of DSN Antennas from 64 to 70 m	22
VLSI Multicode Convolutional Encoder Chip	24
2.5 Bits/Detected Photon Demonstration	26
Data Acquisition and Command of Pioneer 8 From an Unattended Station	29
Microwave Holographic Surface Measurement of the Tidbinbilla 64-m Antenna	30
Diffraction-Coupled Semiconductor Laser Arrays	32

Energy and Energy Conversion Technology

Low-Cost Polycrystalline Silicon Process Development	74
Characterization of Silicon Materials Pertinent to Terrestrial Solar-Cell Applications	76

Further information concerning any project may be obtained by contacting the proper NASA program office, National Aeronautics and Space Administration, Washington, D.C. 20546.